The origin and evolution of LysM receptor-like kinases in plants

Dissertation

zur

Erlangung des Doktorgrades

der Mathematisch-Naturwissenschaftlichen Fakultät

der Universität zu Köln

vorgelegt von

Foo Mung Hsia

aus Serian, Sarawak, Malaysia

accepted in the year 2025

Die vorliegende Arbeit wurde am Max-Planck-Institut für Pflanzenzüchtungsforschung in Köln in der unabhängigen Forschungsgruppe Grundlegendes Immunsystem der Pflanzen unter der Leitung von Dr. Hirofumi Nakagami angefertigt.

This work described in this thesis was conducted under the supervision of Dr. Hirofumi Nakagami in the independent research group Basic Immune System of Plants at the Max Planck Institute for Plant Breeding Research in Cologne.

MAX-PLANCK-INSTITUT
FÜR PFLANZENZÜCHTUNGSFORSCHUNG

Table of Contents

List of figures

Acknowledgements (remove for publication)

List of abbreviations

At- *Arabidopsis thaliana*

Cb- *Chara braunii*

Ccdb- control of cell-death toxin b

CEBiP- chitin elicitor-binding protein

CERK- chitin elicitor receptor kinase

DAMP- damage-associated molecular pattern

ECD- ectodomain

EDTA- ethylenediaminetetraacetic acid

EGF- epidermal growth factor

ETI- effector triggered-immunity

FDR- false discovery rate

flg-22- flagellin 22

FLIM- fluorescence-lifetime imaging microscopy

FRET- Förster resonance energy transfer

GFP- green fluorescent protein

GlcNAc- *N-acetylglucosamine*

HAMP- herbivore-associated molecular pattern

HR- hypersensitive response

Kd- dissociation constant

KO- knockout

LCA- last common ancestor

LCO- lipo-chitooligosaccharides

LED- light-emitting diode

Lj- *Lotus japonicus*

LRR- leucine-rich repeat

LYK- LysM kinase

LYM- LysM domain

LYR- LysM kinase related

LysM- lysin motif

MAMP- microbes-associated molecular pattern

MAPK- mitogen-activated protein kinase

Mp- *Marchantia polymorpha*

MS- mass spectrometry

MST- microscale thermophoresis

MurNAc- *N-acetylmuramic acid*

Myc factor- mycorrhizal factor

NADPH- nicotinamide adenine dinucleotide phosphate

NLR- nucleotide-rich leucine-repeat receptor

Nod factor- nodulation factor

Os- *Oryza sativa*

PAGE- polyacrylamide gel electrophoresis

PAMP- pathogen-associated molecular pattern

PCA- principal component analysis

PGN- peptidoglycan

PRR- pattern recognition receptor

PTI- pattern-triggered-immunity

RBOH- respiratory burst oxidase homolog

RLCK- receptor-like cytoplasmic kinase

RLK- receptor like kinase

RLP- receptor like protein

RLU- relative light unit

ROS- reactive oxygen species burst

rpm- revolutions per minute

SDS- sodium dodecyl sulfate

Sp- *Spirogyra pratensis*

SP- signal peptide

Summary

The cell surface localized lysin motif (LysM) receptor-like kinases/proteins (RLKs/RLPs) function as sensors for pathogenic and symbiotic microbes in land plants, perceiving chitin, lipo-chitooligosaccharides (LCOs), and peptidoglycan. LysM-RLKs/RLPs play a crucial role in activating various responses that lead to defense against pathogens or the establishment of symbiosis. While the functions of LysM-RLKs/RLPs were well-studied in land plants, their evolutionary origin and broader functional roles remain less explored. Streptophyte algae are widely recognized as the sister lineage of land plants. Land plants are believed to have emerged from a streptophyte algal ancestor. Plant–pathogen interactions are ancient and have played a pivotal role in shaping the evolution and complexity of the plant innate immune system. Genomic analyses revealed the presence of LysM-RLKs in two streptophyte algal species, Charophyceae *Chara braunii* and Zygnematophyceae *Spirogyra pratensis*. The functional roles of LysM-RLKs in both species were subsequently characterized.

Through phylogenetic analysis combined with sequence alignment, I propose that LysM-RLKs originated from the last common ancestor of Charophyceae, Zygnematophyceae, and land plants. A conserved CXC motif within the LysM ectodomains (ECDs) was identified in streptophyte algal LysM-RLKs, like those present in land plants. Structural predictions using AlphaFold2 and three-dimensional modeling revealed that the overall architecture of LysM ECD is conserved, including a chitin-binding groove within the LysM2 domain. *In vitro* binding assays further demonstrated the chitin-binding capability of LysM ECDs from both streptophyte algae and bryophytes, suggesting an ancestral role of LysM ECDs in chitin recognition. Intriguingly, however, chitin treatment did not trigger downstream transcriptional responses in streptophyte algae, pointing to a functional divergence in LysM-RLKs during evolution. Furthermore, genetic and interaction studies demonstrated that heterodimerization and the formation of higher-order oligomeric complexes of LysM receptors are essential for proper function in bryophytes. In contrast to bryophytes, chitin treatment did not promote homodimerization of algal LysM receptors. Overall, this study new provides an insight into the evolutionary origin and functional diversification of LysM RLKs/RLPs in plants.

Introduction

1.1 Streptophyta

The green lineage split into the clades of Chlorophyta and Streptophyta. Streptophyta includes paraphyletic streptophyte algae and embryophytes (land plants) (Figure 1.1). The streptophyte algae are divided into six distinct lineages: Mesostigmatophyceae, Chlorokybophyceae, Klebsormidiophyceae, Charophyceae, Coleochaetophyceae, and Zygnematophyceae. These lineages are further categorized into two grades, KCM (Klebsormidophyceae, Chlorokybophyceae, Mesostigmatophyceae) and ZCC (Zygnematophyceae, Charophyceae, Coleochaetophyceae) (Figure 1.1). Streptophyte algae are also referred to as charophytes. Land plants represent the remaining plant species that thrive on land. While many streptophyte algae adopt an aquatic lifestyle, some species can be found in moist terrestrial habitats. It is commonly accepted that land plants evolved from an algal ancestor, with the Zygnematophyceae as the closest sister lineage to land plants. Over more than 500 million years, when plants transitioned from aquatic to terrestrial environments, they were exposed to adverse environmental conditions and pathogen invasions. This facilitated the evolution of adaptive mechanisms that enabled plants to overcome the challenges of moving to land.

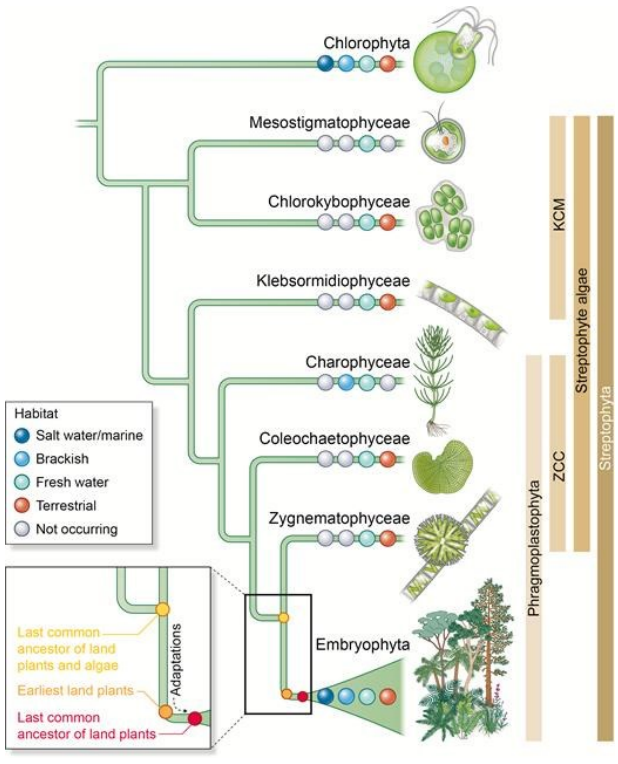

Figure 1.1 The cladogram shows split of the green lineage of Chlorophyta and Streptophyta. The Streptophyta consists of paraphyletic streptophyte algae and monophyletic land plants. The habitats are illustrated. Illustration from (Fürst-Jansen et al., 2020)

1.2 Plant–pathogen relationships

Bacteria are thought to have already existed roughly around 3.2–3.5 billion years ago (Battistuzzi et al., 2004; Betts et al., 2018), well before the emergence of the streptophyte algal ancestor of land plants around one billion years ago (Strother et al., 2011). Land plants are exposed to a wide diversity of bacteria, many of which can cause disease in plants. Likewise, algae also host diverse bacterial communities, some of which might also become pathogenic (Han, 2019).

Fungi appeared approximately one billion years ago, with the earliest fungi were mainly aquatic (Loron et al., 2019; Naranjo-Ortiz & Gabaldón, 2019). Fungi can infect land plants, including liverworts and mosses (Ponce De LeÓN et al., 2012; Redkar et al., 2022). The ancient aquatic fungi may have acquired plant cell wall-digesting enzymes, enabling them to extract nutrients from land plants and algae, suggesting that fungi may have been associated with plants since their origin (Chang et al., 2015).

Oomycetes are fungi-like heterotrophs that are found ubiquitously in both aquatic and terrestrial environments, and many species are also plant pathogens (Beakes et al., 2012). The discovery of *Paleonitella* fossils, a streptophyte algae displaying infection by oomycete-like filamentous structures, suggests that the association between oomycetes and plants is ancient (Taylor et al., 1992).

The origin of viruses remains elusive; however, their existence predates the earliest forms of life, which is widely accepted. They likely existed in the pre-cellular world as self-replicating entities and later evolved into microbes that parasitize other cells (Forterre, 2006). Viruses infect cells across all domains of life, Archaea, Bacteria, and Eukarya. Numerous pieces of evidence showed that viruses have been infecting plants, including green algae, suggesting an ancient association. (Perini et al., 2024; Van Etten et al., 1991)

Pathogenic microbes reduce plant fitness and increase mortality rates. Plants must counter these threats to ensure survival. Consequently, plants have evolved an elegant and sophisticated innate immune system to combat a wide range of pathogens. The evolutionary arms race between plants and microbes has shaped the landscape of plant innate immunity over hundreds of millions of years.

1.3 Plant innate immunity

The threat of pathogenic microbes to plants is persistent, as pathogens continually evolve new tools for infection, while plants, in turn, develop innovative ways to combat these pathogens. Unlike mammals, plants lack mobile immune cells and an adaptive immune system. Plants rely solely on the innate immune system. The plant's innate immune system consists of a two-tier system. The first layer involves cell-surface pattern recognition receptors (PRRs) that activate pattern-triggered immunity (PTI) (Zipfel, 2008). The second layer of plant immunity consists of intracellular receptors that detect pathogen effectors, activating effector-triggered immunity (ETI) (Jones & Dangl, 2006; Ngou et al., 2022).

The PRRs recognize pathogen-associated molecular patterns (PAMPs), microbes-associated molecular patterns (MAMPs), and herbivore-associated molecular patterns (HAMPs) derived from bacteria, fungi, oomycetes, and herbivores, thereby activating PTI (Ge et al., 2022). Some PRRs also recognize self-derived molecules, called damage-associated molecular patterns (DAMPs), which are released upon damage that can be caused by pathogen invasion (Gust et al., 2017; Jones et al., 2024; Reymond, 2021). Frequently, ligand-sensing PRRs require co-receptors to transmit non-self signals and initiate a full immune response. Generally, the PTI response is less drastic and does not result in host cell death.

Pathogens, on the other hand, secrete effectors into host cells to suppress PTI. Plants can recognize certain effectors and trigger ETI. Plants recognize effectors by utilizing nucleotide-binding, leucine-rich repeat (NLR) proteins. NLR proteins detect effectors either directly or indirectly, leading to immune defense responses. Activation of NLR proteins often results in the hypersensitive response (HR), in which cells at the infection site undergo programmed cell death, thereby limiting the growth of biotrophic and hemibiotrophic pathogens.

PTI and ETI were once considered independent branches of the plant immune system. However, growing evidence suggests that PTI and ETI engage in crosstalk rather than functioning as two distinct modes, resulting in a more robust immune response (Igarashi et al., 2013; Ngou et al., 2021; Pruitt et al., 2021; Tian et al., 2021; Wang et al., 2023; Yuan et al., 2021). In land plants, particularly angiosperms, PTI, ETI, and their crosstalk have been extensively studied.

1.4 Types of PRRs

PRRs are cell-surface localized receptors that can be broadly categorized into two types: receptor-like kinases (RLKs) and receptor-like proteins (RLPs). Both RLKs and RLPs contain various types of extracellular domains (ECDs) at their N-termini, which are responsible for MAMP recognition. Based on their ECD types, including leucine-rich repeat (LRR), lysin motif (LysM), epidermal growth factor (EGF)-like, and malectin-like domain, RLKs and RLPs can be grouped into distinct classes (Albert et al., 2020; Boutrot & Zipfel, 2017; Ngou et al., 2022). RLKs consist of an ECD, a single-pass transmembrane domain that anchors the protein in the plasma membrane, and an intracellular kinase domain. RLPs lack an intracellular kinase domain. Depending on their type, RLPs either contain a glycosylphosphatidylinositol (GPI)-anchor or possess a transmembrane domain that anchors them to the plasma membrane. The key difference between RLKs and RLPs is that RLKs possess an intracellular kinase domain at their C terminus, whereas RLPs do not. Consequently, RLPs often rely on RLKs as co-receptors to initiate and transmit signals.

The types of ECDs primarily determine the nature of ligand specificity. Ligand binding promotes the formation of complexes between PRRs and their co-receptors, leading to *cis*- and /or *trans*-phosphorylation of the intracellular kinase domain. This phosphorylation subsequently activates receptor-like cytoplasmic kinase (RLCKs). RLCKs activate responses, including the production of reactive oxygen species (ROS) by respiratory burst oxidase homologs (RBOHs) that are NADPH oxidases, cytosolic calcium ion bursts, activation of mitogen-activated protein kinase (MAPK) cascades, and induction of defense-related gene expression (DeFalco & Zipfel, 2021; Lu & Tsuda, 2020). The ROS production by RBOHs depends on phospho-regulation by RLCKs and calcium-dependent kinase (Dubiella et al., 2013; Kadota et al., 2014; Kobayashi et al., 2007; Li et al., 2014; Monaghan et al., 2014). These responses collectively serve as effective host defense mechanisms, contributing to broad-spectrum resistance.

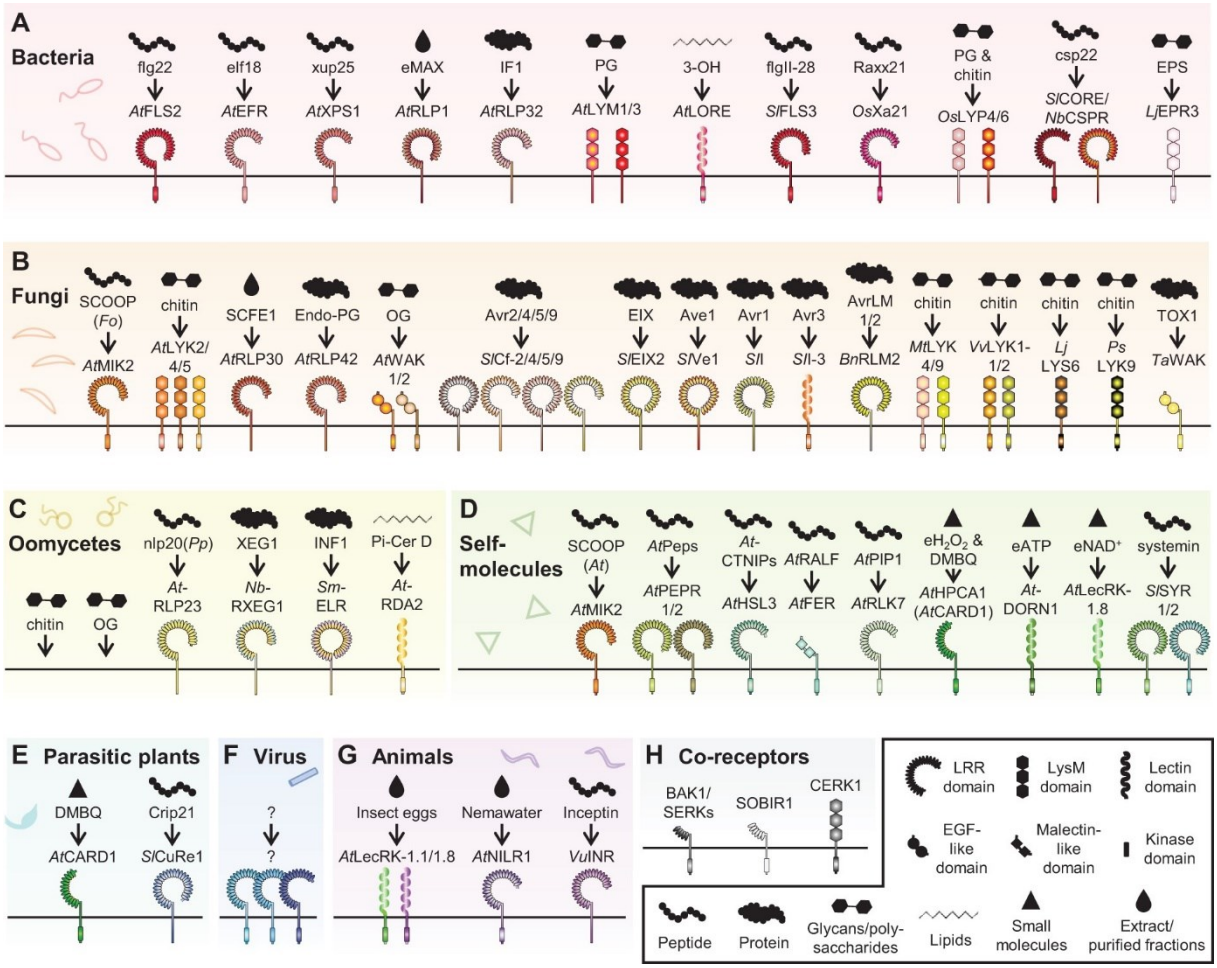

Figure 1.2 Overview of plant PRRs and co-receptors from vascular plants with known elicitors/ligands from bacteria, fungi, oomycetes, self-molecules, parasitic plants, viruses, and herbivores from vascular plants. Abbreviations represent different plant species. Illustration from (Ngou et al., 2022).

1.5 LysM domain; an ancient protein domain

The LysM domain is an ancient protein domain with carbohydrate-binding modules, first identified in the lysozyme of the *Bacillus* bacteriophage phi29, which functions as an enzyme that hydrolyzes bacterial cell walls (Garvey et al., 1986). Subsequent studies have revealed that LysM domain-containing proteins are present across nearly all kingdoms of life, including bacteriophages, bacteria, fungi, and eukaryotes, but are absent in Archaea (Buist et al., 2008). In both bacteria and fungi, the LysM domain-containing proteins often exhibit enzymatic activities

such as glycoside hydrolase, transglycosylase, peptidase, amidase, and chitinase (Akcapinar et al., 2015; Buist et al., 2008).

The LysM domain is a small, non-catalytic globular protein comprising approximately 40–50 amino acids. It exhibits high sequence conservation primarily in the first sixteen amino acids and contains none or only one conserved cysteine residue (Oguiza, 2022). The tertiary structure of the LysM domain typically adopts a βααβ fold, in which both α-helices are packed on the same side of two antiparallel β-sheets. This type of βααβ arrangement is a conserved structural feature of the LysM domain (Bateman & Bycroft, 2000).

Several studies have shown that LysM domains bind the *N-acetylglucosamine* (GlcNAc), a carbohydrate monomer, and can recognize peptidoglycan (PGN) and chitin (Mesnage et al., 2014; Salamaga et al., 2023; Visweswaran et al., 2014). PGN, a key component of the bacterial cell wall, is composed of linear glycan strands made up of alternating GlcNAc and *N-acetylmuramic acid* (MurNAc) residues linked by β-1,4 bonds (Vollmer et al., 2008). The fungal cell wall is composed of polysaccharides such as branched β-(1,3) glucan and chitin, with chitin consisting of linear chains of β-(1,4)-GlcNAc (Gow Neil et al., 2017).

1.6 LysM domain-containing protein in plants: LysM-RLKs/RLPs

LysM-RLKs and LysM-RLPs also play crucial roles in symbiosis (Radutoiu et al., 2003; Radutoiu et al., 2007). LysM-RLKs can be further classified into two subgroups, LYK and LYR, based on the nature of their kinase domains. LYKs possess both *in vitro* and *in vivo* protein phosphorylation activity and contain canonical RD kinase domains. LYR functions as pseudo-kinase, lacking the conserved feature typically found in canonical kinases, such as the glycine-rich loop. The LysM-RLPs are also referred to as LYP (Buendia et al., 2018; Zhang et al., 2007). LysM-RLKs/RLPs typically have three tandem LysM domains in their ECDs. Each LysM is connected by a highly conserved cysteine pair that flanks a single amino acid, forming a CXC motif. This feature was found in all land plants LysM-RLKs/RLPs (Buendia et al., 2018; Lefebvre et al., 2012). LysM receptors in land plants display remarkable diversity. Phylogenetic analyses have shown that the LysM ECDs of land plants LysM receptor homologs form four major classes: LYKa, LYKb, LYR, and LYP (Yotsui et al., 2023). The LysM RLKs/RLPs have been extensively studied genetically, biochemically, and structurally, and the knowledge of LysM-RLKs/RLPs is rapidly advancing.

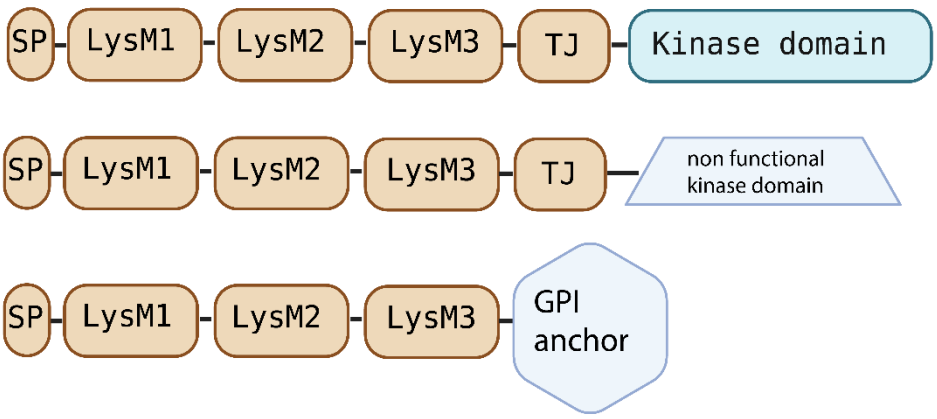

Figure 1.3 Three different types of LysM-RLKs and LysM-RLPs. The receptors comprise an SP (signal peptide), three tandem LysM domains (LysM1–LysM3), forming the ECD, and, in certain receptors, a TJ (transmembrane and juxtamembrane) domain.

In *Arabidopsis thaliana*, there are eight members of LysM-RLKs/RLPs: one LYKa, AtCERK1; one LYKb, AtLYK3; three LYRs, AtLYK2, AtLYK4, and AtLYK5; and three LYPs, AtLYM1, AtLYM2, and AtLYM3. AtCERK1 has been reported to function as a chitin receptor (Liu et al., 2012). The At*cerk1* mutant displays deficiencies in chitin responses, including MAPK activation, ROS production, and transcriptional reprogramming (Miya et al., 2007). Chitin treatment induces autophosphorylations of AtCERK1 at its kinase domain, which is required for downstream signaling (Suzuki et al., 2016). Among its phosphorylation sites, Y428 serves as the "master" regulatory site, dictating interactions with downstream RLCKs for immune activation (Suzuki et al., 2018). In addition to Y428, chitin treatment induced phosphorylation at T519 and Y557, which are required for triggering the ROS burst but not MAPK activation (Liu et al., 2018; Suzuki et al., 2016). Several RLCKs have been shown to interact with AtCERK1, including AtPBL27, which is preferentially phosphorylated by AtCERK1 (Shinya et al., 2014). AtPBL27, in turn, phosphorylates AtMAPKKK5, thereby initiating the activation of the MAPK cascade (AtMAPKKK5–AtMKK4/5–AtMPK3/6) (Yamada et al., 2016). Additionally, AtCERK1 interacts with AtPBL19, which also phosphorylates AtMAPKKK5 to activate the AtMAPKKK5–AtMKK4/5–AtMPK3/6 cascade. Furthermore, AtCERK1-activated AtPBL19 phosphorylates AtMEKK1, leading to activation of the AtMEKK1–AtMKK1/2–AtMPK4 cascade, thereby adding further complexity to the signaling network (Bi et al., 2018). Notably, AtPBL27 does not participate in chitin-induced ROS production. Instead, another RLCK, AtBIK1, which functions downstream of LRR-type PRRs, including AtFLS2, a receptor for the bacterial flagellin-derived peptide flg22, regulates chitin-induced immune responses by directly phosphorylating NADPH

oxidase RBOHD (Kadota et al., 2015). AtLYK5 has also been identified as a chitin receptor, which heterodimerizes with AtCERK1 upon chitin treatment (Cao et al., 2014). The At*lyk5* mutant shows partial defects in chitin-induced responses. AtLYK5 functions redundantly with AtLYK4 in mediating chitin signaling: AtLYK5 regulates the autophosphorylation of AtCERK1, whereas AtLYK4 contributes to ROS production (Mittendorf et al., 2024). There is evidence suggesting that AtLYK4 forms a tripartite complex with AtLYK5 and AtCERK1, acting concertedly in plant defense (Cao et al., 2014; Xue et al., 2019). Chitin binds to the LysM ECDs of both AtCERK1 and AtLYK5 (Cao et al., 2014; Liu et al., 2012). AtLYM1 and AtLYM3, together with AtCERK1, play a role in sensing bacterial PGN, contributing to resistance against bacterial infection (Willmann et al., 2011). AtLYM2, together with AtLYK4 and AtLYK5, regulates plasmodesmata closure as a defense mechanism (Cheval et al., 2020; Faulkner et al., 2013). Besides, AtCERK1 is required for immune responses induced by linear 1,3-β-D-glucans derived from the fungal cell wall (Mélida et al., 2018). Binding of 1,3-β-D-glucans to the ECD of AtCERK1 has not been detected, suggesting that AtCERK1 functions as a co-receptor in this signaling (del Hierro et al., 2021). AtLYK2 is required for chitin- and flg22-induced resistance against *Botrytis cinerea* and *Pseudomonas syringae* infection, even though it is not required for chitin-induced early immune responses (Giovannoni et al., 2021). AtLYK3 is required for nodulation (Nod) factor-induced repression of flg22-triggered immunity (Liang et al., 2013). AtLYK3 also contributes to the crosstalk between plant immunity and abscisic acid responses by negatively regulating basal and early pathogen-induced expression of defense genes as well as abscisic acid-related genes (Paparella et al., 2014).

Rice LYP OsCEBiP (chitin-elicitor binding protein) was the first chitin receptor identified in plants (Kaku et al., 2006). OsCEBiP binds chitin and forms homodimers, playing a key role in signal transduction and the defense responses (Akamatsu et al., 2013; Hayafune et al., 2014; Kaku et al., 2006; Liu et al., 2016). Subsequent studies showed that the rice homolog of AtCERK1, OsCERK1, is recruited to form a heterocomplex upon OsCEBiP homodimerization, highlighting the importance of their cooperative function in regulating chitin signaling in rice (Shimizu et al., 2010). Moreover, OsCERK1 participates in the recognition of short-chain chitin (Xu et al., 2023), which is important for arbuscular mycorrhizal symbiosis (Carotenuto et al., 2017). OsLYK2/OsMYR1 forms a heterodimer with OsCERK1 upon perception of short-chain chitin. The Os*myr1* and Os*cerk1* mutants are less sensitive to the mycorrhizal (Myc) factor, and colonization by symbiotic fungi is disrupted (He et al., 2019). When OsMYR1 perceives short-chain chitin, it prevents complex formation of OsCERK1 between OsCEBiP, thereby inhibiting the phosphorylation of downstream substrates. Two OsCEBiP homologs, OsLYP4 and OsLYP6, have

also been shown to bind chitin and potentially form a complex with OsCERK1. The formation of distinct receptor complexes enables rice to differentiate between symbiotic and immune signals (He et al., 2019). During *Magnaporthe oryzae* infection, secreted endoglucanases degrade the plant cell wall, releasing two glucan oligosaccharides: trisaccharide 3-β-D-Cellobiosyl-glucose and tetrasaccharide 3-β-D-Cellotriosyl-glucose. OsCERK1, but not OsCEBiP, binds these oligosaccharides, triggering heterodimerization of OsCERK1 with OsCEBiP. Both Os*cerk1* and Os*cebip* mutants exhibit compromised responses to these oligosaccharides (Yang et al., 2021). In *A. thaliana* and rice, CERK1 functions as a multifunctional receptor-like kinase in chitin-induced response, with the execution of immune signaling relying on CERK1.

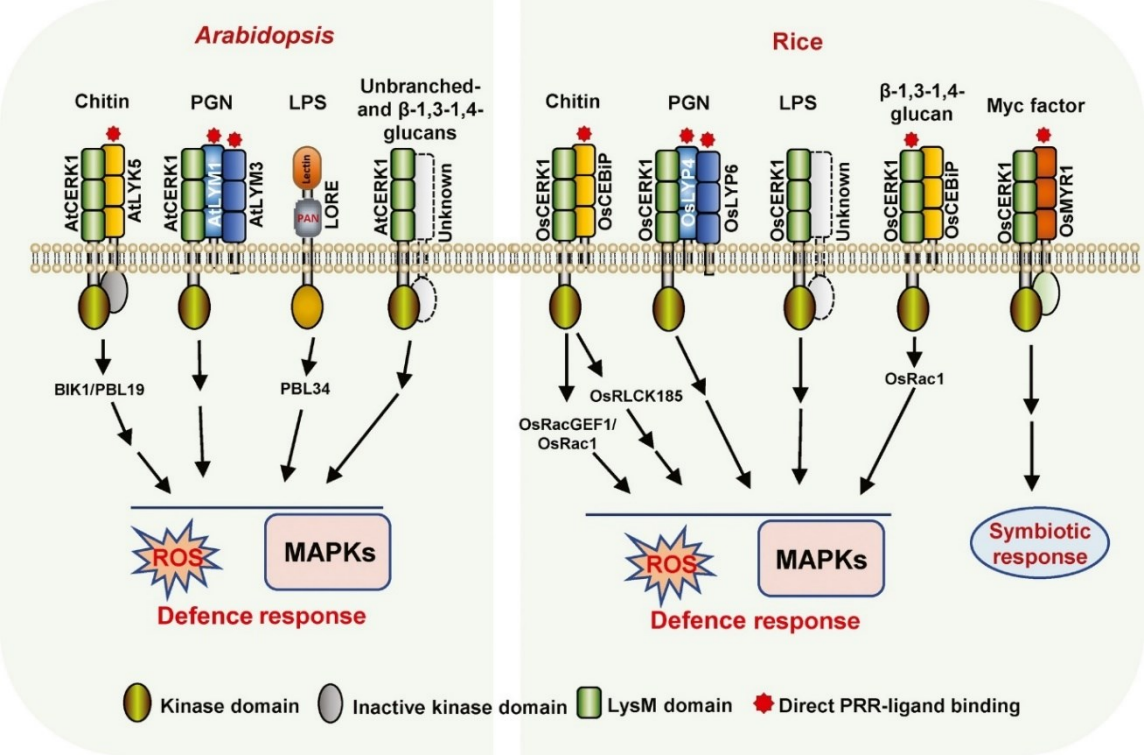

Figure 1.4 The LysM-RLKs/RLP in Arabidopsis and rice perceive different ligands, activating downstream response. Illustration from (Yang et al., 2022).

In *Lotus japonicus*, LYKa LjNFR1 and LYR LjNFR5 are essential for the initiation of nodulation. These receptors recognize lipo-chitooligosaccharides (LCOs), also known as Nod factors, which are secreted by the symbiotic bacterium *Mesorhizobium loti* (Broghammer et al., 2012). Mutations in either Lj*NFR1* or Lj*NFR5* fail to initiate infection thread formation and nodule primordium development following inoculation with *M. loti* or treatment with purified LCOs (Radutoiu et al., 2003). Expression of key symbiotic genes, such as *NIN* and *ENOD2*, is significantly impaired in these mutants upon inoculation. LjNFR1 and LjNFR5 form heterodimers

in vivo, as demonstrated in *Nicotiana benthamiana. In vitro* analyses reveal that LjNFR1 possesses kinase activity, whereas LjNFR5 lacks detectable kinase function (Madsen et al., 2011). Another LYKa LjCERK6/LjLYS6 plays a role in chitin perception and is involved in chitin-triggered ROS production and defense responses. The ECD of LjCERK6 shows high sequence conservation with that of AtCERK1 (Bozsoki et al., 2017), suggesting functional similarity. Interestingly, symbiotic and immune signaling appear to be genetically and functionally separable in *L. japonicus*, highlighting the plant's ability to distinguish between beneficial and pathogenic microbial signals through structurally related LysM-type receptors (Bozsoki et al., 2017).

In the liverwort *Marchantia polymorpha*, the single LYKa MpLYK1 and the single LYR MpLYR are required for chitin- and PGN-induced immune responses (Yotsui et al., 2023). Chitin treatment induces defense-related gene expression and ROS production, both of which are absent in Mp*lyk1* and Mp*lyr* mutants, indicating that MpLYK1 and MpLYR function together to sense chitin to trigger intercellular signaling. MpLYK1 is also critical for defense against bacterial pathogens. Moreover, phosphoproteomic analyses revealed that chitin treatment potentially activates homologs of key PTI components found in *A. thaliana*, including RLCKs, RBOH, and MAPK, suggesting that LysM receptor-mediated signaling mechanisms are conserved in liverworts. The single LYP MpLYP and the single LYKb, MpLYK2 do not appear to be involved in chitin- or PGN-induced ROS production (Yotsui et al., 2023). In *Marchantia paleacea*, which can form symbiosis with arbuscular mycorrhizal (AM) fungi, the single LYKa MpaLYKa, also known as MpaCERK1, and the single MpaLYR are involved in both immunity and symbiosis (Tan et al., 2025). ECD of MpaLYR, but not MpaCERK1, binds both short- and long-chain chitin as well as LCOs *in vitro* (Tan et al., 2025; Teyssier et al., 2025). MpaCERK1 and MpaLYR form a complex in *N. benthamiana*, and their intracellular domains interact in yeast (Tan et al., 2025). Both Mpa*cerk1*and Mpa*lyr* mutants are impaired in chitin- and LCO-induced early responses, similar to observations in *M. polymorpha*. While MpaCERK1 is essential for AM symbiosis, the role of MpaLYR in this process remains debated (Tan et al., 2025; Teyssier et al., 2025).

Taken together, these findings highlight the intricate regulatory architecture of LysM receptor-mediated signaling in land plants. The interplay of multiple kinases and pseudo-kinases, along with differential phosphorylation dynamics and the concurrent ROS production and activation of MAPK pathways, underscores the complexity, redundancy, and specialization of this signaling network. Such sophisticated mechanisms likely played a pivotal role in the adaptive responses required for successful terrestrialization.

1.7 LysM protein structure and ligand recognition

As mentioned earlier, the LysM domain is a highly conserved carbohydrate module that recognizes polysaccharides containing GlcNAc. Structural studies of LysM proteins in complex with their ligands have provided critical insights into the molecular basis of this recognition.

In 2012, Liu et al. reported the crystal structure of the ECD of AtCERK1 in complex with a chitin pentamer (Liu et al., 2012). They provided the first molecular insights into how chitin is recognized by plant LysM-RLK. The AtCERK1 ECD adopts a globular conformation, with three tightly packed LysM domains. Each LysM portrays the canonical βααβ fold that is a conserved feature of LysM domains. The two β strands form an antiparallel β-sheet. The chitin pentamer was observed to bind specifically to the second LysM domain (LysM2), with no conformational changes occurring upon chitin binding. Electron density maps revealed that four of the five GlcNAc residues are anchored within a shallow groove of LysM2 via hydrogen bonds and van der Waals interactions, with specific recognition for the *N-acetyl* moieties of GlcNAc (Liu et al., 2012).

In 2013, Sánchez-Vallet et al. investigated the structural basis of chitin recognition by the LysM effector Ecp6 from the fungal pathogen *Cladosporium fulvum* (Sánchez-Vallet et al., 2013). Their findings revealed that chitin binding in Ecp6 occurs through intrachain dimerization of its LysM domains, which creates a novel chitin-binding groove. The Ecp6 protein contains three LysM domains (LysM1–LysM3), each exhibiting the characteristic βααβ fold that defines the LysM structural family. Interestingly, despite crystallization in the absence of chitin, electron density maps unexpectedly revealed a bound chitin tetramer positioned within a large interdomain groove formed between LysM1 and LysM3. This configuration brings together the two domains to create a deeply embedded chitin-binding site. The tetramer is almost entirely buried within the groove and stabilized by multiple noncovalent interactions, including extensive hydrogen bonding. This unique binding mode represents a previously uncharacterized LysM-mediated carbohydrate recognition mechanism.

In 2016, Liu et al. further advanced our understanding of LysM–chitin interactions by solving the crystal structure of the ECD of OsCEBiP, both free and bound to chitin (Liu et al., 2016). Like AtCERK1, the three LysM domains of OsCEBiP are tightly packed together and each adopts the conserved βααβ fold. Notably, their analysis showed that chitin binding was restricted to the LysM2. Electron density maps showed that three of the four GlcNAc residues in the chitin tetramer were resolved, appearing to be sandwiched between two surface loops of LysM2, stabilized by a network of hydrogen bonds and van der Waals interactions. These findings support

a conserved mechanism for oligomeric GlcNAc recognition by LysM-containing proteins and highlight amino acid conservation at key ligand-binding sites

LysM domains are not limited to recognizing chitin; they also exhibit binding affinity for PGN, a key component of bacterial cell walls. A notable example is the multimodular LysM domain from AtIA, an autolysin produced by *Enterococcus faecalis* (Mesnage et al., 2014). Structural studies of this bacterial protein have elucidated the molecular basis of LysM–PGN interactions. Specifically, the LysM domain was shown to recognize GlcNAc–X–GlcNAc motifs, where X can be either another GlcNAc or MurNAc. The study further demonstrated that ligand specificity, such as the ability to distinguish between PGN, chitin, and Nod factors, is influenced not only by carbohydrate composition but also by the surrounding secondary structure of the LysM domain.

In summary, these findings suggest that subtle structural adaptations within the LysM scaffold contribute to its functional diversity, enabling selective recognition of chemically similar glycans across diverse biological contexts.

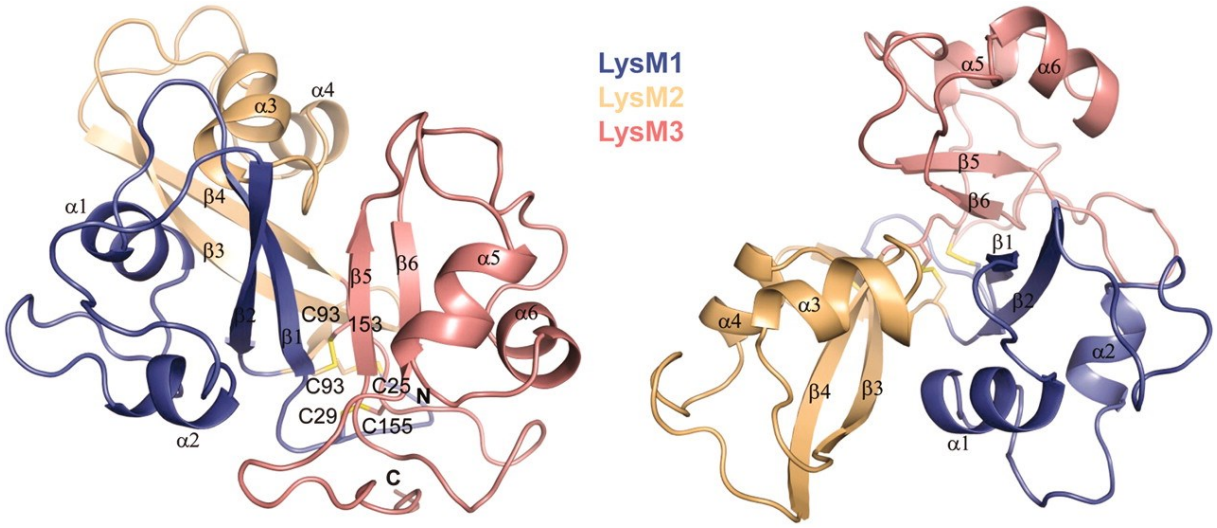

Figure 1.5 Structure of the AtCERK1 ECD presented in ribbon form in two orientations. Each LysM domain was presented as βααβ fold and colored differently. PDB for AtCERK1 is 4EBZ. Illustration is from (Liu et al., 2012).

1.8 Origin and evolution of LysM receptors

The advancement of sequencing technology has opened new avenues for evolutionary research, providing valuable insights from genome sequences. Comparative genomics and phylogenomics have shed light on the evolution of PRRs. In the case of LysM receptors, multiple studies have proposed different origins. Ngou et al. (2024) proposed that the LysM-RLKs originated from the last common ancestor of land plants, whereas LysM-RLPs have emerged earlier during the evolution of Archaeplastida (Ngou et al., 2024). However, a previous study showed that the streptophyte algae *Chara braunii* encodes LysM receptors, referred to as CbLYKs (Nishiyama et al., 2018) . This observation has led to the hypothesis that the last common ancestor of land plants was already equipped with a LysM receptor, which may have originated from a streptophyte algae LysM receptor (Delaux et al., 2015; Delaux & Schornack, 2021).

Scope of thesis

Plant-microbe interactions have played a crucial role in the evolution and stability of terrestrial ecosystems for over 450 million years, influencing both plant physiology and ecological dynamics. These interactions include mutualistic symbioses, such as those formed with nitrogen-fixing bacteria and mycorrhizal fungi, as well as pathogenic relationships that have driven the evolution of plant defense mechanisms. Despite extensive research on land plants, significant gaps remain in our understanding of the origin, diversification, and functional roles of LysM receptors in the plant-microbe interactions within streptophyte algae.

This dissertation aims to address the following key questions:

1. What is the evolutionary origin of plant LysM receptors, and what was their ancestral role?
2. What is the functional role of LysM-RLKs in streptophyte algae?
3. How did LysM receptors diversify and evolve functionally to assume essential roles in plant–microbe interactions in land plants?

By integrating phylogenetic, transcriptomic, proteomic, and biochemical analyses, this dissertation provides an evolutionary perspective on LysM-mediated signaling across the plant lineage.

2. Result

2.1 Plant LysM receptors originated in the last common ancestor (LCA) of Charophyceae, Zygnematophyceae, and land plants

Previous studies have discussed the origin of plant LysM-RLKs and LysM-RLPs (Delaux et al., 2015; Ngou et al., 2024; Yotsui et al., 2023). However, the available information remains fragmented, making it difficult to trace the origin of LysM-RLKs/RLPs. To address this, I analyzed publicly available genome and transcriptome datasets from thirty species spanning rhodophytes, chlorophytes, streptophyte algae, bryophytes, and tracheophytes. The datasets comprised one rhodophytes (*Chondrus crispus*), two chlorophytes (*Volvox carteri* and *Chlamydomonas reinhardtii*), twelve streptophyte algae (*Chlorokybus atmophyticus*, *Mesostigma viride*, *Nitella mirabilis*, *Klebsormidium nitens*, *Chara braunii*, *Penium margaritaceum*, *Spirogyra pratensis*, *Mougeotia sp., Zygnema circumcarinatum*, *Mesotaenium endlicherianum*, *Mougeotiopsis calospora,* and *Spirogloea muscicola*), and fifteen land plants. The land plant set includes two mosses (*Sphagnum fallax* and *Physcomitrium patens*), two liverworts (*Ricciocarpos natans* and *Marchantia polymorpha*), two hornworts (*Anthoceros punctatus* and *Anthoceros agrestis*), one lycophyte (*Selaginella moellendorffii*), and eight spermatophytes comprising gymnosperms and angiosperms (*Azolla filiculoides*, *Amborella trichopoda*, *Oryza sativa*, *Cuscuta campestris*, *Cuscuta australis*, *Arabidopsis thaliana*, *Lotus japonicus*, and *Medicago truncatula*). The surveyed species were illustrated in a cladogram depicting their species-level evolutionary relationship. (Figure 2.1 A). LysM-receptors were defined according to the following criteria. First, they must contain three LysM domains, each linked by two cysteine residues flanked by variable amino acids, forming the characteristic CXC motif. Second, LysM-RLKs must possess a transmembrane domain and an intercellular kinase domain.

Consistent with previous reports, all land plants analyzed in this study were found to encode LysM-RLKs. In contrast, no LysM-RLKs were identified in rhodophytes, commonly known as red algae, or chlorophytes. Among streptophyte algae, the presence of LysM-RLKs varied, with some species encoding them while others did not (Figure 2.1 A). Members of Charophyceae, including *C. braunii* and *N. mirabilis*, were found to encode LysM-RLKs. Within Zygnematophyceae, the closest algal sister lineage to land plants, only a few species encoded LysM-RLKs, including *S. pratensis* and *Mougeotia sp*. (Figure 2.1 A). LysM proteins with CXC motifs were also identified in *M. endlicherianum* and *M. calospora*; however, these proteins lacked an entire intracellular

kinase domain, indicating that they do not qualify as true or functional LysM-RLKs (Figure 2.1 A).

To investigate the phylogenetic relationships among LysM receptors, a phylogenetic tree was constructed using the ECDs of LysM receptors. Consistent with previous reports, ECDs of LysM receptors from land plants clustered into four major groups: LYKa, LYKb, LYR, and LYP. Interestingly, the ECDs of streptophyte algae LysM-RLKs did not form a single monophyletic group but were instead distributed across several distinct clades (Figure 2.2 B). The ECD of LysM receptors is characterized by the conserved CXC motif, and alignment analysis of the LysM ECDs of streptophyte algae LysM-RLKs, compared with representative ECDs from land plant LysM-RLKs, revealed a high level of conservation in this motif, similar to that observed in land plants (Figure 2.1 C). Collectively, these data suggest that LysM receptors evolved from a common ancestor shared by Charophyceae, Zygnematophyceae, and land plants, and may have been lost in certain species of streptophyte algae. The loss of LysM receptors in certain species may reflect adaptations to specific environmental habitats.

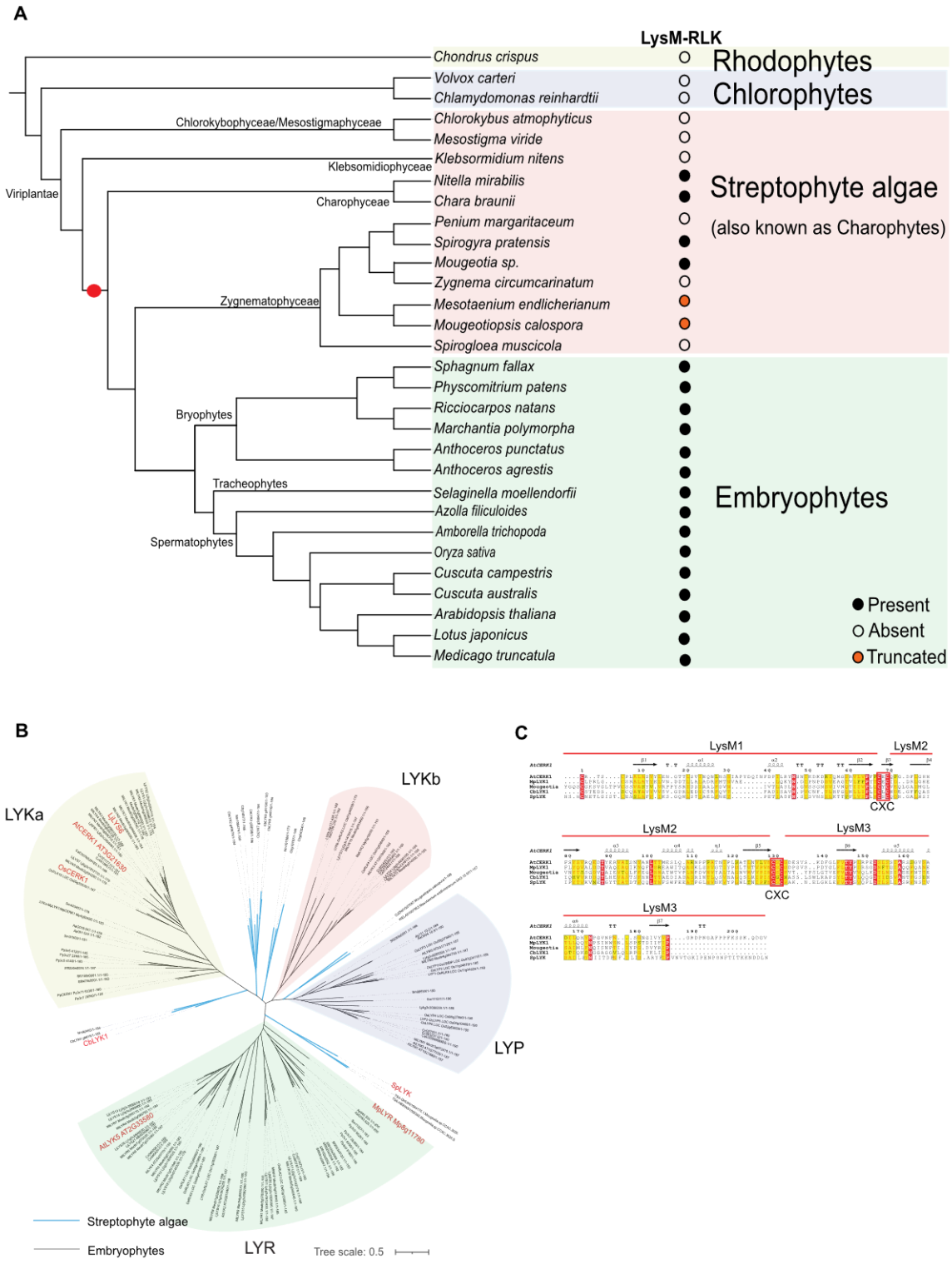
A
LysM-RLK
Chondrus crispus
Volvox carteri
Chlamydomonas reinhardtii
Chlorokybophyceae/Mesostigmaphyceae
Chlorokybus atmophyticus
Mesostigma viride
Klebsormidiophyceae
Klebsormidium nitens
Viriplantae
Nitella mirabilis
Charophyceae
Chara braunii
Penium margaritaceum
Spirogyra pratensis
Mougeotia sp.
Zygnema circumcarinatum
Zygnematophyceae
Mesotaenium endlicherianum
Mougeotiopsis calospora
Spirogloea muscicola
Sphagnum fallax
Physcomitrium patens
Bryophytes
Ricciocarpos natans
Marchantia polymorpha
Anthoceros punctatus
Anthoceros agrestis
Tracheophytes
Selaginella moellendorfii
Azolla filiculoides
Spermatophytes
Amborella trichopoda
Oryza sativa
Cuscuta campestris
Cuscuta australis
Arabidopsis thaliana
Lotus japonicus
Medicago truncatula
Rhodophytes
Chlorophytes
Streptophyte algae
(also known as Charophytes)
Embryophytes
Present
Absent
Truncated
B
LYKa
LYKb
LYP
LYR
AtCERK1 AT3G21630
OsCERK1
CbLYK1
SpLYK
MpLYR Mp8g11780
AtLYK5 AT2G33580
Streptophyte algae
Embryophytes
Tree scale: 0.5
C
LysM1
LysM2
LysM3
CXC
CXC

Figure 2.1 Origin and evolution of LysM-RLKs.
(A) LysM-RLKs in thirty species ranging from rhodophytes, chlorophytes, streptophyte algae and land plants. **(B)** Unroot phylogenetic tree of the ECD of LysM receptors showing that land plants ECD of (gray) were clustered into four major clades and LysM streptophyte algae ECDs (blue) were clustered into several distinct clades. Tree scale = 0.5 **(C)** The architecture of the LysM ECDs in representative streptophyte algae, compared with land plants LysM ECDs represented by AtCERK1 (*A. thaliana*) and MpLYK1 (*M. polymorpha*) shows a conserved CXC motif in the sequence alignment.

2.2 Features of LysM-RLK in Charophyceae *C. braunii* and Zygnematophyceae *S. pratensis*

A previous study identified seven LysM-RLKs in *C. braunii*, designated as CbLYKs (Nishiyama et al., 2018). In addition, the single LysM-RLK was found in *S. pratensis*, referred to as SpLYK (unpublished, full-length coding-sequence (CDS) information provided by Prof. Dr. Jan de Vries, Georg-August-University Goettingen). This study focuses on characterizing the functions of LysM-RLKs from both species. All seven LysM-RLKs identified in *C. braunii* and SpLYK contain the conserved CXC motif (Figure 2.2 A).

A detailed assessment of the kinase domain showed that only CbLYK1 and SpLYK contain an unmodified glycine-rich P-loop (GXGXF or GXGXYG motif), a catalytic loop with the HRD motif, and a magnesium-binding DFG motif (Figure 2.2 B). The kinase domains of other LYKs in *C. braunii* are defective in at least one of these features, suggesting they may have limited or no kinase activity; however, the possibility of residual activity cannot be excluded. Based on these findings, CbLYK1 and SpLYK were selected for further characterization due to their potential kinase activities and their ability to activate downstream signaling events. First, we generated transgenic *M. polymorpha* lines overexpressing CbLYK1 and SpLYK. CbLYK1 and SpLYK were fused to mCitrine at the C-terminus and expressed under the constitutive MpEF1α promoter. However, in the transgenic lines, the fluorescence of both CbLYK1- and SpLYK-mCitrine fusion proteins could not be detected by confocal microscopy. A key feature of LysM-RLKs is their localization to the plasma membrane. The lack of detectable fluorescence raised questions about the potential incompatibility of the signal peptides and whether the fusion proteins can localize at the plasma membrane in the heterologous system. To investigate whether charophyte LysM-RLKs contain signal peptide sequences indicative of the plasma membrane localization, I analyzed their sequences using SignalP 6.0 (Teufel et al., 2022). Based on published annotations, only CbLYK3 and CbLYK6 were predicted to contain signal peptides (Figure 2.2A). However, I observed that the remaining LysM-RLKs possess atypical N-terminal extensions. Therefore, I hypothesized that

the original annotations may have misidentified the translation start codons. To address this, I searched for downstream methionine residues that could serve as alternative start sites. As a result, alternative start codons were identified for CbLYK1, CbLYK4, and CbLYK7, leading to the prediction of signal peptides in these proteins as well (Figure 2.2A). Besides, SpLYK was predicted to contain a signal peptide (Figure 2.2 A). These findings support the potential for CbLYK1, CbLYK3, CbLYK4, CbLYK6, CbLYK7, and SpLYK to function as receptors at the plasma membrane.

To investigate the subcellular localization of CbLYK1, with the alternative start codon predicting a signal peptide, and SpLYK, I transiently expressed them in *Nicotiana benthamiana* leaves via *Agrobacterium*-mediated infiltration. CbLYK1 and SpLYK were fused to green fluorescent protein (GFP) at their C-termini and expressed under β-estradiol-inducible CaMV35S promoter. This time, I observed fluorescence from the CbLYK1-GFP fusion protein, which localized to the plasma membrane in *N. benthamiana* leaf cells (Figure 2.2 C). In contrast, no fluorescence signal was detected for the SpLYK-GFP fusion protein, consistent with our previous observation in *M. polymorpha*. I hypothesized that the absence of fluorescence from SpLYK-GFP may result from incompatibility between its native signal peptide and the *N. benthamiana* cellular machinery. To test this, I generated a modified version of SpLYK in which its native signal peptide was replaced with the signal peptide from MpLYK1. This chimeric construct named mSpLYK, was expressed under the same promoter and fused to GFP at the C-terminus. Interestingly, expression of mSpLYK in *N. benthamiana* resulted in GFP fluorescence at the plasma membrane (Figure 2.2C). These results suggest that while CbLYK1 is efficiently targeted to the plasma membrane, the native signal peptide of SpLYK may prevent proper translation or localization in *N. benthamiana* and *M. polymorpha.* For simplicity, the modified CbLYK1 and SpLYK constructs retained their original names and were used in subsequent analyses.

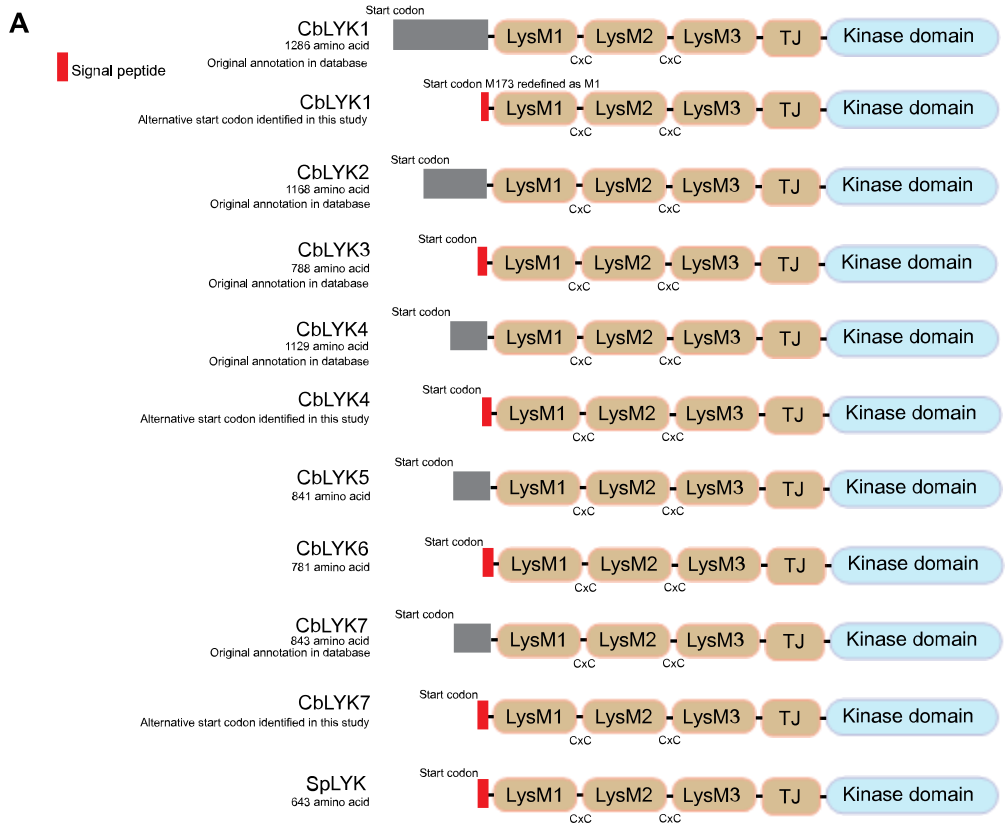
A
Signal peptide
Start codon
CbLYK1
1286 amino acid
Original annotation in database
LysM1
LysM2
LysM3
TJ
Kinase domain
CxC
CxC
Start codon M173 redefined as M1
CbLYK1
Alternative start codon identified in this study
CbLYK2
1168 amino acid
Original annotation in database
CbLYK3
788 amino acid
Original annotation in database
CbLYK4
1129 amino acid
Original annotation in database
CbLYK4
Alternative start codon identified in this study
CbLYK5
841 amino acid
CbLYK6
781 amino acid
CbLYK7
843 amino acid
Original annotation in database
CbLYK7
Alternative start codon identified in this study
SpLYK
643 amino acid

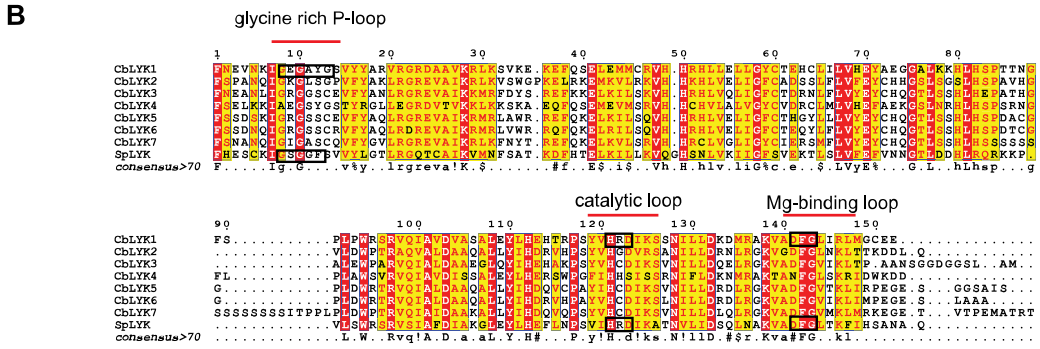
B
glycine rich P-loop
catalytic loop
Mg-binding loop
CbLYK1
CbLYK2
CbLYK3
CbLYK4
CbLYK5
CbLYK6
CbLYK7
SpLYK
consensus>70

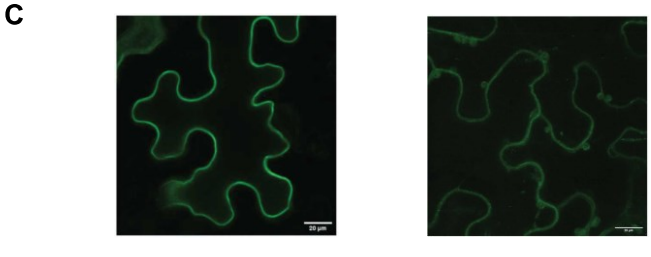
C
CbLYK1-GFP
SpLYK-GFP

Figure 2.2 LysM-RLKs in Charophyceae *C. braunii* and Zygnematophyceae *S. pratensis*. **(A)** Schematic representation of *C. braunii* LysM-RLKs CbLYK1, CbLYK2, CbLYK3, CbLYK4, CbLYK5, CbLYK6, CbLYK7 and *S. pratensis* SpLYK. The protein lengths and predicted signal peptide, determined by SignalP 6.0, for both the original annotations and alternative start codons are shown. **(B)** Alignment of the kinase domain of CbLYK1–CbLYK7 and SpLYK. The glycine-rich P-loop, catalytic loop, and Mg-binding loop are indicated. Only CbLYK1 and SpLYK retain an unmodified P-loop, HRD motif, and DFG motif, with the relevant amino acids highlighted in black boxes. **(C)** Subcellular localization of CbLYK1 and SpLYK in *N. benthamiana*. Scale bar: 20 μm.

2.3 LysM ECDs exhibit structural conservation, including the chitin-binding groove in LysM2

Structural analyses have demonstrated that chitin binds directly to the second LysM domain (LysM2) of AtCERK1 (Liu et al., 2012). Based on the knowledge, I used AlphaFold2 to investigate the structural conservation of the ECDs of LysM receptors across different plant lineages. I have predicted structures of *M. polymorpha* MpLYK1 and MpLYR, both of which are genetically required for chitin-induced responses (Yotsui et al., 2023), *A. thaliana* AtLYK5, *C. braunii* CbLYK1, and *S. pratensis* SpLYK. Structural comparisons were conducted against the crystal structure of the AtCERK1 ECD (PDB: 4EBZ).

In-silico analysis showed that all predicted ECDs adopt the conserved βααβ fold in each LysM domain (Figure 2.3 A, Supplemental Figure 1), consistent with previously reported structures. As previously observed in AtCERK1, chitin binding occurs in the LysM2. Manual modelling of chitin into the predicted structures of AtLYK5, MpLYK1, MpLYR, CbLYK1, and SpLYK revealed a conserved shallow binding groove in the LysM2, resembling the known chitin-binding interface of AtCERK1 (Figure 2.3 B). Comparison of the chitin-binding interface of LysM2 between AtCERK1 and the other LysM-RLKs showed high similarities in Region A and Region B, although slight variations were observed in Region B of AtLYK5 (Figure 2.3 C). In Region A, despite minor differences in amino acid sequence alignment, the position of conserved residues within the secondary structure was maintained (Figure 2.3 C). In Region B, hydrophobic residues such as valine, leucine, and isoleucine are conserved, potentially mediating interactions with the chitin molecule (Figure 2.3 D and E). Moreover, the manual modelling analysis indicated possible hydrogen bonds between chitin and residues in the LysM2 binding groove in AtLYK5, MpLYK1, MpLYR, CbLYK1, and SpLYK (Figure 2.3 E). Overall, these structural models suggest a high structural conservation of LysM ECDs across *A. thaliana*, streptophyte algae, and *M.*

polymorpha. The presence of the chitin-binding groove further suggests the potential of charophyte LysM-RLKs to bind chitin.

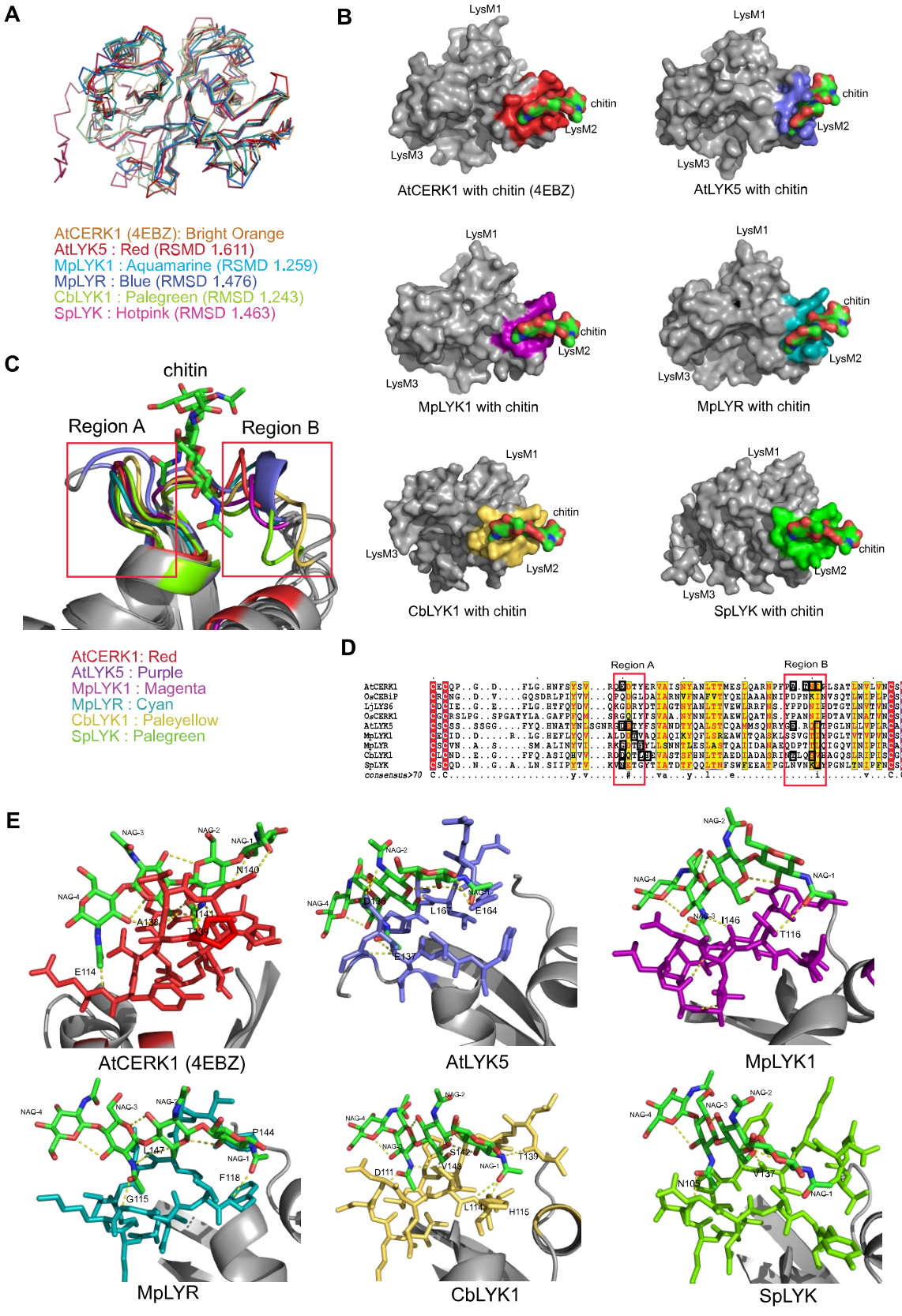
A
AtCERK1 (4EBZ): Bright Orange
AtLYK5 : Red (RSMD 1.611)
MpLYK1 : Aquamarine (RSMD 1.259)
MpLYR : Blue (RMSD 1.476)
CbLYK1 : Palegreen (RMSD 1.243)
SpLYK : Hotpink (RMSD 1.463)
B
LysM1
LysM2
LysM3
chitin
AtCERK1 with chitin (4EBZ)
AtLYK5 with chitin
MpLYK1 with chitin
MpLYR with chitin
CbLYK1 with chitin
SpLYK with chitin
C
chitin
Region A
Region B
AtCERK1: Red
AtLYK5 : Purple
MpLYK1 : Magenta
MpLYR : Cyan
CbLYK1 : Paleyellow
SpLYK : Palegreen
D
Region A
Region B
AtCERK1
OsCEBiP
LjLYS6
OsCERK1
AtLYK5
MpLYK1
MpLYR
CbLYK1
SpLYK
consensus>70
E
NAG-1
NAG-2
NAG-3
NAG-4
N140
A138
I111
T139
E114
AtCERK1 (4EBZ)
D135
L161
E164
E137
AtLYK5
I146
T116
MpLYK1
P144
L147
F118
G115
MpLYR
S142
V146
T139
D111
L114
H115
CbLYK1
N105
V137
SpLYK

Figure 2.3 Structures of LysM ECDs predicted by AlphaFold2 and modeling of potential chitin-binding groove within LysM2 domain.
(A) Structural superposition of the LysM ECDs of AtCERK1, AtLYK5, MpLYK1, MpLYR, CbLYK1, and SpLYK with the corresponding RMSD values indicated. **(B)** The presence of the chitin-binding groove in the LysM2 domain of the AtcERK1 ECD (PDB:4EBZ) was revealed by (Liu et al., 2012). Manual modelling of the chitin molecule was performed on AlphaFold2 models of AtLYK5, MpLYK1, MpLYR, CbLYK1, and SpLYK. The chitin-binding groove was highlighted in different colors for identification. Structures are shown in surface form. **(C)** Close-up representation of the structural superposition of all the LysM domains, focused on the chitin-binding groove at the LysM2 domain, with Region A and Region B indicated. The colors corresponding to each ECD are also indicated. **(D)** Sequence alignment of the LysM2 domain with the chitin-binding groove of Region A and Region B is highlighted in red boxes. **(E)** Potential hydrogen bonds (shown in yellow) between chitin (bicolor red/green stick) and the LysM ECDs of AtLYK5, MpLYK1, MpLYR, CbLYK1, and SpLYK. Amino acids that are potentially involved in hydrogen bond formation are labeled for each protein and were highlighted with black boxes in panel D.

2.4 ECDs of LysM receptor homologs from bryophytes and algae exhibit chitin-binding activity *in vitro*

To evaluate the chitin-binding capacity of LysM receptor ECDs, I performed a microscale thermophoresis (MST) binding assay. Chitin heptamer, a long-chain chitin that functions as MAMP, was used as a ligand. I prepared histidine-tagged ECDs of LysM receptors, *M. polymorpha* MpLYK1 and MpLYR, *C. braunii* CbLYK1, and *S. pratensis* SpLYK, along with *A. thaliana* AtCERK1 and AtLYK5 as positive controls (Liu et al., 2012; Cao et al., 2014). Recombinant proteins were expressed in insect cells, purified, and fluorescently labeled prior to MST analysis (Figure 2.4 A). Binding was assessed using increasing concentrations of chitin heptamer, and dissociation constants (Kd) were calculated from the binding curves. All tested ECDs exhibited chitin-binding activity, although with varying affinities. The observed Kd ranged widely: 154 µM ± 90 µM for AtCERK1, 208 µM ± 60 µM for AtLYK5, 626 µM ± 801 µM for MpLYK1, 395 µM ± 291 µM for MpLYR, 290 µM ± 300 µM for CbLYK1, and 939 µM ± 400 µM for SpLYK (Figure 2.4 B to G). Consistent with previous reports, the positive controls AtCERK1 and AtLYK5 displayed chitin-binding activity. These data suggest that the ECDs of LysM receptor homologs from bryophytes and streptophyte algae can directly bind chitin, and the observed differences in

affinity may be attributed to variations in amino acids residue within the chitin-binding groove in LysM2.

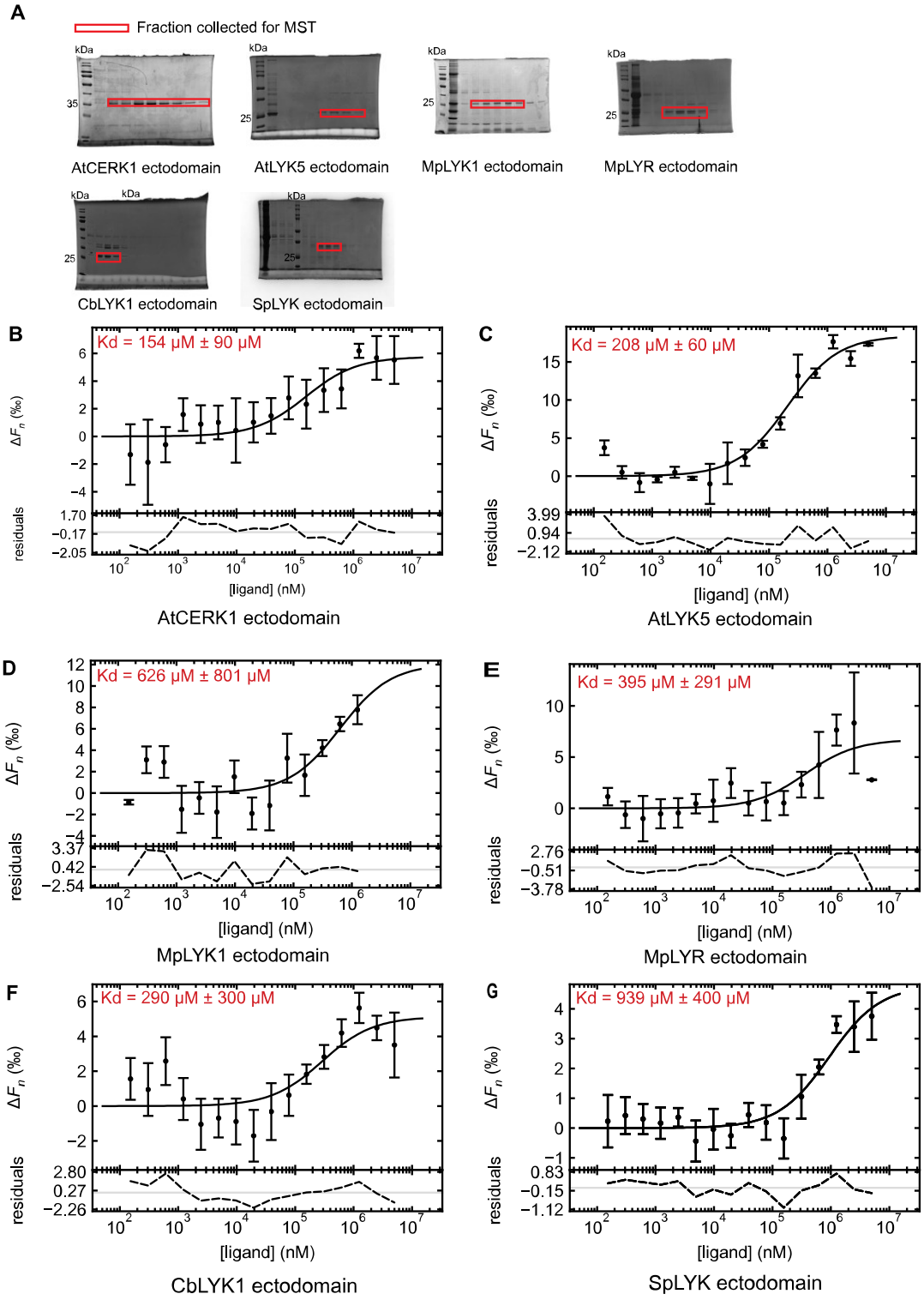

Figure 2.4 LysM ECDs purified from insect cells and MST binding curves.
(A) SDS-PAGE gel images showing the purified ECDs of AtCERK1, AtLYK5, MpLYK1, MpLYR, CbLYK1, and SpLYK purified from insect cell expression, along with the protein fractions used for the MST assay. **(B)** Binding curve of the AtCERK1 ECD with chitin heptamer obtained by MST, used to calculate the Kd value, Kd value was 154 ± 90 μM. **(C)** Binding curve of the AtLYK5 ECD with chitin heptamer obtained by MST, used to calculate the Kd value, Kd value was 208 ± 60 μM. **(D)** Binding curve of the MpLYK1 ECD with chitin heptamer obtained by MST, used to calculate the Kd value, Kd value was 626 ± 801 μM. **(E)** Binding curve of the MpLYR ECD with chitin heptamer obtained by MST, used to calculate the Kd value, Kd value was 395 ± 291 μM. **(F)** Binding curve of the CbLYK1 ECD with chitin heptamer obtained by MST, used to calculate the Kd value, Kd value was 290 ± 300 μM. **(G)** Binding curve of the SpLYK ECD with chitin heptamer obtained by MST, used to calculate the Kd value, Kd value was 939 ± 400 μM. The change in fluorescence in a thermal gradient (△Fn) as a function of ligand concentration are plotted for each LysM ECD. The MST experiment were performed three times (n=3, error bars indicate SD).

2.5 Chitin bead pull-down from protein extracts, followed by mass-spectrometry (MS), identified LysM receptor homologs in land plants but not in algae

To confirm the chitin-binding activity of the LysM ECDs observed in the MST analysis, I performed an affinity pull-down assay followed by MS. Chitin beads containing long-chain chitin polymers were used to selectively enrich chitin-binding proteins from total protein extracts. Affinity pull-downs were carried out using total protein extracts from *A. thaliana*, *M. polymorpha*, *S. pratensis*, and *M. endlicherianum*. *Chara braunii* was excluded from this analysis due to the difficulty of obtaining sufficient tissue for total protein extraction, whereas *M. endlicherianum* was included because of the potential presence of a truncated LysM receptor. In *A. thaliana*, MS analysis identified known chitin-binding LysM receptors, including AtCERK1, AtLYK5, AtLYK4, and AtLYM2, thereby confirming the validity of the assay (Figure 2.5 A). In *M. polymorpha*, MpLYR and MpLYP were identified, whereas MpLYK1 was not (Figure 2.5 B). Meanwhile, SpLYK was not recovered from the *S. pratensis* extract, and no LysM receptor homologs were identified in the *M. endlicherianum* extract (Figure 2.5 C and D). The successful identification of known LysM receptors in *A. thaliana* demonstrated the robustness of the chitin bead pull-down MS approach for studying LysM receptors in plants. The absence of MpLYK1 and SpLYK in the pull-down assay is likely due to either low protein abundance in the total extracts or

relatively weak chitin-binding affinity (Figure 2.4 D and G), which may have limited their enrichment by chitin beads.

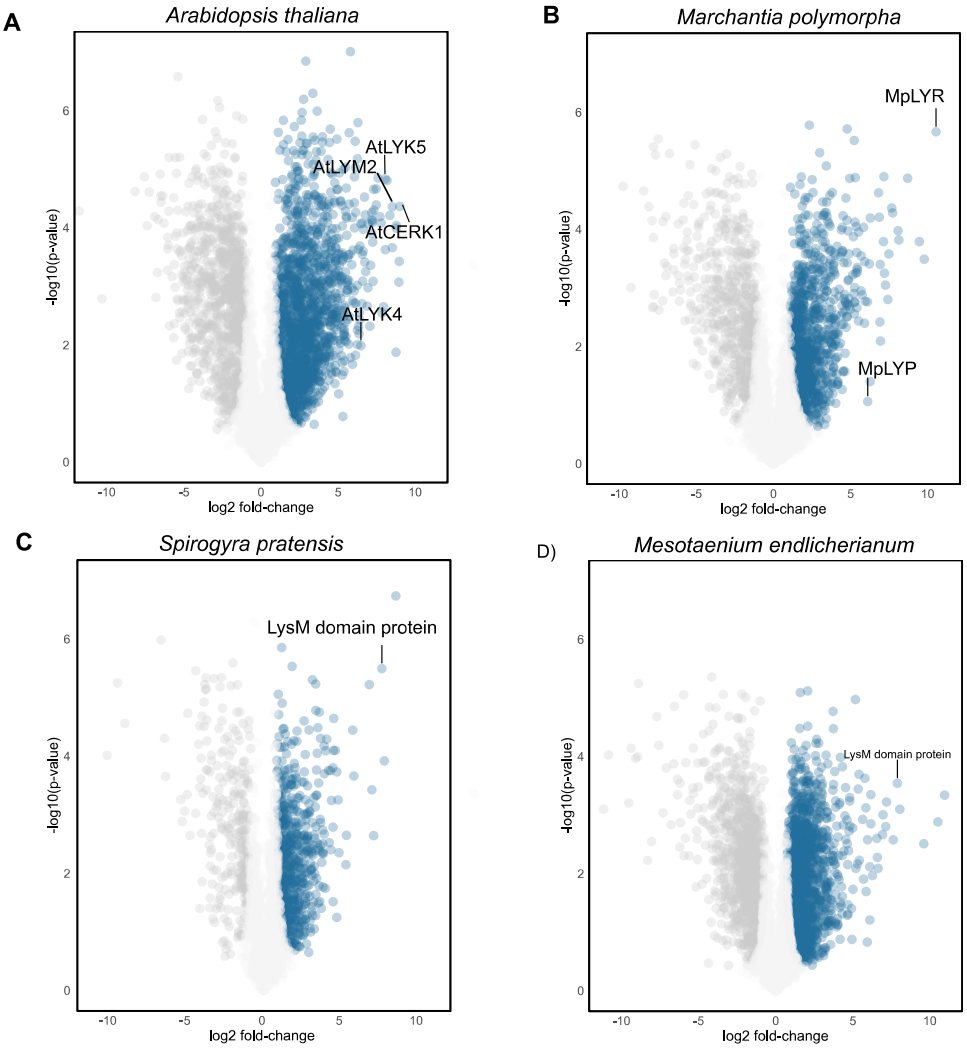

Figure 2.5 LysM receptors identified by chitin bead pull-down followed by MS analysis in *A. thaliana*, *M. polymorpha*, *S. pratensis*, and *M. endlicherianum*.
(A) Proteins significantly enriched by chitin bead pull-down in *A. thaliana* are labeled in blue. Three biological replicates were used for analysis. (**B)** Proteins significantly enriched by chitin bead pull-down in *M. polymorpha* are labeled in blue. Three biological replicates were used for analysis. **(C)** Proteins significantly enriched by chitin bead pull-down in *S. pratensis* were labeled in blue. Three biological replicates were used for analysis. **(D)** Proteins significantly enriched by chitin bead pull-down in *M. endlicherianum* were labeled with blue. Two biological replicates were used for analysis.

2.6 Charophyceae *C. braunii* and Zygnematophyceae *S. pratensis* do not respond to chitin

Previous studies have demonstrated that a wide range of land plants recognize chitin via LysM receptors, triggering immune responses such as ROS burst and transcriptional reprogramming. To investigate whether streptophyte algae can sense chitin, I treated *C. braunii* and *S. pratensis* with chitin heptamer and monitored their responses. First, I measured ROS production following chitin exposure. As a positive control *M. polymorpha* Tak-1, exhibited a clear ROS burst following chitin treatment. In contrast, neither *C. braunii* nor *S. pratensis* showed detectable ROS production under the tested conditions (Figure 2.6 A and 2.6 C). Next, I performed RNA sequencing analysis to assess transcriptional responses. *Chara braunii* was treated with chitin heptamer or mock for one hour (with the help of Prof. Keiko Sakakibara at Rikkyo University), while *S. pratensis* was treated for one, three, and twenty-four hours. Principal component analysis (PCA) of global gene expression profiles did not separate chitin-treated samples from mock-treated samples (Figure 2.6 B and 2.6 D). Furthermore, no differentially expressed genes (DEGs) were detected between chitin and mock treatments in either species. These results indicate that chitin does not induce transcriptional reprogramming in these algal species. Taken together, these data suggest that *C. braunii* and *S. pratensis* may not recognize chitin to activate downstream signaling, despite encoding LysM-RLKs in their genomes whose ECDs exhibit chitin-binding activity.

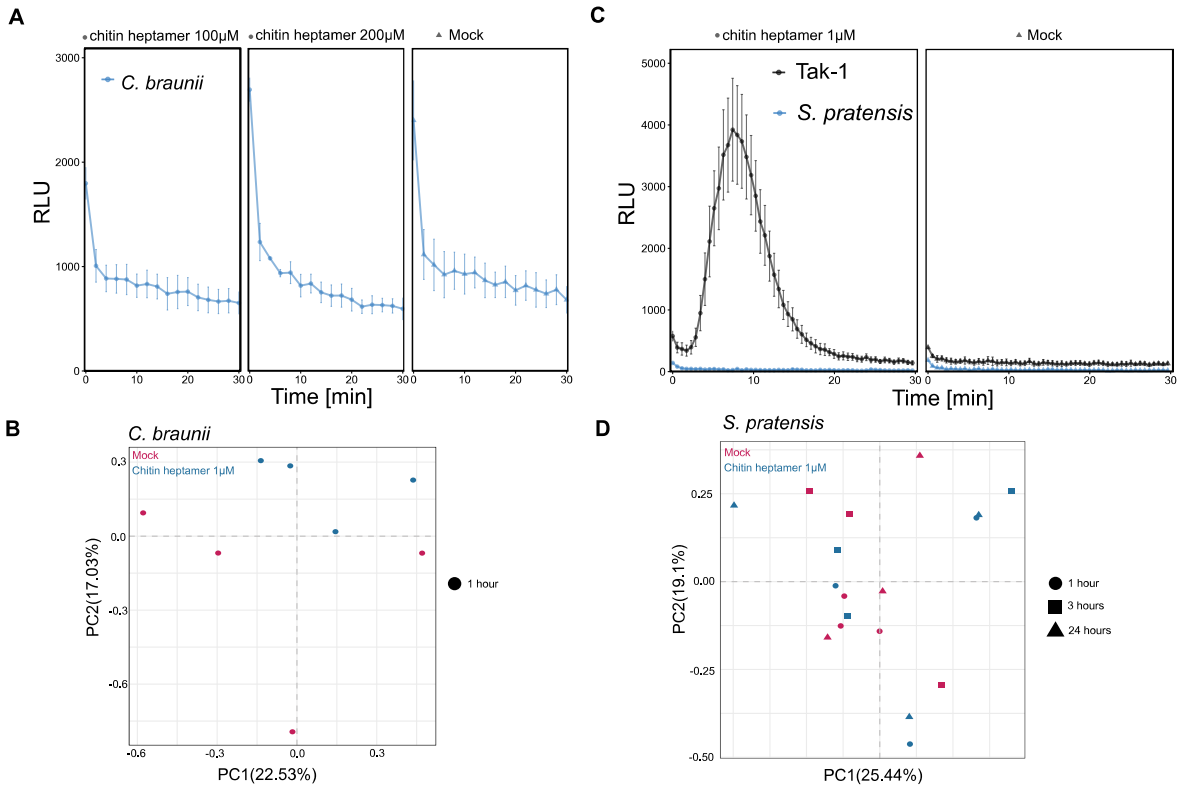

Figure 2.6 Response of *C. braunii* and *S. pratensis* to chitin treatment.
(A) ROS measurement of *C. braunii* treated with mock, 100 μM chitin heptamer, or 200 μM chitin heptamer. Measurements were performed at least two times. **(B)** PCA of RNA-sequencing data from *C. braunii* treated with mock and 1 μM chitin heptamer. Data were from four biological replicates. **(C)** ROS measurement of *S. pratensis* treated with mock, or 1 μM chitin heptamer. Seven-day-old *M. polymorpha* Tak-1 gemmae were used as a positive control. Measurements were performed at least two times. **D** PCA of RNA-sequencing data from *S. pratensis* treated with mock or 1 μM chitin heptamer. Data were from three biological replicates.

2.7 Species-specific LysM ECD is required for a chitin response in *M. polymorpha*

A previous study showed that MpLYK1 is required for chitin-induced responses, as Mp*lyk1* mutants fail to trigger a ROS burst upon chitin treatment (Yotsui et al., 2023). To assess the chitin-sensing capabilities of ECDs from different species in the context of chitin-induced responses, I employed a trans-species domain-swapping complementation approach in Mp*lyk1*. A full-length trans-species complementation, which includes the intracellular kinase domain, was not performed because the downstream signaling targets of the kinase domain are likely to be species-specific. I generated chimera constructs by replacing the ECD of MpLYK1 with that of AtCERK1, CbLYK1, or SpLYK, and fused each to mCitrine at their C-terminus. (Figure 2.7 A). These chimeric proteins were expressed under the constitutive MpEF1α promoter. Confocal microscopy confirmed that all

domain-swapped fusion proteins were expressed and correctly localized to the plasma membrane, similar to MpLYK1-mCitrine (Figure 2.7 B). For ROS burst measurements, wild-type Tak-1 was used as a positive control. The expression of MpLYK1-mCitrine in the Mp*lyk1* restored the chitin-induced ROS burst (Figure 2.7 C). In contrast, the transgenic plants expressing the chimeric receptors did not exhibit a ROS burst in response to chitin treatment (Figure 2.7 C). These results indicate that, although chitin-binding ability may be conserved, replacing the MpLYK1 ectodomain with those from other species is insufficient to restore downstream immune signaling, suggesting that species-specific LysM receptor complex is critical in *M. polymorpha*.

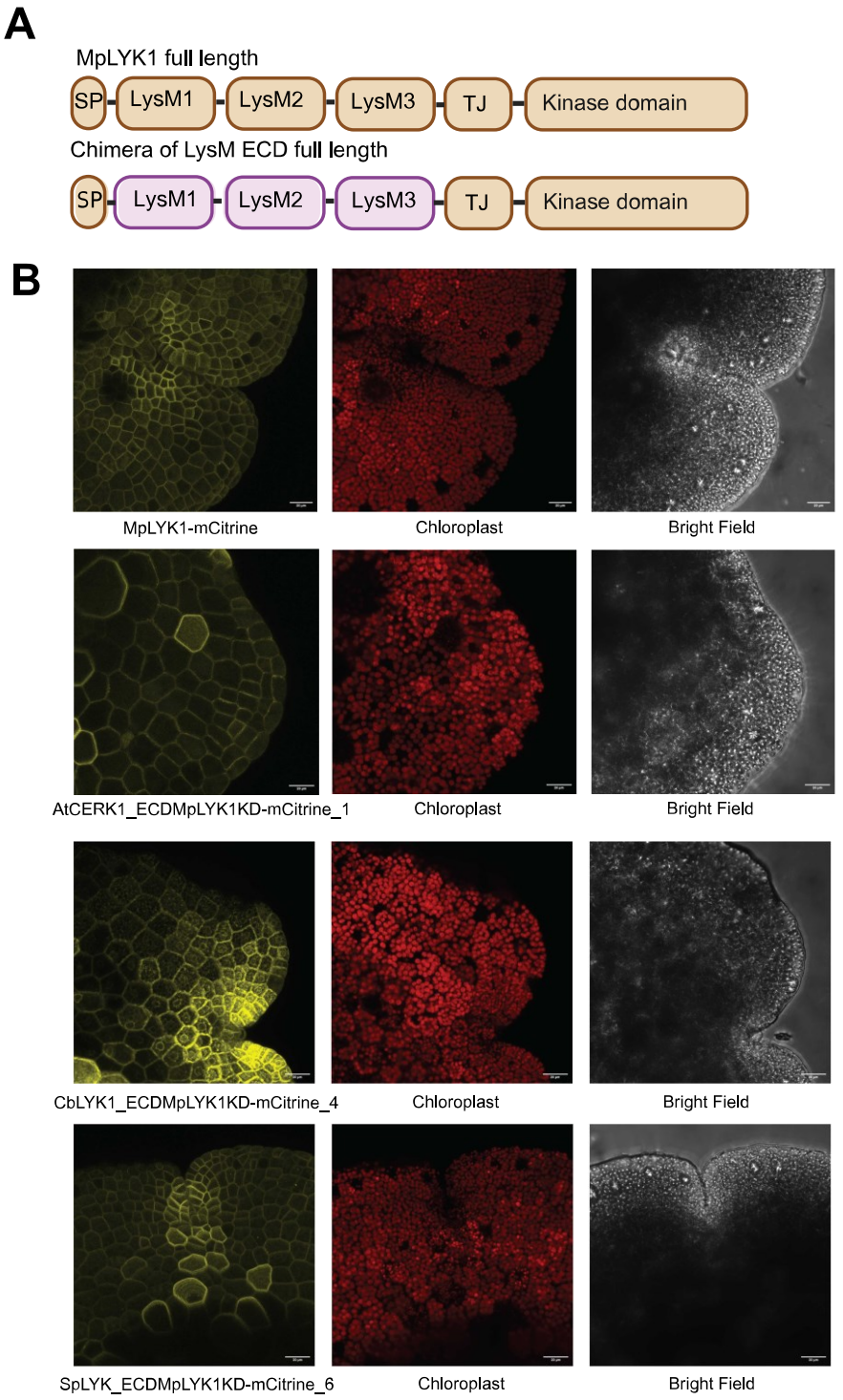
A
MpLYK1 full length
SP
LysM1
LysM2
LysM3
TJ
Kinase domain
Chimera of LysM ECD full length
SP
LysM1
LysM2
LysM3
TJ
Kinase domain
B
MpLYK1-mCitrine
Chloroplast
Bright Field
AtCERK1_ECDMpLYK1KD-mCitrine_1
Chloroplast
Bright Field
CbLYK1_ECDMpLYK1KD-mCitrine_4
Chloroplast
Bright Field
SpLYK_ECDMpLYK1KD-mCitrine_6
Chloroplast
Bright Field
C
RLU
Time [min]
Tak-1
Mplyk1_COMP
Mplyk1_KO
AtCERK1 ECD chimera_1
AtCERK1 ECD chimera_2
CbLYK1 ECD chimera_4
CbLYK1 ECD chimera_15
SpLYK ECD chimera_6
SpLYK ECD chimera_16
chitin heptamer 1μM
Mock

Figure 2.7 ECD domain-swapped, trans-species complementation of LysM-RLKs into *M. polymorpha lyk1* mutant

(A) Schematic representation of the domain replacement constructs. **(B)** Plasma membrane localization of chimera receptors in *M. polymorpha*. Confocal microscopy images for MpLYK1-mCitrine, AtCERK1_ECD-MpLYK1_KD-mCitrine chimera, CbLYK1_ECD-MpLYK1_KD-mCitrine chimera, and SpLYK_ECD-MpLYK1_KD-mCitrine. Scale bars, 20 μm. (**C)** ROS production in *M. polymorpha* upon mock or 1μM chitin heptamer treatment. Seven-day-old gemmae were used. The experiment was repeated twice with similar results.

2.8 Role of chitin in homodimerization and heterodimerization of *M. polymorpha* LysM receptors

In *A. thaliana*, the LysM receptors AtCERK1 and AtLYK5 are known to form heterodimer, and a similar interaction occurs between MpaCERK1 and MpaLYR in *M. paleacea*. Given that the domain-swapped chimera complementation lines containing ECDs from AtCERK1, CbLYK1, and SpLYK failed to restore the chitin-induced ROS burst, it is possible that heterodimer formation between the LysM receptors was impaired.

To test this possibility, I first examined whether MpLYK1 and MpLYR form a heterodimeric complex *in planta* and whether this interaction is chitin-inducible. Förster resonance energy transfer–fluorescence lifetime imaging (FRET–FLIM) experiment was employed to assess their interaction. MpLYK1 was fused to mCherry at the C-terminus, and MpLYR was fused to GFP at the C-terminus. These fusion proteins were expressed in *N. benthamiana* leaves via *Agrobacterium*-mediated transformation, and FRET–FLIM measurements were taken one- or two-days post-infiltration. Both proteins localized to the plasma membrane (Figure 2.8A). Firstly, the fluorescence lifetime (τ) of MpLYR-GFP alone, used as a negative control, was measured under mock and chitin-treated conditions, showing no significant difference (Figure 2.8 B). Co-expression with MpLYK1-mCherry resulted in a reduced lifetime of MpLYR-GFP under mock conditions, which was further reduced upon chitin treatment (Figure 2.8 B). These results indicate that MpLYK1 and MpLYR can form a complex at the plasma membrane, and that their interaction is enhanced in the presence of chitin.

Previous studies have demonstrated that both AtCERK1 and AtLYK5 can homodimerize in addition to forming heterodimers (Petutschnig et al., 2024). Therefore, I investigated whether MpLYK1 and MpLYR are also able to homodimerize. I performed FRET–FLIM measurements under the following combinations: MpLYK1-GFP donor alone, MpLYR-GFP donor alone, MpLYK1-GFP donor co-expressed with MpLYK1-mCherry acceptor (to assess MpLYK1

homodimerization), and MpLYR-GFP co-expressed with MpLYR-mCherry acceptor (to assess MpLYR homodimerization). Measurements were conducted under both mock- and chitin-treated conditions. For MpLYK1-GFP, co-expression with MpLYK1-mCherry led to a reduced GFP fluorescence lifetime, indicating homodimerization; however, no significant difference was observed between the mock and chitin treatments (Figure 2.8 C). For MpLYR-GFP, co-expression with MpLYR-mCherry also resulted in reduced GFP fluorescence lifetime, and this reduction was further enhanced upon chitin treatment, indicating that MpLYR homodimerization is promoted by chitin (Figure 2.8 D). To conclude, the LysM receptors complex in *M. polymorpha* may consist of a least an MpLYK1 homodimer and an MpLYR homodimer, which could assemble into a higher-order oligomer complex upon chitin perception.

Next, I examined whether the chimeric LYKs can properly form a complex with MpLYR using FRET–FLIM analysis. Using MpLYR-GFP as the donor, GFP fluorescence lifetime was measured in the presence of MpLYK1-mCherry or chimeric receptors containing the ECDs of AtCERK1, SpLYK, or CbLYK1 fused to mCherry. Co-expression of MpLYR-GFP with MpLYK-mCherry resulted in a clear reduction in fluorescence lifetime, consistent with previous results. By contrast, co-expression with the domain-swapped chimeras resulted in a less pronounced reduction in fluorescence lifetime (Figure 2.8 E). Notably, expression of the SpLYK ECD chimera induced lesions in *N. benthamiana*, which interfered with FRET–FLIM measurements. As a result, only a single replicate of measurement could be obtained (Supplemental Figure 2).

These results indicate that proper pairing of ECDs is critical for stable receptor–co-receptor complex formation, potentially explaining why chimeric receptors failed to restore MpLYK1 function in *M. polymorpha* (Figure 2.7 C).

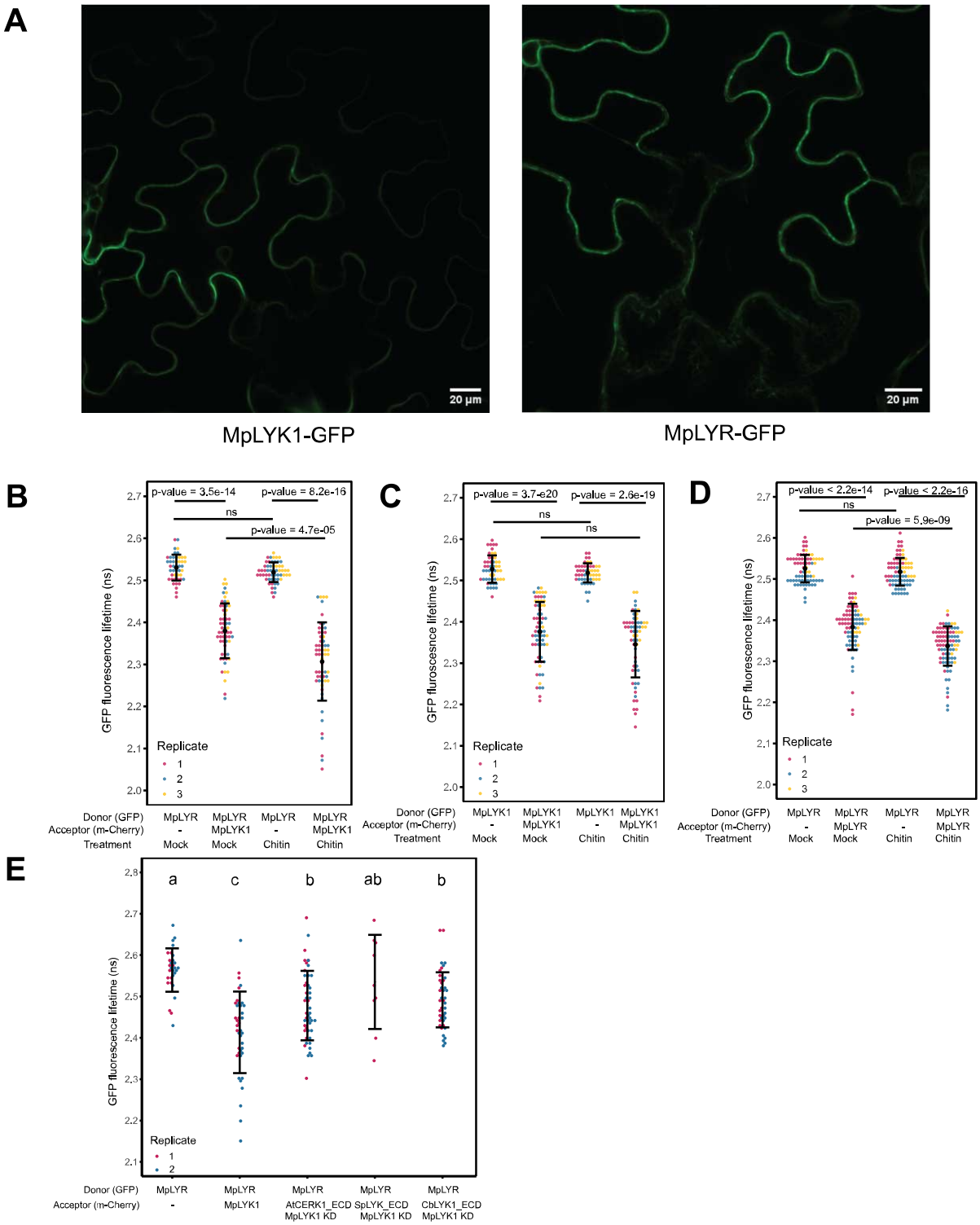
A
20 µm
MpLYK1-GFP
20 µm
MpLYR-GFP
B
p-value = 3.5e-14
p-value = 8.2e-16
ns
p-value = 4.7e-05
GFP fluorescence lifetime (ns)
Replicate
1
2
3
Donor (GFP)
Acceptor (m-Cherry)
Treatment
MpLYR
-
Mock
MpLYR
MpLYK1
Mock
MpLYR
-
Chitin
MpLYR
MpLYK1
Chitin
C
p-value = 3.7-e20
p-value = 2.6e-19
ns
ns
GFP fluroscesnce lifetime (ns)
Replicate
1
2
3
Donor (GFP)
Acceptor (m-Cherry)
Treatment
MpLYK1
-
Mock
MpLYK1
MpLYK1
Mock
MpLYK1
-
Chitin
MpLYK1
MpLYK1
Chitin
D
p-value < 2.2e-14
p-value < 2.2e-16
ns
p-value = 5.9e-09
GFP fluorescence lifetime (ns)
Replicate
1
2
3
Donor (GFP)
Acceptor (m-Cherry)
Treatment
MpLYR
-
Mock
MpLYR
MpLYR
Mock
MpLYR
-
Chitin
MpLYR
MpLYR
Chitin
E
a
c
b
ab
b
GFP fluorescence lifetime (ns)
Replicate
1
2
Donor (GFP)
Acceptor (m-Cherry)
MpLYR
-
MpLYR
MpLYK1
MpLYR
AtCERK1_ECD
MpLYK1 KD
MpLYR
SpLYK_ECD
MpLYK1 KD
MpLYR
CbLYK1_ECD
MpLYK1 KD

Figure 2.8 Multimer formation of MpLYK1, MpLYR, and the chimeric receptors in *N. benthamiana*.
(A) Subcellular localization of transiently expressed MpLYK1 and MpLYR at the plasma membrane in *N. benthamiana* leaf cells. **(B)** FRET–FLIM analysis of MpLYR-GFP and MpLYK1 m-Cherry expressed in *N. benthamiana*. The graph shows the fluorescence lifetime of the donor alone or with the acceptor, under mock (water) or 10 μM chitin heptamer treatment. The significant reduction in the donor's lifetime in the presence of the acceptor indicates energy transfer and physical interaction. Dots represent the values of each datapoint, N > 45. Statistical analysis was calculated by the Kruskal-Wallis test followed by Dunn's test. Significant differences are indicated by p-value, while 'ns' indicated non-significant differences. Experiments were performed in three independent replicates. **(C)** FRET–FLIM analysis of MpLYK1-GFP and MpLYK1-mCherry in *N. benthamiana.* The graph illustrates the fluorescence lifetime of the donor alone or with the acceptor, under mock (water) or 10 μM chitin heptamer treatment. The significant reduction in the donor's lifetime with the acceptor demonstrates energy transfer and physical interaction. Dots represent values of each datapoint, N > 45. Statistical analysis was calculated by the Kruskal-Wallis test followed by Dunn's test. Significant differences are indicated by p-value, while 'ns' indicated non-significant differences. Experiments were performed in three independent replicates. **(D)** FRET–FLIM analysis of MpLYR-GFP and MpLYR-mCherry in *N. benthamiana.* The graph illustrates the fluorescence lifetime of the donor alone or with the acceptor, under mock (water) or 10 μM chitin heptamer treatment. The significant reduction in the donor's lifetime with the acceptor demonstrates energy transfer and physical interaction. Dots represent values of each datapoint, N > 45. Statistical analysis was calculated by the Kruskal-Wallis test followed by Dunn's test. Significant differences are indicated by p-value, while 'ns' indicated non-significant differences. Experiments were performed in three independent replicates. **(E)** FRET-FLIM analysis of MpLYR-GFP and the domain-swapped chimera receptors. The graph displays the fluorescence lifetime of the donor alone or with the acceptor. The significant reduction in the donor's lifetime with the acceptor confirms energy transfer and physical interaction. Dots represent the values of each datapoint. Statistical analysis was calculated by one-way ANOVA followed by Tukey HSD test. Significant differences are indicated by different letters (adjusted $P < 0.05$). Experiments were performed in two independent replicates, except for the MpLYR-GFP and SpLYK_ECD-MpLYK1_KD-mCherry pair.

2.9 CbLYK1 and SpLYK form homodimers, but are not induced by chitin

Previous studies have suggested that the formation of homo- and heterodimer formation of LysM receptors is crucial for their activation and signal transduction. To assess whether this property is conserved in charophyte LysM-RLKs, I examined the homodimerization potential of *C. braunii* CbLYK1 and *S. pratensis* SpLYK using FRET–FLIM. GFP fluorescence lifetimes were measured for CbLYK1-GFP expressed alone or co-expressed with CbLYK1-mCherry, and for SpLYK-GFP expressed alone or co-expressed with SpLYK-mCherry. Measurements were

conducted under both mock- and chitin-treated conditions. For CbLYK1-GFP, co-expression with CbLYK1-mCherry led to a reduction in GFP fluorescence lifetime, indicating homodimer formation. However, the extent of lifetime reduction was not significantly different between mock- and chitin-treated samples (Figure 2.9A). A similar pattern was observed for SpLYK-GFP, where co-expression with SpLYK-mCherry led to a modest reduction in GFP fluorescence lifetime that was likewise unaffected by chitin treatment (Figure 2.9 B). These results suggest that CbLYK1 and SpLYK can form homodimers *in vivo*. However, as observed for MpLYK1, their homodimerization is not enhanced by chitin treatment. The absence of LYR-type or LYP-type LysM receptors may hinder the assembly of a chitin-induced oligomeric formation. Taken together, these findings suggest that chitin-induced complex formation is a feature that evolved specifically within land plant lineages. An alternative, and not mutually exclusive, hypothesis is that chitin is not the activating ligand for CbLYK1 and SpLYK.

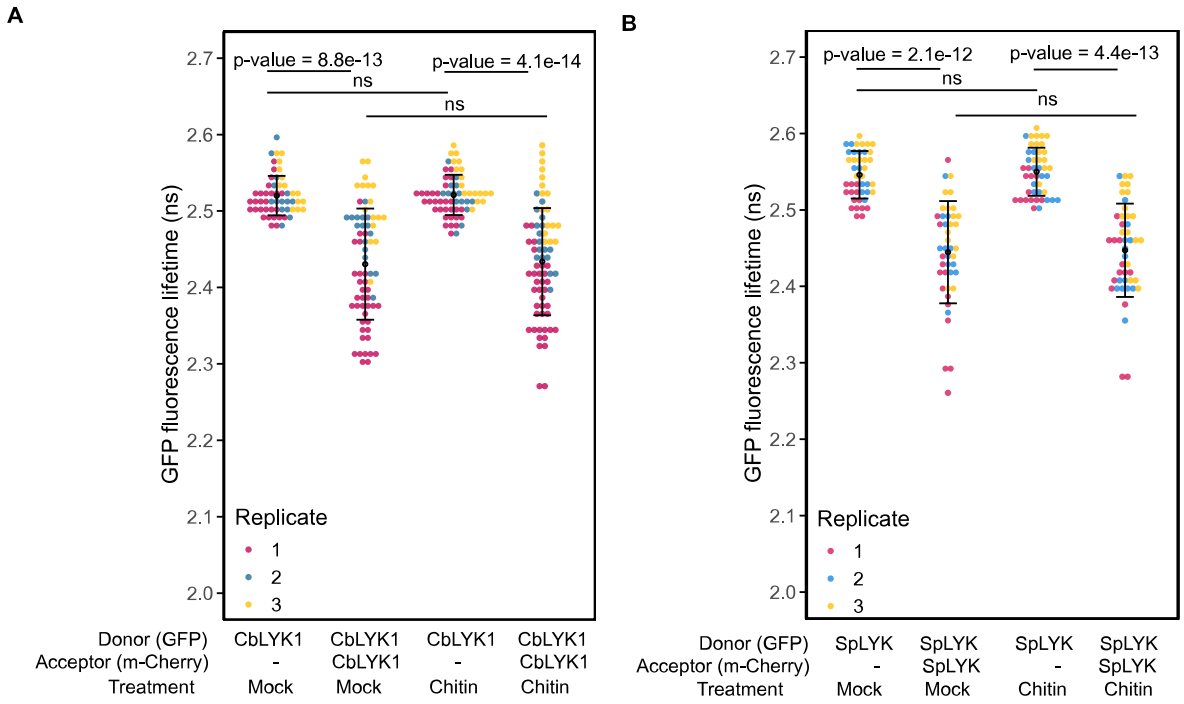

Figure 2.9 CbLYK1 and SpLYK can homodimerize, which is not enhanced by chitin treatment.

(A) FRET-FLIM analysis of CbLYK1-GFP and CbLYK1-mCherry expressed in *N. benthamiana*. The graph shows the fluorescence lifetime of the donor alone or with the acceptor, under mock (water) or µM chitin heptamer treatment. The significant reduction in donor lifetime in the presence of the acceptor indicates energy transfer and physical interaction. Dots represent values of each datapoint, N > 45. Statistical analysis was calculated by the Kruskal-Wallis test followed by Dunn's test. Significant differences are indicated by p-value, while 'ns' indicated non-significant differences. Experiments were performed in three independent replicates. (**B)** FRET-FLIM analysis

of SpLYK-GFP and SpLYK m-Cherry expressed in *N. benthamiana*. The graph shows the fluorescence lifetime of the donor alone or with the acceptor, under mock (water) or 10 µM chitin heptamer treatment. The significant reduction in donor lifetime in the presence of the acceptor indicates energy transfer and physical interaction. Dots represent values of each datapoint, N > 45. Statistical analysis was calculated by the Kruskal-Wallis test followed by Dunn's test. Significant differences are indicated by p-value, while 'ns' indicated non-significant. Experiments were performed in three independent replicates.

2.10 SpLYK was not detected in the plasma membrane-enriched fraction of *S. pratensis*

The SpLYK protein could not be heterologously expressed either in *M. polymorpha* or *N. benthamiana* using its native signal peptide sequence. Moreover, chitin beads failed to pull-down SpLYK from the protein extract of *S. pratensis* (Figure 2.5 C). To further investigate the expression status of SpLYK in *S. pratensis*, I enriched the plasma membrane fraction and analyzed the proteome using MS approach. As a result, I did not identify SpLYK from the plasma membrane-enriched fraction or in other fractions. Of note, MpLYK1, MpLYK2, MpLYR, and MpLYP of *M. polymorpha* were identified from fractionated or non-fractionated samples using similar conditions (Supplemental table 1). These results suggest that SpLYK is either expressed at very low levels, not translated, or not targeted to the plasma membrane in *S. pratensis*. This could be an alternative reason why chitin does not trigger responses in *S. pratensis*.

3. Discussion

LysM-RLKs are PRRs that play pivotal roles in PTI in land plants. Extensive studies have demonstrated their function in recognizing MAMPs and initiating downstream immune signaling pathways in land plants. Streptophyte algae, the closest living relatives of land plants, offer a valuable evolutionary context for tracing the origins of the plant immune mechanisms. With recent advances in genome sequencing, LysM-RLK homologs have been identified in multiple streptophyte algae species. However, their functional roles remain unknown. In this study, I investigated the molecular properties and potential signaling functions of LysM-RLKs in two streptophyte algae: the Charophyceae *C. braunii* and the Zygnematophyceae *S. pratensis*. Through this analysis, I provided new insights into the origin and function of LysM receptors, revealing aspects of their ancestral functions and highlighting key divergences that may have contributed to the emergence of PTI in land plants.

3.1 The origin and emergence of LysM-RLK

LysM-RLKs are characterized by three tandem repeats of the LysM domain connected by CXC motif. It is worth noting that LysM domain-containing proteins are prevalent across all kingdoms of life; however, LysM-RLKs with the specific domain-motif features described appear to be unique to Streptophyta (Buendia et al., 2018; Zhang et al., 2007). Genome analyses indicated that LysM-RLKs are absent in certain early-diverging streptophyte algae lineages with sequenced genomes, including members of Mesostigmatophyceae, Chlorokybophyceae, and Klebsormidiophyceae. The presence of LysM-RLK-encoding genes in the Charophyceae *C. braunii* and Zygnematophyceae *S. pratensis*, suggested that the plant LysM receptors originated from the last common ancestor of Charophyceae, Zygnematophyceae, and land plants (Figure 2.1 A).

Phylogenetic analysis of LysM ECDs revealed that LysM-RLKs from streptophyte algae do not form a monophyletic clade and are divided into distinct clades. This pattern suggests that streptophyte algae LysM-RLKs and land plant LysM receptors share a common evolutionary origin, with individual streptophyte algae lineages likely evolved their LysM-RLKs independently (Figure 2.1 A and B). Therefore, LysM-RLKs in Charophyceae *C. braunii* and Zygnematophyceae *S. pratensis* may have diverged to fulfill distinct functions in each species. Following the divergence of streptophyte algae and land plants, LysM receptors underwent significant expansion in land plants, forming four major clades, prior to the divergence of bryophytes and tracheophytes.

This expansion may have enabled LysM receptors to function in immune signaling and symbiotic interactions, both of which are thought to be essential for survival in terrestrial environments.

Among the Charophyceae species with available genomic databases, not all encode LysM-RLKs. This observation suggests that the loss of LysM-RLKs may have occurred independently in certain algal species, both before and after the divergence of streptophyte algae and land plants. The phenomenon could potentially be linked to specific ecological conditions, possibly due to differences in the microbial communities they interact with. Meanwhile, the presence of a partial LysM-RLK gene in some streptophyte algae suggests that the last common ancestor possessed a complete LysM-RLK gene, which subsequently lost the kinase domain and became non-functional. This observation raises the possibility that streptophyte algae are gradually losing LysM-RLK genes over evolutionary time. Taken together, these findings highlight the Charophyceae as a key phylogenetic group for elucidating the origin and evolution trajectory of LysM-RLKs.

3.2 Ancestral property of the ECD of plant LysM-RLKs in ligand recognition

Chitin binding is likely an ancient property of the LysM domain, predating the emergence of the green lineage. *In vitro* binding analyses conducted in this study demonstrated that chitin-binding capacity is also an ancestral feature of the plant LysM receptor-specific ECDs (Figure 2.4 B-G). These findings indicate that LysM ECDs from both streptophyte algae and land plants retain the ability to bind chitin, supporting the hypothesis that this function is evolutionarily conserved.

The observed differences in binding affinities among various LysM ECDs may reflect the amino acid variations within conserved chitin-binding grooves. The reliability of the MST-based approach was confirmed by the detection of chitin binding in both AtCERK1 and AtLYK5. However, in contrast to my results, Cao et al. (2014) reported that AtLYK5 exhibits a chitin-binding affinity approximately 200 times higher than that of AtCERK1. This discrepancy may result from differences in protein expression systems used. Cao et al. (2014) employed the *Escherichia coli* protein expression system, whereas the insect cell protein expression system was used in this study, which can lead to distinct post-translational modifications of the expressed LysM ECDs. Additionally, the binding assays differed: Cao et al. (2014) used isothermal titration calorimetry (ITC), while MST was used in this study. Liu et al. (2012) also used ITC with an insect cell expression system and reported a binding affinity of 45 μM for AtCERK1 to a chitin octamer. In this study, I used MST and measured AtCERK1 binding affinity to a chitin heptamer, resulting in a different value.

Tan et al. (2025) reported that the ECD of MpLYK1, as well as its homologs in *M. paleacea*. MpaCERK1, does not bind chitin, which contrasts with the findings of this study, where I demonstrated chitin binding of MpLYK1 ECD using MST. Again, this discrepancy may arise from differences in experimental approaches employed to assess chitin binding. Tan et al. (2025) used a chitin bead pull-down approach, in which the ECD of MpLYR but not MpLYK1 was recovered. Intriguingly, my chitin bead pull-down MS analyses also identified but failed to detect MpLYK1. One possible explanation is that the form of chitin presented on beads is not suitable for stable interaction with MpLYK1 ECD. Taken together, these observations highlight that differences in protein expression systems, chitin oligomer lengths, and binding assay methods strongly influence outcomes, and therefore, direct comparison of binding affinities across studies should be made with caution.

My MST results were partly validated using chitin bead pull-down MS-based analyses (Figure 2.5). The lack of detection of MpLYK1 and SpLYK may reflect technical limitations, such as low expression levels in the native tissues, or biological factors such as relatively weaker interactions with long-chain chitin. An affinity pull-down MS-based approach using total protein extracts from *C. braunii* would be valuable for further validating my MST results. Future studies employing additional complementary methods will be important to confirm and reconcile these findings.

Binding of chitin to the LysM2 domain has been reported in previous studies (Liu et al., 2016; Liu et al., 2012; Yu et al., 2024). Based on structural prediction and modelling analyses, it is plausible that chitin-binding occurs through a conserved shallow groove within the LysM2 domain of both algal and *M. polymorpha* LysM ECDs (Figure 2.3 B-E). Binding assays combined with site-directed mutagenesis could be conducted to assess the functional significance of key residues within the LysM2 domain. Very recently, a structural study of the LYR-type LysM receptor LYS13 (renamed as CHIP13 in that study) from *Lotus japonicus* revealed that chitin octamer binding involves not only a groove in the LysM2 domain but also an additional interface in the LysM3 domain, demonstrating a binding module not previously observed LysM ECD (Gysel et al., 2025). Therefore, the possibility that LYR-type LysM receptors engage chitin through multiple interfaces within the LysM ECD cannot be ruled out.

Previous studies have shown that LysM ECDs can bind to various ligands, such as glycan oligosaccharides, lipo-chitooligosaccharides (LCOs), and PGN. Therefore, it is possible that the LysM ECDs from streptophyte algae and *M. polymorpha* may also have the capacity to bind additional ligands. Testing a broader range of ligands in binding assays is worth pursuing.

3.3 *Chara braunii* and *Spirogyra pratensis* do not respond to chitin treatment

Land plants, including *M. polymorpha* and *A. thaliana*, can perceive chitin, typically triggering a ROS burst and the induction of defense-related genes expression (Miya et al., 2007; Yotsui et al., 2023). In contrast, *C. braunii* and *S. pratensis* showed no detectable response to chitin treatment, as evidenced by the absence of ROS production and transcriptional responses. This suggests that these streptophyte algae either do not perceive chitin or do not mount canonical immune responses (Figure 2.6). This difference in chitin response between streptophyte algae and land plants can be attributed to the functional divergence of LysM-RLKs or LysM receptors. In land plants, chitin-induced homo- or heterodimerization of LysM receptors is required for downstream signal transduction. While chitin-binding ability appears to be an evolutionarily conserved feature in LysM-RLKs, FRET–FLIM analysis revealed that chitin does not enhance homodimerization of streptophyte algae LysM-RLKs (Figure 2.9 A and B). This lack of chitin-induced homodimerization may suggest that, despite the conservation of chitin-binding ability, the signal transduction in streptophyte algae may rely on other, yet unidentified ligands that promote homodimerization and downstream signaling.

Another notable feature of land plants is the high diversity of LysM receptors, including additional LYR- and LYP-type receptors (Figure 2.1 B). In contrast, *C. braunii* and *S. pratensis* show no evidence of LysM receptor diversification, and LYR- or LYP-type receptors are absent. This raises an important question: why are LysM receptors in these algae not diversified? One plausible hypothesis is that the diversification of LysM receptors was driven by selective pressures associated with terrestrialization, including interactions with different microbes

It is possible that the LysM-RLKs encoded in the genomes of *C. braunii* and *S. pratensis* are not translated or properly localized to the plasma membrane, and therefore, they cannot perceive exogenously applied chitin. Indeed, fluorescence from the SpLYK-GFP fusion protein expressed in *M. polymorpha* or *N. benthamiana* was not detectable by confocal microscopy. However, when the signal peptide of SpLYK was replaced with that of MpLYK1, SpLYK-GFP fluorescence was observed at the plasma membrane of *N. benthamiana* when expressed heterologously (Figure 2.2 C). Despite this, SpLYK was not detected in either the crude extract or the plasma membrane-enriched fraction of *S. pratensis* using an MS-based proteomics approach. Additionally, SpLYK was also not detected in the chitin-bead pulldown samples (Figure 2.5 C). Among the seven LysM-RLKs in *C. braunii*, only CbLYK3 and CbLYK6 were predicted to contain signal peptides in the original annotation (Figure 2.2 A). In this study, alternative start codons were identified for CbLYK1, CbLYK4, and CbLYK7, which would result in the prediction of signal

peptides in these proteins. However, there is currently no evidence that these alternative start codons are utilized. Furthermore, among the seven CbLYKs, only CbLYK1, along with SpLYK, is predicted to possess protein kinase activity based on its kinase domain sequence (Figure 2.2 B). It is important to investigate whether streptophyte algae LysM-RLKs possess the catalytic activity required to trigger intracellular signaling cascades.

In land plants, RLCKs, RBOHs, and MAPK cascades play crucial roles downstream of LysM receptors in chitin responses, including ROS production and transcriptional reprogramming (Bi et al., 2018; Kadota et al., 2014; Liu et al., 2018; Miya et al., 2007). Although previous studies suggested that RLCK, RBOH, and MAPK cascade components are widely conserved, including in streptophyte algae, their functions in streptophyte algae remain uncharacterized (Gong & Han, 2021; Ngou et al., 2024). Indeed, I found that subfamily VII RLCKs, which act downstream of various PRRs in land plants, are highly conserved both in *C. braunii* and *S. pratensis* (Supplemental Figure 3 A). However, it remains unclear whether these RLCK-VII homologs function downstream of LysM-RLKs for signal transduction in streptophyte algae as they do in land plants. By contrast, streptophyte algae appeared to lack land plant-type RBOH homologs (Supplemental Figure 3B). RBOHs are NADPH oxidases that, in land plants, mediate MAMP-induced ROS burst. Land plant RBOHs possess a characteristic N-terminal extension, which is phosphorylated by calcium-dependent protein kinases and RLCKs upon MAMP recognition, leading to ROS production (Kadota et al., 2015). As far as I investigated, NADPH oxidases identified in streptophyte algae likely lack this N-terminal region, suggesting that the calcium-dependent protein kinase and RLCK-dependent RBOH-mediated ROS production mechanism is not conserved in streptophyte algae. This may explain the absence of chitin-induced ROS production in *C. braunii* and *S. pratensis*.

Overall, my findings suggest a potential evolutionary decoupling between chitin recognition and the capacity to activate immune signaling in streptophyte algae, possibly representing an intermediate stage in the emergence of LysM-mediated PTI. Future investigations into the molecular architecture and activation potential of LysM-RLKs in streptophyte algae may provide critical insights into how PTI evolved from ancestral lineages to the sophisticated defense mechanisms observed in land plants.

3.4 How does the immune system function in streptophyte algae?

The absence of a chitin response in *C. braunii* and S. *pratensis* underscores a key difference from land plants and raises the question of how the immune system functions in streptophyte algae. Streptophyte algae exhibit remarkable diversity, ranging from the complex morphology of *C. braunii* to filamentous forms like *S. pratensis,* and unicellular types such as *M. endlicherianum*. Their habitats are also highly variable, spanning both aquatic and terrestrial environments. Considering these morphological and environmental differences, it is conceivable that streptophyte algae have evolved distinct immune strategies independently of land plants, potentially relying more on metabolite-based defenses and/or physical protective barriers. Establishing a pathosystem between algae and a compatible pathogen would therefore be valuable for elucidating algal immune system. Another important question concerns the function of *LYK* genes in the studied species. Although genetic transformation techniques have been developed for *Closterium peracerosum-strigosum-littorale* (*C. psl*), a Zygnematophyceae species, no such methods exist for *C. braunii* or *S. pratensis* (Kawai et al., 2022). Notably, *C. psl* does not encode any *LysM-RLK* genes, highlighting a major limitation for functional studies in both species. Future efforts to develop genetic transformation techniques for *C. braunii* and *S. pratensis* will be critical for enabling functional studies in these species.

3.5 The role of chitin in homo- and/or hetero-dimerization of LysM receptors in *M. polymorpha*

In *A. thaliana*, LYKa AtCERK1 interacts with LYR AtLYK5 to form heterodimers, and both AtCERK1 and AtLYK5 can also form homodimers, collectively playing a key role in regulating chitin-triggered PTI (Cao et al., 2014; Petutschnig et al., 2024). Through FRET–FLIM analysis in *N. benthamiana*, I demonstrated that LYKa MpLYK1 interacts with LYR MpLYR, and importantly, this interaction is enhanced by chitin treatment (Figure 2.8 B). This represents the first evidence that chitin mediates homo- and/or heterodimerization of LysM receptors in bryophytes. A previous study in *M. paleacea* showed that LYKa MpaCERK (a homolog of MpLYK1) interacts with LYR MpaLYR (a homolog of MpLYR), but the role of chitin in enhancing this interaction was not investigated (Tan et al., 2025).

My FRET–FLIM results of *M. polymorpha* LYKaLYR heterodimerization are consistent with previous observations in *A. thaliana*, where the interaction between AtCERK1 and AtLYK5 is enhanced by chitin treatment, as demonstrated using FRET–FLIM in transgenic plants and co-immunoprecipitation (Cao et al., 2014; Petutschnig et al., 2024). In contrast, although LYKa

MpLYK1 formed homodimers, this interaction was not enhanced by chitin treatment (Figure 2.8 C), differing from *A. thaliana*, where LYKa AtCERK1 homodimerization is induced by chitin treatment (Petutschnig et al., 2024). This discrepancy may be due to differences in the experimental system, as my study relied on heterologous transient expression, whereas the previous study used transgenic plants expressing fluorescent protein-tagged LysM receptors. Alternatively, the chitin-enhances homodimerization of LYKa can be species-specific.

Cao et al. (2014) also showed that LYR AtLYK5 forms homodimer both before and after chitin treatments using co-immunoprecipitation. However, because co-immunoprecipitation is not quantitative, it remains unclear whether chitin enhances the homodimerization. By contrast, my FRET–FLIM analysis demonstrated that LYR MpLYR forms homodimers both prior to and after chitin treatment, and further revealed that chitin enhanced MpLYR homodimerization (Figure 2.8 D).

Heterodimerization between LYK and LYR proteins plays a critical role in initiating PTI response, as demonstrated by the impaired chitin-triggered immunity observed in plants lacking either AtCERK1 or AtLYK5. Consistently, chitin-triggered ROS production in the Mp*lyk1* mutant was not restored by the expression of the ECD-swapped chimera MpLYK1s (Figure 2.7 C), suggesting that proper heterodimerization between LYKa and LYR is essential for this response. Supporting this, FRET–FLIM analysis demonstrated that the ECD-swapped chimera MpLYK1 failed to form heterodimers and/or only weakly interacted with MpLYR (Figure 2.8 E). However, it remains unresolved whether these chimera receptors are also incapable of activating the downstream MAPK signaling cascade or triggering transcriptional reprogramming upon chitin treatment.

Importantly, by integrating the results of *in vitro* chitin-binding assays and FRET–FLIM analyses from this study (Figure 2.4, 2.5, 2.7 A B) with the genetic evidence provided by Yotsui et al. (2023), I conclude that both MpLYK1 and MpLYR function as bona fide chitin receptors that form chitin-induced higher-order oligomeric complexes. Nonetheless, the precise role of chitin in regulating homo- and/or heterodimerization of LysM receptors remains to be fully resolved. Further studies employing complementary experimental approaches will be essential to achieve a more comprehensive understanding of these molecular mechanisms.

3.6 Conclusion

In conclusion, to my knowledge, this is the first study to investigate the origin and function of LysM-RLKs in streptophyte algae. My findings provide evidence that LysM ECDs in both

streptophyte algae and land plants shared functional similarity in chitin binding, while also revealing key differences in the LysM-mediated chitin response between these two lineages. Furthermore, this study provides the first evidence that chitin promotes homo- and/or heterodimerization of LysM receptors in *M. polymorpha*, suggesting the formation of a higher-order oligomeric complex that may represent a feature specific to land plant and absent in streptophyte algae (Figure 3). Collectively, these findings contribute to a deeper understanding of the molecular mechanisms underlying chitin-triggered PTI in land plants.

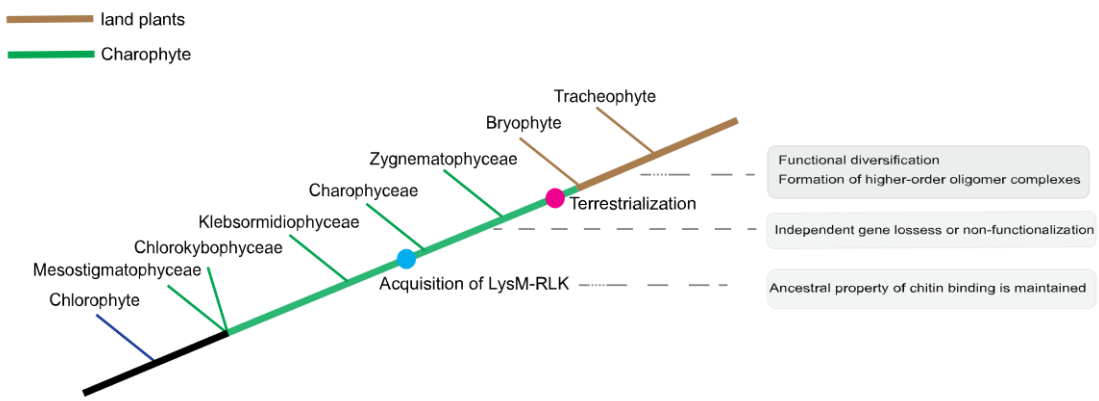

Figure 3 Scenario of stepwise evolution of LysM receptors during plant evolution. A simplified cladogram illustrates the proposed origin and stepwise neofunctionalization of LysM receptors.

3.7 General discussion and outlooks

It is well established that chitin triggers the complex formation and activation of LysM-RLKs, leading to downstream signaling responses. These receptors are localized at the plasma membrane, with their LysM ECDs facing the extracellular space. Evidence suggests that complex formation is mediated through these ECDs (Liu et al., 2012; Cao et al., 2014). However, the detailed mechanism of this process at the single-molecule level remains unclear. It would be particularly interesting to investigate how chitin influences the dynamics of LysM receptors at the single-particle level, and how the ratio of heterodimerization to homodimerization of LysM-RLKs

changes between the resting and active states. Single-particle tracking photoactivated localization microscopy may be useful to map the dynamics.

The development of AlphaFold2 by DeepMind, as reported by Jumper et al. (2021), has revolutionized the field of structural biology by enabling highly accurate prediction of three-dimensional (3D) protein structures directly from amino acid sequences. This breakthrough has significantly accelerated our understanding of protein architecture and function, making AlphaFold2 an indispensable tool not only in structural biology but also in hypothesis generation and the design of experimental studies. Importantly, to fully grasp the biological functions of proteins, it is essential to also consider their interactions with ligands, as some proteins will have conformational changes in the bound or unbound state. More importantly, several studies emphasize that while AlphaFold predictions are valuable, they do not replace experimental structure determination, and also point out the limitations of AlphaFold's accuracy and reliability (Agarwal & McShan, 2024; Akdel et al., 2022; Terwilliger et al., 2024). Thus, structural biology with ligand remains essential.

In the context of this dissertation, the ligand of interest is a glycan, which serves as the substrate for LysM proteins. Although the primary focus of my dissertation does not extensively address the glycan side, it is important to acknowledge the structural and functional relevance of glycans. Glycans (also known as carbohydrates, saccharides, or sugars) are among the most structurally complex biomolecules, participating in a wide range of physiological functions. Their complexity arises from the vast enzymatic repertoire involved in their biosynthesis, degradation, and modification. Unlike proteins, where structural prediction has been vastly improved due to the abundance of structural data and sequence homology-based approaches, glycan structural biology has lagged. Predicting glycan structure remains a major challenge, as traditional sequence-based strategies are not readily applicable. Furthermore, glycans often undergo extensive chemical modifications that significantly influence their structural properties. Adding to this complexity, glycans are inherently flexible molecules that can adopt multiple, well-defined conformational states under physiological conditions. This conformational flexibility complicates structural characterization and poses limitations for studying protein-ligand interactions involving glycans. Understanding the glycan itself may help in the acceleration of our knowledge of the protein it interacts with.

4. Materials and methods

4.1 Plant materials

Marchantia polymorpha

M. polymorpha lines used in this study are listed in the table below.

Table 1: *M. polymorpha* and transgenic lines used and generated in this study

Name	Description	Vector	Selection marker	Source
Tak-1	Wild type male *M. polymorpha*	-	-	Takaragaike, Japan
Mplyk1-1 KO	MpLYK1 loss-of-function mutant in Tak-1 and Tak-2 background			
MpLYK1/Mplyk1-1 KO	MpLYK1 complementation in Mplyk1-1 KO mutant background			
CbLYK1-mCitrine	CbLYK1-mCitrine utilizing information in original annotation were created by Katharina Melkonian, a former lab member			
AtCERK1 ECD chimera_1	MpLYK1 ECD swapped with AtCERK1 ECD chimera driven by EF1α promoter complementation in Mplyk1-1 KO mutant background	pMpGWB308	Chlorsulfuron	This work

AtCERK1 ECD chimera_2	MpLYK1 ECD swapped with AtCERK1 ECD chimera driven by EF1α promoter complementation in Mplyk1-1 KO mutant background	pMpGWB308	Chlorsulfuron	This work
CbLYK1 ECD chimera_4	MpLYK1 ECD swapped with CbLYK1 ECD chimera driven by EF1α promoter complementation in Mplyk1-1 KO mutant background	pMpGWB308	Chlorsulfuron	This work
CbLYK1 ECD chimera_15	MpLYK1 ECD swapped with CbLYK1 ECD chimera driven by EF1α promoter complementation in Mplyk1-1 KO mutant background	pMpGWB308	Chlorsulfuron	This work
SpLYK ECD chimera_6	MpLYK1 ECD swapped with SpLYK ECD chimera driven	pMpGWB308	Chlorsulfuron	This work

	by EF1α promoter complementation in Mplyk1-1 KO mutant background			
SpLYK ECD chimera_16	MpLYK1 ECD swapped with SpLYK ECD chimera driven by EF1α promoter complementation in Mplyk1-1 KO mutant background	pMpGWB308	Chlorsulfuron	This work

Chara braunii

C. braunii S276 was originally isolated from Lake Kasumigaura (Ibaraki, Japan) (Nishiyama et al., 2018) and obtained from the laboratory of Prof. Dr. Wolfgang Hess (University of Freiburg)

Spirogyra pratensis

S. pratensis strain MZCH10213 was from the Microalgae and Zygnematophyceae Collection Hamburg and obtained from the laboratory of Prof. Dr. Jan de Vries (Göttingen University)

Mesotaenium endlicherianum

M. endlicherianum SAG 12.97 was obtained from the Culture Collection of Algae at Göttingen University (SAG).

Arabidopsis thaliana

A. thaliana ecotype Columbia (Col-0) was used.

Nicotiana benthamiana

N. benthamiana wild type was used.

4.2 Plant growth conditions and cultivation

Marchantia polymorpha

A male accession of *M. polymorpha*, Tak-1 was used as wild-type, mutants, and transgenic lines were grown from single gemmae or thallus. The plants were grown on ½ Gamborg's B5 medium containing 1% (w/v) agar, under continuous white LED light with intensity of 50-60 µmol photons m^{-2} s^{-1} at 22 °C.

For transgenic plants generation, 14-day-old plants were grown from single gemmae on ½ Gamborg's B5 medium containing 1% (w/v) agar at 22 °C under continuous white LED light with intensity of 50-60 µmol photons m^{-2} s^{-1} at 22 °C.

For ROS assay, 7-day-old gemmae were cultured in liquid ½ Gamborg's B5 medium supplemented with 0.1% (w/v) sucrose with shaking at 130 rpm under continuous white LED light with intensity of 50-60 µmol photons m^{-2} s^{-1} at 22 °C.

For *in-vitro* chitin beads pull-down with mass spectrometry analysis, 3-weeks-old Tak-1 wild -type plants were grown from single gemmae on ½ Gamborg's B5 medium containing 1% (w/v) agar at 22 °C under continuous white LED light with intensity of 50-60 µmol photons m^{-2} s^{-1}.

Algae

C. braunii were grown using the protocol of (Holzhausen et al., 2022) in glass jars containing compost (Gardol Pure Nature, Bauhaus), lime (Gardol Garten- & Rasenkalk, Bauhaus), quartz sand (0.4–0.8 mm in diameter and distilled water, sealed with surgical tape (Micropore, 3 M). Algae were kept under long-day condition with 16 hours light/8 hours dark under white LED light with intensity of 50-60 µmol photons m^{-2} s^{-1}.

For RNA sequencing analysis, *in-vitro* chitin beads pull-down with mass-spectrometry analysis, 13-day-old *S. pratensis and 7-day-old M. endlicherianum* were grown on sterilized cellophane on WHM medium containing 11% (w/v) agar and were kept under long-day condition with 16 hours light/8 hours dark under white LED light with intensity of 50-60 µmol photons m^{-2} s^{-1}.

A. thaliana

For *in-vitro* chitin beads pull-down with mass spectrometry analysis, *A. thaliana* seeds were vapor-sterilized using and grown on ½ Murashige-Skoog medium containing 1% (w/v) agar for 3 weeks and were kept under long-day condition with 16 hours light/8 hours dark under white LED light with intensity of 50-60 µmol photons m^{-2} s^{-1}.

N. benthamiana

N. benthamiana plants were grown on soil at the greenhouse of the Max Planck Institute for Plant Breeding Research, Cologne, with a controlled environment.

4.3 Bacterial and insect cell strains

Table 2: Bacterial and insect cell strains used in this study

Name	Supplier	Genotype	Purpose
E. coli DH10B	Invitrogen (now Thermo Fisher Scientific)	F– mcrA Δ(mrr-hsdRMS-mcrBC) φ80lacZΔM15 ΔlacX74 recA1 endA1 araD139 Δ (ara-leu)7697 galU galK λ– rpsL (StrR) nupG	Molecular cloning
E. coli MACH1	Invitrogen (now Thermo Fisher Scientific)	F- φ80(lacZ)ΔM15 ΔlacX74 hsdR(rK-mK+) ΔrecA1398 endA1 tonA	Molecular cloning
E. coli DB3.1	Invitrogen (now Thermo Fisher Scientific)	gyrA462 endA1 Δ(sr1-recA) mcrB mrr hsdS20 glnV44 (=supE44) ara14 galK2 lacY1 proA2 rpsL20 xyl5 leuB6 mtl1	Amplification of gateway binary vector containing toxic CcdB cassette
E. coli DH10Bac	Invitrogen (now Thermo Fisher Scientific)	F-mcrA Δ (mrr-hsdRMS-mcrBC) Φ80lacZΔM15 Δ lac X74 recA1 endA1 araD139 Δ (ara, leu)7697 galU galK λ - rps L nupG /pMON14272 / pMON7124	Production of recombinant bacmids used in the Bac-to-Bac Baculovirus Expression System.
A. tumefaciens GV3101		pMP90RK, Gm^r, Km^r	*M. polymorpha* transformation and transient expression in *N. benthamiana*

S. frugiperda Sf21	Invitrogen (now Thermo Fisher Scientific)	IPLB-Sf21-AE, isolated from *Spodoptera frugiperda* (Fall Armyworm) ovary	Generation of baculovirus
T. ni High Five™	Invitrogen (now Thermo Fisher Scientific)	BTI-TN-5B1-4, a clonal isolate derived from the parental *Trichoplusia ni* cell line (cabbage looper ovary)	Expression of recombinant proteins using the Baculovirus Expression Vector System (BEVS)

4.4 Other materials

Oligonucleotides

All oligonucleotides were synthesized by and purchased from Sigma-Aldrich (Darmstadt, Germany).

Table 3: Oligonucleotides used in this study

Name	Description	Sequence
MpLYK1_ectodel_F	To delete MpLYK1 ectodomain	CAAAGAGTGTTTGCCACTGGTGC
MpLYK1_ectodel_R		ATCACCCTCCGAGGTCGGA
ChaLYK1_ecto_F	To amplify CbLYK1 ectodomain and in-fusion cloning for generating chimera receptor	ACCTCGGAGGGTGATTGTTCTACGGAAGACTCCTCTTGC
ChaLYK1_ecto_R		GGCAAACACTCTTTGAGGGATGATCAGCTTAATGCCAG
AtCERK1_ecto_F	To amplify AtCERK1 ectodomain and in-fusion cloning for generating chimera receptor	ACCTCGGAGGGTGATTGCAGGACTAGCTGTCCTTTAGC

AtCERK1_ecto_R		GGCAAACACTCTTTGAACACCATCTTGTTTACTTGATTTGAATGGT
Polyhedrin_F	To sequence pFastBac1 vector	AAATGATAACCATCTCGCAAA
SpLYK_F	SpLYK cds amplification	ATGCAATTTTACGTAATCCTTAAT
SpLYK_R		GTCTTCTAATAAGCATTCGAAA
att_CbLYK1_Fnew	CbLYK1 cds amplification with signal peptide and attB site added	GGGGACAAGTTTGTACAAAAAAGCAGGCTTAATGAGATGCCGCCCT
att_CbLYK1_Rnew		GGGGACCACTTTGTACAAGAAAGCTGGGTTCCTCAGCAATTGCGC
MpLYK1_Sigp_F	MpLYK1 signal peptide amplification that will be replaced to SpLYK signal peptide	GCAGGCTCCACCATGATTGCGACGGGAGTTAT
MpLYK1_Sigp_R		TGAGAATGACCCTCCGAGGTCGG
SpLYK_noSP_F	SpLYKcds amplification without signal peptide sequence	GGAGGGTCATTCTCATTGCAACGAAACATTAGG
SpLYK_noSP_R		GAAAGCTGGGTCTAGGTCTTCTAATAAGCATTCGAAAATGGCT
P0-hem	Sequential primer to add BamH1 and hemolin	GGATCCATGGCGTTCAAGAGTATAGCAGTTTTAAGCGCCTGCATAA

P1_hem	Sequential primer for hemolin	ATAGCAGTTTTAAGC GCCTGCATAATTGTG GGTTCAGCGCTTCCC
P2-AtCERK1_hem	Sequential primer partial hemolin with partial AtCERK1	TTGTGGGTTCAGCGC TTCCcAAGTGCAGGA CTTCTTGCCC
P2_SpLYK_hem	Sequential primer partial hemolin with partial SpLYK	TTGTGGGTTCAGCGC TTCCCCACTCTCACT GCAACGAAAC
P2_MpCERK_hem	Sequential primer partial hemolin with partial MpLYK1	TTGTGGGTTCAGCGC TTCCCATCCCTACCT CTGAAGGCGA
P2_AtLYK5_hem	Sequential primer partial hemolin with partial AtLYK5	GGTTCAGCGCTTCCC CAGCCCTACGTCAAC AACC
P2_MpLYR_hem	Sequential primer partial hemolin with partial MpLYR	GGTTCAGCGCTTCCC CAGGTCTACGGCGA AACC
P2_CbLYK1_hem	Sequential primer partial hemolin with partial CbLYK1	GGTTCAGCGCTTCCC ATCCCTGCTGCTTGC GCC
R_AtCERK1_his	Reverse primer for amplification of AtCERK1 ectodomain with histidine tag and Xho1 site	CTCGAGTTAGTGATG GTGATGGTGATGGA CACCGTCCTGCTTAG A
R_AtLYK5_his	Reverse primer for amplification of AtLYK5 ectodomain with histidine tag and Xho1 site	CTCGAGTTAGTGATG GTGATGGTGATGCCA CTTGTGAGAGCTAGA
R_MpCERK1_his	Reverse primer for amplification of MpLYK1 ectodomain with histidine tag and Xho1 site	CTCGAGTTAGTGATG GTGATGGTGATGTCC GGCGTTGGTCTTAGA

R_MpLYR_his	Reverse primer for amplification of MpLYR ectodomain with histidine tag and Xho1 site	CTCGAGTTAGTGATGGTGATGGTGATGGTTGGTGGAAGAGGAGCT
R_CbLYK_his	Reverse primer for amplification of CbLYK1 ectodomain with histidine tag and Xho1 site	CTCGAGTTAGTGATGGTGATGGTGATGCTGGTTTCCGTCAGAGTGA
R_SpLYK_his	Reverse primer for amplification of SpLYK ectodomain with histidine tag and Xho1 site	CTCGAGTTAGTGATGGTGATGGTGATGGTTCAGGTCGTCGTTCTT
infuse_P0_F	Amplification for BamH1 and hemolin and ectodomain for in-fusion into pFastBac1	ATCGGGCGCGGATCCATGGCGTTCAAGAGTATAGCAG
infuse_his_R	Amplification for histidine tag for in-fusion into pFastBac1	TACCGCATGCCTCGAGTTAGTGATGGTGATGGTGATG
pFB_lin_R	In-fusion cloning pFastBac1	CTCGAGGCATGCGGTACCA
pFB_lin_F	In-fusion cloning pFastBac1	GGATCCGCGCCCGATGGT

Plasmids

Table 4: Plasmids used and generated in this study

Name	Description	Vector	Selection marker
pDONR207	Gateway® donor vector with attP1 and attP2 sites	pDONR207	Gentamycin
pDONR207-SpLYK	Gateway® donor vector with SpLYK cds	pDONR207	Gentamycin
pENTR4-mSpLYK	Gateway® enrty vector with SpLYK cds with	pENTR4	Kanamycin

	replacement of MpLYK1 signal peptide		
pDONR207-CbLYK1 real	Gateway® donor vector with CbLYK1 cds with new signal peptide	pDONR207	Gentamycin
pENTR4-AtCERK1ED_MpLYK1 KD	Gateway® entry vector MpLYK1 ECD swapped with AtCERK1 ECD chimera	pENTR4	Kanamycin
pENTR4-CbLYK1ED_MpLYK1 KD	Gateway® entry vector MpLYK1 ECD swapped with CbLYK1 ECD chimera	pENTR4	Kanamycin
pENTR4-SpLYKED_MpLYK1 KD	Gateway® entry vector MpLYK1 ECD swapped with CbLYK1 ECD chimera	pENTR4	Kanamycin
pAB117 (Somssich & Simon, 2017)	Gateway® binary vector with estradiol inducible promoter and GFP (C terminal on insert)	pABindGFP	Spectinomycin
pAB118 (Somssich & Simon, 2017)	Gateway® binary vector with estradiol inducible promoter and mCherry (C terminal on insert)	pABindmCherry	Spectinomycin
pAB117-mSpLYK	Expression of mSpLYK fused with GFP at the C terminal	pAB117	Spectinomycin
pAB118-mSpLYK	Expression of mSpLYK fused with mCherry at the C-terminal	pAB118	Spectinomycin
pAB117-CbLYK1	Expression of CbLYK1 fused with GFP at the C terminal	pAB117	Spectinomycin

pAB118-CbLYK1	Expression of CbLYK1 fused with mCherry at the C terminal	pAB118	Spectinomycin
pAB117-MpLYK1	Expression of MpLYK1 fused with GFP at the C terminal	pAB117	Spectinomycin
pAB118-MpLYK1	Expression of MpLYK1 fused with mCherry at the C terminal	pAB118	Spectinomycin
pAB117-MpLYR	Expression of MpLYR fused with GFP at the C terminal	pAB117	Spectinomycin
pAB118-MpLYR	Expression of MpLYR fused with mCherry at the C terminal	pAB118	Spectinomycin
pFastBac1	Vector for high-level expression of proteins in insect cells using the Bac-to-Bac® baculovirus system	pFastBac1	Ampicillin
pFastBac1-AtCERK1 ECD	Expression of AtCERK1 ectodomain protein with 6× histidine tag at C-terminal	pFastBac1	Ampicillin
pFastBac1-AtLYK5 ECD	Expression of AtLYK5 ectodomain protein with 6× histidine tag at C-terminal	pFastBac1	Ampicillin
pFastBac1-MpLYK1 ECD	Expression of MpLYK1 ectodomain protein with 6× histidine tag at C-terminal	pFastBac1	Ampicillin
pFastBac1-MpLYR ECD	Expression of MpLYR ectodomain protein with 6× histidine tag at C-terminal	pFastBac1	Ampicillin
pFastBac1-CbLYK1 ECD	Expression of CbLYK1 ectodomain protein with 6× histidine tag at C-terminal	pFastBac1	Ampicillin

pFastBac1-SpLYK ECD	Expression of SpLYK ectodomain protein with 6× histidine tag at C-terminal	pFastBac1	Ampicillin
pMpGWB308 (Ishizaki et al., 2015)	Gateway® binary vector with MpEF1α promoter and Citrine (C terminal on insert)	pMpGWB308	Chloramphenicol and Spectinomycin
pMH3	MpLYK1 ECD swapped with CbLYK1 ECD chimera driven by EF1α promoter	pMpGWB308	Chloramphenicol and Spectinomycin
pMH5	MpLYK1 ECD swapped with SpLYK ECD chimera driven by EF1α promoter	pMpGWB308	Chloramphenicol and Spectinomycin
pMH6	MpLYK1 ECD swapped with AtCERK1 ECD chimera driven by EF1α promoter	pMpGWB308	Chloramphenicol and Spectinomycin

Gene synthesis

Gene for protein expression, SpLYK and CbLYK1 were commercially purchased from GeneArt (Thermo Fisher Scientific).

Chemicals

All chemicals were purchased from Carl Roth GmbH (Karlsruhe, Germany), Sigma-Aldrich (St. Louis, USA) or Merck (Darmstadt, Germany), unless otherwise mentioned in the respective section.

Molecular biology kits and reagents

The section below provides information of general molecular biology kits and reagents used in this study. Standard protocols for molecular biology methods that were used in this study were performed according to the manufacturer's instructions unless otherwise stated. Specific reagents that were used will be mentioned in particular section.

Table 5: Kits and reagents used in this study

Kits / Reagents	Purpose	Supplier
NucleoSpin Plasmid, Mini Kit for Plasmid SNA	Isolation of plasmid	Macherey-Nagel
NucleoSpin Gel and PCR Clean-up, Mini Kit for Gel Extraction and PCR Clean-up	PCR product clean up	Macherey-Nagel
Spectrum Plant Total RNA Kit	RNA extraction	Sigma-Aldrich
Gateway BP Clonase	BP cloning	Thermo Fisher Scientific
Gateway LR Clonase	LR cloning	Thermo Fisher Scientific
LightRun tubes	Sanger sequencing	Eurofins Genomics
In-Fusion cloning kit	Cloning	Takara Bio
NEBuilder® HiFi DNA Assembly Cloning Kit	Cloning	New England Biolabs
PrimeSTAR® GXL DNA Polymerase	PCR	Takara Bio
Q5 DNA polymerase	PCR	New England Biolabs
BamH1-HF	Restriction digest	New England Biolabs
Xho1-HF	Restriction digest	New England Biolabs
Nco1-HF	Restriction digest	New England Biolabs
Xba1-HF	Restriction digest	New England Biolabs

Software

The softwares that were used in this study is mentioned in respective section.

4.5 Methods

4.5.1 Plasmid construction

The information about primers was listed in the table provided in the previous section.

For plasmids with pENTR4 backbone, the pENTR4 vector were digested with Nco1 and Xba1 to linearize the vectors, and gel purified. The inserts were PCR amplified. The entry vector and inserts were recombined with In-fusion cloning kit or NEBuilder® HiFiDNA Assembly Cloning Kit (New England Biolabs). For plasmids with pDONR backbone, the inserts were PCR amplified with primer with attB site added. The inserts were recombined into pDONR vector with BP clonase. For generating transgenic line, the entry vectors were cloned into pMpGWB308 binary vector using LR clonase. For generating estradiol-inducible expression vectors with GFP or mCherry as translational fusions at the C-terminus for transient expression in *N. benthamiana* leaves. The entry vectors were further cloned into pABind117 and pABind118 by LR clonase (Thermo Fisher Scientific). For generating protein expression plasmids, the pFastBac1 vector was digested with BamH1 and Xho1 enzymes, the cds sequences of genes of ectodomains that were synthesized from GeneArt were PCR amplified sequentially to add BamH1 site, followed by hemolin signal peptide at the N terminus and 6 ×histidine sequences followed by Xho1 site. The pFastBac1 vector and the inserts were recombined using In-Fusion cloning kit. All plasmids generated were verified by Sanger sequencing.

4.5.2 *Agrobectrium*-mediated Marchantia stable transformation

M. polymorpha transgenic lines were produced using the cut thallus method for Agrobacterium-mediated stable transformation, as shown by Kubota et al. 2013, with minor modifications. Candidate transformants were selected using the same conditions as mentioned before but on ½ Gamborg's B5 medium containing 1% agar and corresponding antibiotics supplemented with 100 mg/L cefotaxime for killing of residual agrobacteria. The transgenic plants were selected by visualizing fluorescence under confocal microscope.

4.5.3 Transient expression in *N. benthamiana*

Agrobacterium cells transformed with the desired plasmids were grown at 28 °C and were cultured on Luria-Bertani (LB) medium containing 1 % (w/v) agar with antibiotics for 2 days. A single colony was selected and inoculated into 5 mL LB liquid medium with appropriate antibiotics and then cultured overnight at 28 °C with shaking at 200 rpm. To prepare a fresh liquid culture, 1 mL

of overnight culture was added to 4 mL of LB liquid culture and further grown with shaking at 200 rpm for 4 hours. The bacteria were then collected by centrifugation for 5000 x g and the bacteria pellets were resuspended with infiltration solution (10 mM $MgCl_2$, 10 mM MES, 450 µM acetosyringone, adjusted to pH 5.6). The bacterial suspension was kept on ice before infiltration. The optical density was measured using spectrophotometer and adjusted to an OD600 of 0.2 for strain expressing GFP fusion protein or 0.4 for strain expressing mCherry fusion protein. Agrobacteria strain carrying p19 construct was mixed with a ratio of 1:1 respectively. *N. benthamiana* leaves were infiltrated with suspension using a needless syringe. The plants were kept in growth chamber at 22 °C with continuous white LED light of intensity of of 50-60 µmol photons m^{-2} s^{-1}. The expression of proteins was induced by brushing the abaxial side of leaves using induction solution (20 µM β-estradiol and 0.1% Tween 20) for 24-48 hours.

4.5.4 LysM RLK/RLP homologs identification

The publicly available genome and transcriptome database of thirty plant species were searched for LysM RLK/RLP homologs identification. The *M. polymorpha* MpLYK1 and MpLYP amino acid were used as query sequences for BLASTp search. The identified proteins were then subjected to InterProScan to confirm the presence of LysM domain and kinase domain for in LysM RLK and LysM domain for LysM RLP. Sequences were obtained from Yotsui et al. (2023) and the database from JGI Genome Portal. The presence of CXC motif was further inspected. Species tree was drawn based on the information from Timetree5 for land plants (Kumar et al., 2017) and for Charophyceae (Hess et al., 2022).

4.5.5 Phylogenetic tree generation

LysM ectodomain

Phylogenetic analysis for LysM ectodomain was performed by Yosuke Hoshino.

RBOH

The Marchantia RBOH1 (Mp3g20340.1) amino acid sequence was used as query in BLASTp search with an E-value threshold of 1e-3. The sequences were aligned with MAFFT using default parameters (Katoh et al., 2019) and phylogenetic analysis was performed using IQ-tree with ModelFinder and ultrafast bootstrap of 1000 replicates (Hoang et al., 2018; Kalyaanamoorthy et al., 2017; Trifinopoulos et al., 2016). Phylogenetic tree was visualized using iTOL.

Subfamily VII RLCK

The *M. polymorpha* and *A. thaliana* subfamily VII RLCK sequences were obtained from Izumi et al. The MpRLCKVIIa (Mp3g25360.1) amino acid sequence was used as query in BLASTp with an E-value threshold of 1e-30. The sequences were aligned with MAFFT using default parameters (Katoh et al., 2019) and phylogenetic analysis was performed using IQ-tree with ModelFinder and ultrafast bootstrap of 1000 replicates (Hoang et al., 2018; Kalyaanamoorthy et al., 2017; Trifinopoulos et al., 2016)Phylogenetic tree was visualized using iTOL.

4.5.6 Multiple sequence alignment

Multiple sequence alignment was performed with MAFFT or T-COFFEE using default parameters and visualized using ESPript 3.0 ENDscript - https://endscript.ibcp.fr ((Robert & Gouet, 2014).

4.5.7 Signal peptides prediction

The signal peptides of LysM RLK were predicted using amino acid sequence submitted to SignalP 6.0 server (Teufel et al., 2022).

4.5.8 Subcellular localization

For imaging of subcellular localization of CbLYK1 and SpLYK, the *N. benthamiana* leaves that were transiently expressing CbLYK-GFP and SpLYK-GFP were used. GFP was detected using an excitation wavelength of 485 nm and emission of 492-540 nm using Leica SP8 FALCON-DIVE confocal system with 40× water immersion lenses. The images were processed using Fiji Image J.

For imaging subcellular localization of chimera constructs, gemma was taken from gemma cup of the transgenic lines carrying respective constructs. mCitrine was excited using 514 nm and emission of 500-550 nm using Zeiss LSM 880 confocal system with 40× water immersion lenses. Z-stack projection images were taken, and the images were processed using Fiji Image J.

4.5.9 Molecular modelling

The three-dimensional structure of AtLYK5 ectodomain (residues 27-278), MpLYK1 ectodomain (residues 29-247), MpLYR ectodomain (residues 24-262), CbLYK1 ectodomain (residues 26-289), and SpLYK ectodomain (residues 22-232) were modelled using AlphaFold2 provided by Colabfold (Jumper et al., 2021). The structure of AtCERK1 ectodomain (4EBZ) was retrieved from protein data bank (RCSB PDB). The ligand was extracted from 4EBZ and was manually docked

to each protein of interest according to surface complementarity with no energy minimization involved. The visualization of three-dimensional structure model and analysis were done using PyMOL by Schrödinger.

4.5.10 Protein expression in insect cells

Bacmid generation

The ectodomains of AtCERK1 (residues 25-230), AtLYK5 (residues 27-278), MpLYK1(residues 29-247), MpLYR (residues 24-262), CbLYK1 (residues 26-289), and SpLYK (residues 22-232) were synthesized and codon optimized for expression in insect cell. 6 × histidine tag was added at the C-terminal and hemolin peptide sequence was added at the N-terminal. The genes were cloned into pFastBac1 vector. Plasmids were transformed into DH10Bac competent cells and incubated on LB medium containing 1 % (w/v) agar with supplemented with antibiotics (50 µg/ml kanamycin sulfate, 7 µg/ml gentamicin, and 10 µg/ml tetracycline, 100 µg/ml X-gal, 40 µg/ml IPTG) for 48 hours. The white colonies were selected for positive bacmids. The bacmids DNA were extracted using alkaline lysis method.

Preparation of P0 and P1 virus

The transfection of bacmids to Sf21 insect cells were performed to generate P0 and P1 virus. Sf21 cells were grown and cultured to a density of 2.0× 10^6 cells/mL in incubator shaker 28°C and 120 rpm. The cells were diluted to 1.0× 10^6 cells/mL, and the cells were seeded to 6 well plate. The cells were allowed to attach for 30 minutes at room temperature and the media were remove and 2 mL of Sf-900™ II SFM medium were added to each well. Transfection mixture were prepared in two Eppendorf tubes. For first tube, 6 µl of Cellfectin®, 100 µl of Sf-900™ II SFM (Thermo Fisher Scientific) medium and 8 µl of purified bacmid were mixed by pipetting. For second tube, 6 µl of Cellfectin® and 100 µl of Sf-900™ II SFM medium (Thermo Fisher Scientific) were mixed. The mixture in first and second tubes were mixed and incubated at room temperature for 30-40 minutes. After that, 800 µl of Sf-900™ II SFM medium were added to the mixture and the transfection mixture were further added into wells containing Sf21 cells. The cells were incubated in 28°C for 6 hours. After 6 hours, the mixture was removed and replaced with Sf-900™ II SFM medium containing 1 × Penicillin-Streptomycin (Gibco, Thermo Fisher Scientific). The cells were incubated at 28°C for 4-5 days. Once Sf21 cells displayed signs of late-stage infection with increasing cell size and detachment, the medium was harvested by centrifugation at 2000 ×g for 5 minutes. The P1 virus was generated by infecting 30 mL of Sf21 cells in the density of 1.0-1.5 × 10^6 cells/mL with P0 virus for 5 days at 28°C and medium were harvested by 2000 ×g for 5 minutes.

Once the P1 virus stock was obtained, it was amplified by infecting more Sf21 cells. The viruses were amplified until a third passage which is P2.

Protein expression and purification

Protein purification steps in this study were performed at 4 °C unless otherwise stated. The protein was expressed in High Five™ cells at 28 °C with shaking at 120 rpm. One liter of High Five™ cells (2.0×10^6 cells/mL) were infected with 30 mL of P2 virus in ESF91 (Expression Systems) medium supplemented with 1 × Penicillin-Streptomycin. The cells were infected for 48 hours. Afterward, the protein was harvested by centrifugation for 6000 ×g at 4 °C and the medium was collected. The collected medium was mixed with 4 mL Nuvia IMAC Affinity Resin (Biorad Laboratories) and incubated for 1 hour at 4 °C. The medium was applied 1.5 × 10 cm gravity Econo-column (Bio-Rad Laboratories) and washed with 10 CV of washing buffer (25 mM Tris HCl pH 8.0, 150 mM NaCl, 30 mM imidazole). The protein was eluted with 20 mL of elution buffer (25 mM Tris HCl pH 8.0, 150 mM NaCl, 500 mM imidazole).

For AtCERK, MpLYK1, and SpLYK, after affinity purification, the proteins were concentrated to 500 µl using centrifugal concentrator 10-kD molecular-mass cut-off Amicon Ultra Filter (Merck Millipore). Proteins were further purified using size exclusion chromatography (SEC) using Superdex 200 Increase 10/300 GL column (Cytiva) connected to Biorad NGC choromtaography system (Biorad Laboratories) using 1 × PBS buffer (137 mM NaCl, 2.7 mM KCl, 10 mM Na_2HPO_4, 1.8 mM KH_2 PO_4 pH 7.0).

For AtLYK5, MpLYR and CbLYK1 ectodomain, 2 mL of concentrated protein was diluted with 4 CV of start buffer (25 mM Tris HCl pH 8.0), were passed through 1 mL HiTrap Capto Q ImpRes anion exchange chromatography column (Cytiva) using syringe manually, washed with 5 CV of start buffer and protein were eluted with up to 10 CV of buffer (25 mM Tris HCl pH 8.0) with increasing salt concentration up to 0.5 M NaCl. Ten fractions (each fraction contained 1 mL of eluted protein) were performed (Tris HCl pH 8.0 with NaCl concentration ranging from 50 mM to 500 mM). All purification fractions were examined using denaturing SDS-PAGE followed by Coomassie blue R-250 staining. The fractions that contained target protein were further collected and concentrated to 500 µl using centrifugal concentrator 10-kD molecular-mass cut-off Amicon Ultra Filter (Merck Millipore). SEC were performed as described before.

The purified samples were checked again with SDS-PAGE followed by Coomassie blue R-250 staining. The proteins concentration was assessed using NanoDrop or Pierce 660 nm Protein Assay Kit (Thermo Fisher Scientific).

4.5.11 Microscale thermophoresis (MST) assay

Proteins were labeled with Monolith His-Tag Labeling Kit RED-tris-NTA 2nd Generation dye (Nanotemper Technologies) according to the manufacturer's instructions. A serial dilution of chitin heptamer (Elicityl) starting from 10 mM using 10 µL was prepared in low-binding microfuge tubes and 10 µL of labeled protein (200 nM final concentration) was added to each serial dilution. The mixtures were incubated for 30 minutes at room temperature to facilitate complex formation. Then, approximately 5-8 µL of each reaction was loaded into a standard Monolith capillary tube (Nanotemper Technologies) where each sample contained MST buffer (1 ×PBS containing 0.05% Tween 20) to prevent aggregation. The capillary tubes were loaded into the Monolith MST machine (Nanotemper Technologies) and ran at 100% excitation power and 50% MST Power at 25°C. Data were analyzed using PALMIST Analysis Software and rendered with GUSSI (Scheuermann et al., 2016). The raw data were imported to PALMIST and 1:1 Kd fitting parameter was applied with 95% CI. The resulting dissociation constant were shown as Kd value. To generate figure, the analyzed data were rendered in GUSSI, upper panel showing data curve of the change in normalized fluorescence (ΔFnorm in [‰]) against the concentration of the ligand and lower panel showing residual of a plot between the fitted line and the data. The error bars represent standard deviation. The binding experiments were performed in three independent replicates.

4.5.12 *In vitro* chitin beads pull-down mass spectrometry (MS) analysis

Three-week-old *M. polymorpha*, 13-day-old *S. pratensis*, 7-day-old *M. endlicherianum*, 3-week-old *A.thaliana* were used. The experiment was performed in cold unless otherwise mentioned. Plant tissues were frozen and ground in liquid nitrogen using mortar and pestles. Total protein was extracted using fresh extraction buffer (50 mM Tris HCl pH 7.5, 150 mM NaCl, 10% glycerol, 2 mM EDTA, 5 mM DTT, 1 % Triton X-100 supplemented with plant protease and phosphatase inhibitor) and incubated for 30 minutes on ice. The samples were centrifuged at 10,000 ×g for 10 minutes and repeated twice. The concentration of total proteins was measured using Pierce 660 nm Protein Assay Kit (Thermo Fisher Scientific). Fifty microliter of chitin magnetic beads (New England Biolabs) or amylose magnetic beads were mixed with 500 µg of total protein, topping up to a final volume of 1 mL. The mixtures were incubated for 3 hours on a rolling wheel. The tubes were washed with wash buffer (50 mM Tris HCl pH 7.5, 150 mM NaCl, 10% glycerol, 2 mM EDTA) for four times. The magnetic beads were kept in -20 °C and submitted to mass spectrometry analysis.

Sample preparation and LC-MS/MS data acquisition.

Enriched proteins were submitted to an on-bead digestion using trypsin. In brief, dry beads were re-dissolved in 25 µL digestion buffer 1 (50 mM Tris, pH 7.5, 2M urea, 1mM DTT, 5 ng/µL trypsin) and incubated for 30 min at 30 °C in a Thermomixer with 400 rpm. Next, beads were pelleted, and the supernatant was transferred to a fresh tube. Digestion buffer 2 (50 mM Tris, pH 7.5, 2M urea, 5 mM CAA) was added to the beads. After mixing the beads were pelleted, the supernatant was collected and combined with the previous one. The combined supernatants were then incubated o/n at 32 °C in a Thermomixer with 400 rpm; samples were protected from light during incubation. The digestion was stopped by adding 1 µL TFA and desalted with C18 Empore disk membranes according to the StageTip protocol (Rappsilber et al, Anal. Chem. 2003, 75, 663.).

Dried peptides were re-dissolved in 2% ACN, 0.1% TFA (10 µL) for analysis. Samples from *A. thaliana*, *M. polymorpha* and *S. pratensis* were analyzed using an EASY-nLC 1200 (Thermo Fisher) coupled to a Q Exactive Plus mass spectrometer (Thermo Fisher). Peptides were separated on 16 cm frit-less silica emitters (MSWil, 75 µm inner diameter), packed in-house with reversed-phase ReproSil-Pur C18 AQ 1.9 µm resin (Dr. Maisch). Peptides were loaded on the column and eluted for 115 min using a segmented linear gradient of 5% to 95% solvent B (0 min : 5%B; 0-5 min -> 5%B; 5-65 min -> 20%B; 65-90 min ->35%B; 90-100 min -> 55%; 100-105 min ->95%, 105-115 min ->95%) (solvent A 0% ACN, 0.1% FA; solvent B 80% ACN, 0.1%FA) at a flow rate of 300 nL/min. Mass spectra were acquired in data-dependent acquisition mode with a TOP15 method. MS spectra were acquired in the Orbitrap analyzer with a mass range of 300–1750 m/z at a resolution of 70,000 FWHM and a target value of 3×10^6 ions. Precursors were selected with an isolation window of 1.3 m/z. HCD fragmentation was performed at a normalized collision energy of 25. MS/MS spectra were acquired with a target value of 10^5 ions at a resolution of 17,500 FWHM, a maximum injection time (max.) of 55 ms and a fixed first mass of m/z 100. Peptides with a charge of +1, greater than 6, or with unassigned charge state were excluded from fragmentation for MS^2, dynamic exclusion for 30s prevented repeated selection of precursors.

Samples from *M. endlicherianum* were analyzed using an Ultimate 3000 RSLC nano (Thermo Fisher) coupled to an Orbitrap Exploris 480 mass spectrometer equipped with a FAIMS Pro interface for Field asymmetric ion mobility separation (Thermo Fisher). Peptides were pre-concentrated on an Acclaim PepMap 100 pre-column (75 µM x 2 cm, C18, 3 µM, 100 Å, Thermo Fisher) using the loading pump and buffer A** (water, 0.1% TFA) with a flow of 7 µl/min for 5 min. Peptides were separated on 16 cm frit-less silica emitters (New Objective, 75 µm inner diameter), packed in-house with reversed-phase ReproSil-Pur C18 AQ 1.9 µm resin (Dr. Maisch).

Peptides were loaded on the column and eluted for 130 min using a segmented linear gradient of 5% to 95% solvent B (0 min : 5%B; 0-5 min -> 5%B; 5-65 min -> 20%B; 65-90 min ->35%B; 90-100 min -> 55%; 100-105 min ->95%, 105-115 min ->95%, 115-115.1 min -> 5%, 115.1-130 min ->5%) (solvent A 0% ACN, 0.1% FA; solvent B 80% ACN, 0.1%FA) at a flow rate of 300 nL/min. Mass spectra were acquired in data-dependent acquisition mode with a TOP_S method using a cycle time of 2 seconds. For field asymmetric ion mobility separation (FAIMS) two compensation voltages (-45 and -60) were applied, the cycle times for both compensation voltages were set to 1 second. MS spectra were acquired in the Orbitrap analyzer with a mass range of 320–1200 m/z at a resolution of 60,000 FWHM and a normalized AGC target of 300%. Precursors were filtered using the MIPS option (MIPS mode = peptide), the intensity threshold was set to 5000, Precursors were selected with an isolation window of 1.6 m/z. HCD fragmentation was performed at a normalized collision energy of 30%. MS/MS spectra were acquired with a target value of 75% ions at a resolution of 15,000 FWHM, at an injection time of 120 ms and a fixed first mass of m/z 120. Peptides with a charge of +1, greater than 6, or with unassigned charge state were excluded from fragmentation for MS2.

Data analysis

Raw data were processed using MaxQuant software (version 1.6.3.4, http://www.maxquant.org/) (Cox et al., Nat. Biotechnol. 2008, 26, 1367.) with label-free quantification (LFQ) and iBAQ enabled (Cox et al., Nat. Protoc. 2016, 11, 2301.). MS/MS spectra were searched by the Andromeda search engine against a combined database containing the sequences from *A. thaliana* (TAIR10_pep_20101214; ftp://ftp.arabidopsis.org/home/tair/Proteins/TAIR10_protein_lists/), *M. polymorpha* (Mp_MpTak_v7.1.protein.fasta, https://marchantia.info/data/MpTak1_v7.1/) and *S. pratensis* (Sp_v1.release.gff3.pep.fasta, provided by Prof. Dr. Jan de Vries) or *M. endlichrianium* (Me_Me1_v2.release.gff3.pep.fasta, Dadras et al., 2023), and sequences of 248 common contaminant proteins and decoy sequences. Trypsin specificity was required and a maximum of two missed cleavages allowed. Minimal peptide length was set to seven amino acids. Carbamidomethylation of cysteine residues was set as fixed, oxidation of methionine and protein N-terminal acetylation as variable modifications. The match between runs option was enabled. Peptide-spectrum-matches and proteins were retained if they were below a false discovery rate of 1% in both cases.

Statistical analysis of the MaxLFQ values was carried out using Perseus (version 1.5.8.5, http://www.maxquant.org/). Quantified proteins were filtered for reverse hits and hits “identified by site” and MaxLFQ values were log2 transformed. After grouping samples by condition only

those proteins were retained for the subsequent analysis that had two valid values in one of the conditions. Two-sample t-tests were performed using a permutation-based FDR of 5%. Alternatively, quantified proteins were grouped by condition and only those hits were retained that had three valid values in one of the conditions. Missing values were imputed from a normal distribution (1.8 downshift, separately for each column). Volcano plots were generated in Perseus using an FDR of 5% and an S0=1. The Perseus output was exported and further processed using Excel. The final volcano plots were plotted using R studio.

4.5.13 Transcriptome analysis

For RNA-seq analysis of *C. braunii*, the algae were treated with water as a mock and 1 µM chitin heptamer for 1 hour. Treatment and total RNA extraction were performed by Prof. Dr. Keiko Sakakibara, Rikkyo University, Tokyo, Japan.

For RNA-seq of *S. pratensis*, 13-day-old algae were harvested from WHM agar plates and transferred to WHM liquid medium in 6-well plates. The algae were incubated in a growth chamber overnight. Next, water or chitin heptamer was added in the final concentration of 1 µM. The algae were treated for 1 hour, 3 hours, and 24 hours. The algae were harvested and frozen in liquid nitrogen. Total RNAs were extracted using Spectrum Plant Total RNA Kit (Sigma Aldrich). Samples were sonicated for 1 minute after addition of lysis solution, the subsequent step were performed according to the manufacturer's instructions. On-column DNAse I treatment was performed using DNAse I solution (Sigma Aldrich). Total RNAs were quantified by a Nanodrop spectrophotometer and samples were frozen in liquid nitrogen and kept in -70 °C before being submitted to Novogene UK for RNA sequencing.

RNA samples were shipped on dry ice to Novogene, UK (https://www.novogene.com/eu-en/) where the samples were quality checked with Bioanalyzer (Agilent Technologies), libraries were prepared and subsequently sequenced on Illumina NovaSeq X Plus platform. The *S. pratensis* MZCH10213 genome was supplied by personal communication from Prof. Dr. Jan de Vries, was used for mapping and counting transcripts per gene in STAR aligner. Genes with less than the average of 10 read counts were excluded, and DESeq2 was used for raw count normalization and differentially expressed gene (DEG) analyses. RNA sequencing analysis was performed by Gabriel X. Garcia Ramírez.

4.5.14 ROS burst measurement

For ROS burst measurement in algae, 13-day-old *S. pratensis* or plantlets of *C. braunii* were harvested and transferred to 96-well-plate and were incubated in WHM liquid medium (for *S. pratensis*) or water (for *C. braunii*). The algae were washed with water 3 times and the water were removed. Twenty micromolar L-O12 solutions were added and incubated in the dark for 3 hours at room temperature. At least three technical replicates were performed. The chitin heptamer was dissolved in water supplemented with 2.5 units/mL HRP to desired concentration (2x). The mock solution was prepared in elicitor-free Milli-Q water supplemented with 2.5 units/mL HRP. After incubation with luminol, 100 µL of the 2 × concentration of chitin heptamer and mock solutions were added to the samples and relative RLU were measured in a plate reader.

For ROS burst measurement in *M. polymorpha*, the gemmae from corresponding phenotype were collected from the gemma cups using a sterile tweezer and resuspended in 50 mL liquid ½ Gamborg's B5 medium supplemented with 0.1% sucrose in a 250 mL Erlenmeyer flask and were then cultured in a walk-in growth chamber under 50–60 µmol photons $m^{-2}s^{-1}$ continuous white LED at 22 °C for 7 days, while shaking at 200 rpm. The gemmae were transferred to 50 mL falcon tubes and washed three times with water. Five gemmae of each genotype were carefully transferred into 100 µL water containing 20 µM L-O12. For each genotype and treatment, at least three technical replicates were used. The samples were incubated overnight in dark for 3 hours at room temperature. The chitin heptamer supplemented with 2.5 units/mL HRP to a final concentration of 2 µM (2 ×). The mock solution was prepared in elicitor-free Milli-Q water supplemented with 2.5 units/mL HRP. After incubation with luminol, 100 µL of the 2 × concentration of chitin heptamer and mock solutions were added to the samples and relative RLU were measured in a plate reader.

4.5.15 FRET-FLIM

FRET-FLIM analyses were conducted in transiently expressed *N. benthamiana* plants of 4 to 6 weeks old using a Leica SP8 FALCON-DIVE confocal system, equipped with an InSight X3 pulsed laser from Spectra Physics with a fixed laser line of 1045 and a line tunable from 680 to 1300 nm, in combination with 40x/1.10 W immersion objective. The leaves were transiently expressed with either only with GFP as donor in absence of mCherry as acceptor, or in combination of mCherry. The leaves were punched in pieces in diameter of 5 mM, mounted on microscope slides in water and covered with high precision cover glass. After that, the leaves were used for analysis of fluorescence lifetime. For imaging and FLIM experiments, GFP was excited with 930 nm and the

emission window from 490 to 550 nm was recorded with the RLD detector. To observe FRET between GFP as donor and mCherry as acceptor, only the donor fluorescence was recorded for lifetime imaging. Images with a frame size of 512 by 512 pixels were acquired until a minimum level of 1000 photons was reached for the maximum pixel value. The fluorescence decays of donor only were analyzed to determine the average lifetime using a mono- or biexponential fitting model in the LAS X software (Leica, Germany) and the mean τ intensity weighted lifetimes (ns) were calculated. Regions of interest (ROIs) that showed specific fluorescence of the transformed protein(s) were defined manually. Importantly, areas with contaminating fluorescence signals stemming from subtending or adjacent plastids were excluded. Similarly, the cuticle, regions with stomatal autofluorescence, and air inclusions were avoided.

5. References

Agarwal, V., & McShan, A. C. (2024). The power and pitfalls of AlphaFold2 for structure prediction beyond rigid globular proteins. *Nat Chem Biol*, *20*(8), 950-959. https://doi.org/10.1038/s41589-024-01638-w

Akamatsu, A., Wong, H. L., Fujiwara, M., Okuda, J., Nishide, K., Uno, K., Imai, K., Umemura, K., Kawasaki, T., Kawano, Y., & Shimamoto, K. (2013). An OsCEBiP/OsCERK1-OsRacGEF1-OsRac1 module is an essential early component of chitin-induced rice immunity. *Cell Host Microbe*, *13*(4), 465-476. https://doi.org/10.1016/j.chom.2013.03.007

Akcapinar, G. B., Kappel, L., Sezerman, O. U., & Seidl-Seiboth, V. (2015). Molecular diversity of LysM carbohydrate-binding motifs in fungi. *Curr Genet*, *61*(2), 103-113. https://doi.org/10.1007/s00294-014-0471-9

Akdel, M., Pires, D. E. V., Pardo, E. P., Jänes, J., Zalevsky, A. O., Mészáros, B., Bryant, P., Good, L. L., Laskowski, R. A., Pozzati, G., Shenoy, A., Zhu, W., Kundrotas, P., Serra, V. R., Rodrigues, C. H. M., Dunham, A. S., Burke, D., Borkakoti, N., Velankar, S., . . . Beltrao, P. (2022). A structural biology community assessment of AlphaFold2 applications. *Nat Struct Mol Biol*, *29*(11), 1056-1067. https://doi.org/10.1038/s41594-022-00849-w

Albert, I., Hua, C., Nürnberger, T., Pruitt, R. N., & Zhang, L. (2020). Surface Sensor Systems in Plant Immunity. *Plant Physiology*, *182*(4), 1582-1596. https://doi.org/10.1104/pp.19.01299

Bateman, A., & Bycroft, M. (2000). The structure of a LysM domain from *E. coli* membrane-bound lytic murein transglycosylase D (MltD). *Journal of Molecular Biology*, *299*(4), 1113-1119. https://doi.org/https://doi.org/10.1006/jmbi.2000.3778

Battistuzzi, F. U., Feijao, A., & Hedges, S. B. (2004). A genomic timescale of prokaryote evolution: insights into the origin of methanogenesis, phototrophy, and the colonization of land. *BMC Evol Biol*, *4*, 44. https://doi.org/10.1186/1471-2148-4-44

Beakes, G. W., Glockling, S. L., & Sekimoto, S. (2012). The evolutionary phylogeny of the oomycete "fungi". *Protoplasma*, *249*(1), 3-19. https://doi.org/10.1007/s00709-011-0269-2

Betts, H. C., Puttick, M. N., Clark, J. W., Williams, T. A., Donoghue, P. C. J., & Pisani, D. (2018). Integrated genomic and fossil evidence illuminates life's early evolution and eukaryote origin. *Nature Ecology & Evolution*, *2*(10), 1556-1562. https://doi.org/10.1038/s41559-018-0644-x

Bi, G., Zhou, Z., Wang, W., Li, L., Rao, S., Wu, Y., Zhang, X., Menke, F. L. H., Chen, S., & Zhou, J. M. (2018). Receptor-Like Cytoplasmic Kinases Directly Link Diverse Pattern Recognition Receptors to the Activation of Mitogen-Activated Protein Kinase Cascades in Arabidopsis. *Plant Cell*, *30*(7), 1543-1561. https://doi.org/10.1105/tpc.17.00981

Boutrot, F., & Zipfel, C. (2017). Function, Discovery, and Exploitation of Plant Pattern Recognition Receptors for Broad-Spectrum Disease Resistance. *Annual Review of Phytopathology*, *55*(Volume 55, 2017), 257-286. https://doi.org/https://doi.org/10.1146/annurev-phyto-080614-120106

Bozsoki, Z., Cheng, J., Feng, F., Gysel, K., Vinther, M., Andersen, K. R., Oldroyd, G., Blaise, M., Radutoiu, S., & Stougaard, J. (2017). Receptor-mediated chitin perception in legume roots is functionally separable from Nod factor perception. *Proc Natl Acad Sci U S A*, *114*(38), E8118-e8127. https://doi.org/10.1073/pnas.1706795114

Broghammer, A., Krusell, L., Blaise, M., Sauer, J., Sullivan, J. T., Maolanon, N., Vinther, M., Lorentzen, A., Madsen, E. B., Jensen, K. J., Roepstorff, P., Thirup, S., Ronson, C. W., Thygesen, M. B., & Stougaard, J. (2012). Legume receptors perceive the rhizobial lipochitin oligosaccharide signal molecules by direct binding. *Proc Natl Acad Sci U S A*, *109*(34), 13859-13864. https://doi.org/10.1073/pnas.1205171109

Buendia, L., Girardin, A., Wang, T., Cottret, L., & Lefebvre, B. (2018). LysM Receptor-Like Kinase and LysM Receptor-Like Protein Families: An Update on Phylogeny and Functional Characterization [Review]. *Frontiers in Plant Science*, *9*. https://www.frontiersin.org/journals/plant-science/articles/10.3389/fpls.2018.01531

Buist, G., Steen, A., Kok, J., & Kuipers, O. P. (2008). LysM, a widely distributed protein motif for binding to (peptido)glycans. *Molecular Microbiology*, *68*(4), 838-847. https://doi.org/https://doi.org/10.1111/j.1365-2958.2008.06211.x

Cao, Y., Liang, Y., Tanaka, K., Nguyen, C. T., Jedrzejczak, R. P., Joachimiak, A., & Stacey, G. (2014). The kinase LYK5 is a major chitin receptor in Arabidopsis and forms a chitin-induced complex with related kinase CERK1. *Elife*, *3*, e03766. https://doi.org/10.7554/eLife.03766

Carotenuto, G., Chabaud, M., Miyata, K., Capozzi, M., Takeda, N., Kaku, H., Shibuya, N., Nakagawa, T., Barker, D. G., & Genre, A. (2017). The rice LysM receptor-like kinase OsCERK1 is required for the perception of short-chain chitin oligomers in arbuscular mycorrhizal signaling. *New Phytol*, *214*(4), 1440-1446. https://doi.org/10.1111/nph.14539

Chang, Y., Wang, S., Sekimoto, S., Aerts, A. L., Choi, C., Clum, A., LaButti, K. M., Lindquist, E. A., Yee Ngan, C., Ohm, R. A., Salamov, A. A., Grigoriev, I. V., Spatafora, J. W., &

Berbee, M. L. (2015). Phylogenomic Analyses Indicate that Early Fungi Evolved Digesting Cell Walls of Algal Ancestors of Land Plants. *Genome Biology and Evolution*, *7*(6), 1590-1601. https://doi.org/10.1093/gbe/evv090

Cheval, C., Samwald, S., Johnston, M. G., de Keijzer, J., Breakspear, A., Liu, X., Bellandi, A., Kadota, Y., Zipfel, C., & Faulkner, C. (2020). Chitin perception in plasmodesmata characterizes submembrane immune-signaling specificity in plants. *Proceedings of the National Academy of Sciences*, *117*(17), 9621-9629. https://doi.org/10.1073/pnas.1907799117

DeFalco, T. A., & Zipfel, C. (2021). Molecular mechanisms of early plant pattern-triggered immune signaling. *Molecular Cell*, *81*(17), 3449-3467. https://doi.org/https://doi.org/10.1016/j.molcel.2021.07.029

del Hierro, I., Mélida, H., Broyart, C., Santiago, J., & Molina, A. (2021). Computational prediction method to decipher receptor–glycoligand interactions in plant immunity. *The Plant Journal*, *105*(6), 1710-1726. https://doi.org/https://doi.org/10.1111/tpj.15133

Delaux, P.-M., Radhakrishnan, G. V., Jayaraman, D., Cheema, J., Malbreil, M., Volkening, J. D., Sekimoto, H., Nishiyama, T., Melkonian, M., Pokorny, L., Rothfels, C. J., Sederoff, H. W., Stevenson, D. W., Surek, B., Zhang, Y., Sussman, M. R., Dunand, C., Morris, R. J., Roux, C., . . . Ané, J.-M. (2015). Algal ancestor of land plants was preadapted for symbiosis. *Proceedings of the National Academy of Sciences*, *112*(43), 13390-13395. https://doi.org/doi:10.1073/pnas.1515426112

Delaux, P.-M., & Schornack, S. (2021). Plant evolution driven by interactions with symbiotic and pathogenic microbes. *Science*, *371*(6531), eaba6605. https://doi.org/10.1126/science.aba6605

Dubiella, U., Seybold, H., Durian, G., Komander, E., Lassig, R., Witte, C.-P., Schulze, W. X., & Romeis, T. (2013). Calcium-dependent protein kinase/NADPH oxidase activation circuit is required for rapid defense signal propagation. *Proceedings of the National Academy of Sciences*, *110*(21), 8744-8749. https://doi.org/10.1073/pnas.1221294110

Faulkner, C., Petutschnig, E., Benitez-Alfonso, Y., Beck, M., Robatzek, S., Lipka, V., & Maule, A. J. (2013). LYM2-dependent chitin perception limits molecular flux via plasmodesmata. *Proceedings of the National Academy of Sciences*, *110*(22), 9166-9170. https://doi.org/10.1073/pnas.1203458110

Forterre, P. (2006). The origin of viruses and their possible roles in major evolutionary transitions. *Virus Research*, *117*(1), 5-16. https://doi.org/https://doi.org/10.1016/j.virusres.2006.01.010

Fürst-Jansen, J. M. R., de Vries, S., & de Vries, J. (2020). Evo-physio: on stress responses and the earliest land plants. *Journal of Experimental Botany*, *71*(11), 3254-3269. https://doi.org/10.1093/jxb/eraa007

Garvey, K. J., Saedi, M. S., & Ito, J. (1986). Nucleotide sequence of Bacillus phage phi 29 genes 14 and 15: homology of gene 15 with other phage lysozymes. *Nucleic Acids Res*, *14*(24), 10001-10008. https://doi.org/10.1093/nar/14.24.10001

Ge, D., Yeo, I. C., & Shan, L. (2022). Knowing me, knowing you: Self and non-self recognition in plant immunity. *Essays Biochem*, *66*(5), 447-458. https://doi.org/10.1042/ebc20210095

Giovannoni, M., Lironi, D., Marti, L., Paparella, C., Vecchi, V., Gust, A. A., De Lorenzo, G., Nürnberger, T., & Ferrari, S. (2021). The Arabidopsis thaliana LysM-containing Receptor-Like Kinase 2 is required for elicitor-induced resistance to pathogens. *Plant, Cell & Environment*, *44*(12), 3775-3792. https://doi.org/https://doi.org/10.1111/pce.14192

Gong, Z., & Han, G.-Z. (2021). Flourishing in water: the early evolution and diversification of plant receptor-like kinases. *The Plant Journal*, *106*(1), 174-184. https://doi.org/https://doi.org/10.1111/tpj.15157

Gow Neil, A. R., Latge, J.-P., & Munro Carol, A. (2017). The Fungal Cell Wall: Structure, Biosynthesis, and Function. *Microbiology Spectrum*, *5*(3), 10.1128/microbiolspec.funk-0035-2016. https://doi.org/10.1128/microbiolspec.funk-0035-2016

Gust, A. A., Pruitt, R., & Nürnberger, T. (2017). Sensing Danger: Key to Activating Plant Immunity. *Trends Plant Sci*, *22*(9), 779-791. https://doi.org/10.1016/j.tplants.2017.07.005

Gysel, K., Hansen, S. B., Rübsam, H., Alsarraf, H. M. A. B., Madland, E., Cheng, J. X. J., Baadegaard, C., Poulsen, E. C., Vinther, M., Fort, S., Stougaard, J., & Andersen, K. R. (2025). Structural basis for size-selective perception of chitin in plants. *bioRxiv*, 2025.2007.2009.663820. https://doi.org/10.1101/2025.07.09.663820

Han, G.-Z. (2019). Origin and evolution of the plant immune system. *New Phytologist*, *222*(1), 70-83. https://doi.org/https://doi.org/10.1111/nph.15596

Hayafune, M., Berisio, R., Marchetti, R., Silipo, A., Kayama, M., Desaki, Y., Arima, S., Squeglia, F., Ruggiero, A., Tokuyasu, K., Molinaro, A., Kaku, H., & Shibuya, N. (2014). Chitin-induced activation of immune signaling by the rice receptor CEBiP relies on a unique sandwich-type dimerization. *Proceedings of the National Academy of Sciences*, *111*(3), E404-E413. https://doi.org/10.1073/pnas.1312099111

He, J., Zhang, C., Dai, H., Liu, H., Zhang, X., Yang, J., Chen, X., Zhu, Y., Wang, D., Qi, X., Li, W., Wang, Z., An, G., Yu, N., He, Z., Wang, Y.-F., Xiao, Y., Zhang, P., & Wang, E. (2019). A LysM Receptor Heteromer Mediates Perception of Arbuscular Mycorrhizal

Symbiotic Signal in Rice. *Molecular Plant*, *12*(12), 1561-1576. https://doi.org/https://doi.org/10.1016/j.molp.2019.10.015

Hess, S., Williams, S. K., Busch, A., Irisarri, I., Delwiche, C. F., de Vries, S., Darienko, T., Roger, A. J., Archibald, J. M., Buschmann, H., von Schwartzenberg, K., & de Vries, J. (2022). A phylogenomically informed five-order system for the closest relatives of land plants. *Curr Biol*, *32*(20), 4473-4482.e4477. https://doi.org/10.1016/j.cub.2022.08.022

Hoang, D. T., Chernomor, O., von Haeseler, A., Minh, B. Q., & Vinh, L. S. (2018). UFBoot2: Improving the Ultrafast Bootstrap Approximation. *Mol Biol Evol*, *35*(2), 518-522. https://doi.org/10.1093/molbev/msx281

Holzhausen, A., Stingl, N., Rieth, S., Kühn, C., Schubert, H., & Rensing, S. A. (2022). Establishment and optimization of a new model organism to study early land plant evolution: Germination, cultivation and oospore variation of *Chara braunii* Gmelin, 1826 [Original Research]. *Frontiers in Plant Science*, *Volume 13 - 2022*. https://www.frontiersin.org/journals/plant-science/articles/10.3389/fpls.2022.987741

Igarashi, D., Bethke, G., Xu, Y., Tsuda, K., Glazebrook, J., & Katagiri, F. (2013). Pattern-Triggered Immunity Suppresses Programmed Cell Death Triggered by Fumonisin B1. *PLOS ONE*, *8*(4), e60769. https://doi.org/10.1371/journal.pone.0060769

Ishizaki, K., Nishihama, R., Ueda, M., Inoue, K., Ishida, S., Nishimura, Y., Shikanai, T., & Kohchi, T. (2015). Development of Gateway Binary Vector Series with Four Different Selection Markers for the Liverwort Marchantia polymorpha. *PLOS ONE*, *10*(9), e0138876. https://doi.org/10.1371/journal.pone.0138876

Jones, J. D. G., & Dangl, J. L. (2006). The plant immune system. *Nature*, *444*(7117), 323-329. https://doi.org/10.1038/nature05286

Jones, J. D. G., Staskawicz, B. J., & Dangl, J. L. (2024). The plant immune system: From discovery to deployment. *Cell*, *187*(9), 2095-2116. https://doi.org/10.1016/j.cell.2024.03.045

Jumper, J., Evans, R., Pritzel, A., Green, T., Figurnov, M., Ronneberger, O., Tunyasuvunakool, K., Bates, R., Žídek, A., Potapenko, A., Bridgland, A., Meyer, C., Kohl, S. A. A., Ballard, A. J., Cowie, A., Romera-Paredes, B., Nikolov, S., Jain, R., Adler, J., . . . Hassabis, D. (2021). Highly accurate protein structure prediction with AlphaFold. *Nature*, *596*(7873), 583-589. https://doi.org/10.1038/s41586-021-03819-2

Kadota, Y., Shirasu, K., & Zipfel, C. (2015). Regulation of the NADPH Oxidase RBOHD During Plant Immunity. *Plant Cell Physiol*, *56*(8), 1472-1480. https://doi.org/10.1093/pcp/pcv063

Kadota, Y., Sklenar, J., Derbyshire, P., Stransfeld, L., Asai, S., Ntoukakis, V., Jones, Jonathan D., Shirasu, K., Menke, F., Jones, A., & Zipfel, C. (2014). Direct Regulation of the NADPH Oxidase RBOHD by the PRR-Associated Kinase BIK1 during Plant Immunity. *Molecular Cell*, *54*(1), 43-55. https://doi.org/https://doi.org/10.1016/j.molcel.2014.02.021

Kaku, H., Nishizawa, Y., Ishii-Minami, N., Akimoto-Tomiyama, C., Dohmae, N., Takio, K., Minami, E., & Shibuya, N. (2006). Plant cells recognize chitin fragments for defense signaling through a plasma membrane receptor. *Proceedings of the National Academy of Sciences*, *103*(29), 11086-11091. https://doi.org/10.1073/pnas.0508882103

Kalyaanamoorthy, S., Minh, B. Q., Wong, T. K. F., von Haeseler, A., & Jermiin, L. S. (2017). ModelFinder: fast model selection for accurate phylogenetic estimates. *Nature Methods*, *14*(6), 587-589. https://doi.org/10.1038/nmeth.4285

Katoh, K., Rozewicki, J., & Yamada, K. D. (2019). MAFFT online service: multiple sequence alignment, interactive sequence choice and visualization. *Briefings in Bioinformatics*, *20*(4), 1160-1166. https://doi.org/10.1093/bib/bbx108

Kawai, J., Kanazawa, M., Suzuki, R., Kikuchi, N., Hayakawa, Y., & Sekimoto, H. (2022). Highly efficient transformation of the model zygnematophycean alga *Closterium peracerosum-strigosum-littorale* complex by square-pulse electroporation. *New Phytologist*, *233*(1), 569-578. https://doi.org/https://doi.org/10.1111/nph.17763

Kobayashi, M., Ohura, I., Kawakita, K., Yokota, N., Fujiwara, M., Shimamoto, K., Doke, N., & Yoshioka, H. (2007). Calcium-dependent protein kinases regulate the production of reactive oxygen species by potato NADPH oxidase. *Plant Cell*, *19*(3), 1065-1080. https://doi.org/10.1105/tpc.106.048884

Kumar, S., Stecher, G., Suleski, M., & Hedges, S. B. (2017). TimeTree: A Resource for Timelines, Timetrees, and Divergence Times. *Molecular Biology and Evolution*, *34*(7), 1812-1819. https://doi.org/10.1093/molbev/msx116

Lefebvre, B., Klaus-Heisen, D., Pietraszewska-Bogiel, A., Hervé, C., Camut, S., Auriac, M.-C., Gasciolli, V., Nurisso, A., Gadella, T. W. J., & Cullimore, J. (2012). Role of N-Glycosylation Sites and CXC Motifs in Trafficking of Medicago truncatula Nod Factor Perception Protein to Plasma Membrane. *Journal of Biological Chemistry*, *287*(14), 10812-10823. https://doi.org/https://doi.org/10.1074/jbc.M111.281634

Li, L., Li, M., Yu, L., Zhou, Z., Liang, X., Liu, Z., Cai, G., Gao, L., Zhang, X., Wang, Y., Chen, S., & Zhou, J. M. (2014). The FLS2-associated kinase BIK1 directly phosphorylates the NADPH oxidase RbohD to control plant immunity. *Cell Host Microbe*, *15*(3), 329-338. https://doi.org/10.1016/j.chom.2014.02.009

Liang, Y., Cao, Y., Tanaka, K., Thibivilliers, S., Wan, J., Choi, J., Kang, C. h., Qiu, J., & Stacey, G. (2013). Nonlegumes Respond to Rhizobial Nod Factors by Suppressing the Innate Immune Response. *Science*, *341*(6152), 1384-1387. https://doi.org/10.1126/science.1242736

Liu, J., Liu, B., Chen, S., Gong, B.-Q., Chen, L., Zhou, Q., Xiong, F., Wang, M., Feng, D., Li, J.-F., Wang, H.-B., & Wang, J. (2018). A Tyrosine Phosphorylation Cycle Regulates Fungal Activation of a Plant Receptor Ser/Thr Kinase. *Cell Host & Microbe*, *23*(2), 241-253.e246. https://doi.org/https://doi.org/10.1016/j.chom.2017.12.005

Liu, S., Wang, J., Han, Z., Gong, X., Zhang, H., & Chai, J. (2016). Molecular Mechanism for Fungal Cell Wall Recognition by Rice Chitin Receptor OsCEBiP. *Structure*, *24*(7), 1192-1200. https://doi.org/https://doi.org/10.1016/j.str.2016.04.014

Liu, T., Liu, Z., Song, C., Hu, Y., Han, Z., She, J., Fan, F., Wang, J., Jin, C., Chang, J., Zhou, J.-M., & Chai, J. (2012). Chitin-Induced Dimerization Activates a Plant Immune Receptor. *Science*, *336*(6085), 1160-1164. https://doi.org/10.1126/science.1218867

Loron, C. C., François, C., Rainbird, R. H., Turner, E. C., Borensztajn, S., & Javaux, E. J. (2019). Early fungi from the Proterozoic era in Arctic Canada. *Nature*, *570*(7760), 232-235. https://doi.org/10.1038/s41586-019-1217-0

Lu, Y., & Tsuda, K. (2020). Intimate Association of PRR- and NLR-Mediated Signaling in Plant Immunity. *Molecular Plant-Microbe Interactions®*, *34*(1), 3-14. https://doi.org/10.1094/MPMI-08-20-0239-IA

Madsen, E. B., Antolín-Llovera, M., Grossmann, C., Ye, J., Vieweg, S., Broghammer, A., Krusell, L., Radutoiu, S., Jensen, O. N., Stougaard, J., & Parniske, M. (2011). Autophosphorylation is essential for the in vivo function of the Lotus japonicus Nod factor receptor 1 and receptor-mediated signalling in cooperation with Nod factor receptor 5. *Plant J*, *65*(3), 404-417. https://doi.org/10.1111/j.1365-313X.2010.04431.x

Mélida, H., Sopeña-Torres, S., Bacete, L., Garrido-Arandia, M., Jordá, L., López, G., Muñoz-Barrios, A., Pacios, L. F., & Molina, A. (2018). Non-branched β-1,3-glucan oligosaccharides trigger immune responses in Arabidopsis. *The Plant Journal*, *93*(1), 34-49. https://doi.org/https://doi.org/10.1111/tpj.13755

Mesnage, S., Dellarole, M., Baxter, N. J., Rouget, J.-B., Dimitrov, J. D., Wang, N., Fujimoto, Y., Hounslow, A. M., Lacroix-Desmazes, S., Fukase, K., Foster, S. J., & Williamson, M. P. (2014). Molecular basis for bacterial peptidoglycan recognition by LysM domains. *Nature Communications*, *5*(1), 4269. https://doi.org/10.1038/ncomms5269

Mittendorf, J., Niebisch, J. M., Pierdzig, L., Sun, S., Petutschnig, E. K., & Lipka, V. (2024). Differential contribution of Arabidopsis chitin receptor complex components to defense signaling and ubiquitination-dependent endocytotic removal from the plasma membrane. *New Phytologist*, *244*(3), 934-948. https://doi.org/https://doi.org/10.1111/nph.20074

Miya, A., Albert, P., Shinya, T., Desaki, Y., Ichimura, K., Shirasu, K., Narusaka, Y., Kawakami, N., Kaku, H., & Shibuya, N. (2007). CERK1, a LysM receptor kinase, is essential for chitin elicitor signaling in Arabidopsis. *Proc Natl Acad Sci U S A*, *104*(49), 19613-19618. https://doi.org/10.1073/pnas.0705147104

Monaghan, J., Matschi, S., Shorinola, O., Rovenich, H., Matei, A., Segonzac, C., Malinovsky, Frederikke G., Rathjen, John P., MacLean, D., Romeis, T., & Zipfel, C. (2014). The Calcium-Dependent Protein Kinase CPK28 Buffers Plant Immunity and Regulates BIK1 Turnover. *Cell Host & Microbe*, *16*(5), 605-615. https://doi.org/https://doi.org/10.1016/j.chom.2014.10.007

Naranjo-Ortiz, M. A., & Gabaldón, T. (2019). Fungal evolution: major ecological adaptations and evolutionary transitions. *Biological Reviews*, *94*(4), 1443-1476. https://doi.org/https://doi.org/10.1111/brv.12510

Ngou, B. P. M., Ahn, H.-K., Ding, P., & Jones, J. D. G. (2021). Mutual potentiation of plant immunity by cell-surface and intracellular receptors. *Nature*, *592*(7852), 110-115. https://doi.org/10.1038/s41586-021-03315-7

Ngou, B. P. M., Ding, P., & Jones, J. D. G. (2022). Thirty years of resistance: Zig-zag through the plant immune system. *The Plant Cell*, *34*(5), 1447-1478. https://doi.org/10.1093/plcell/koac041

Ngou, B. P. M., Wyler, M., Schmid, M. W., Kadota, Y., & Shirasu, K. (2024). Evolutionary trajectory of pattern recognition receptors in plants. *Nature Communications*, *15*(1), 308. https://doi.org/10.1038/s41467-023-44408-3

Nishiyama, T., Sakayama, H., de Vries, J., Buschmann, H., Saint-Marcoux, D., Ullrich, K. K., Haas, F. B., Vanderstraeten, L., Becker, D., Lang, D., Vosolsobě, S., Rombauts, S., Wilhelmsson, P. K. I., Janitza, P., Kern, R., Heyl, A., Rümpler, F., Villalobos, L., Clay, J. M., . . . Rensing, S. A. (2018). The Chara Genome: Secondary Complexity and Implications for Plant Terrestrialization. *Cell*, *174*(2), 448-464.e424. https://doi.org/10.1016/j.cell.2018.06.033

Oguiza, J. A. (2022). LysM proteins in mammalian fungal pathogens. *Fungal Biology Reviews*, *40*, 114-122. https://doi.org/https://doi.org/10.1016/j.fbr.2022.02.001

Paparella, C., Savatin, D. V., Marti, L., De Lorenzo, G., & Ferrari, S. (2014). The Arabidopsis LYSIN MOTIF-CONTAINING RECEPTOR-LIKE KINASE3 regulates the cross talk between immunity and abscisic acid responses. *Plant Physiol*, *165*(1), 262-276. https://doi.org/10.1104/pp.113.233759

Perini, L., Sipes, K., Zervas, A., Bellas, C., Lutz, S., Moniruzzaman, M., Mourot, R., Benning, L. G., Tranter, M., & Anesio, A. M. (2024). Giant viral signatures on the Greenland ice sheet. *Microbiome*, *12*(1), 91. https://doi.org/10.1186/s40168-024-01796-y

Petutschnig, E. K., Pierdzig, L., Mittendorf, J., Niebisch, J. M., & Lipka, V. (2024). A novel fluorescent protein pair facilitates FLIM-FRET analysis of plant immune receptor interaction under native conditions. *J Exp Bot*, *75*(3), 746-759. https://doi.org/10.1093/jxb/erad418

Ponce De LeÓN, I., Schmelz, E. A., Gaggero, C., Castro, A., ÁLvarez, A., & Montesano, M. (2012). Physcomitrella patens activates reinforcement of the cell wall, programmed cell death and accumulation of evolutionary conserved defence signals, such as salicylic acid and 12-oxo-phytodienoic acid, but not jasmonic acid, upon Botrytis cinerea infection. *Molecular Plant Pathology*, *13*(8), 960-974. https://doi.org/https://doi.org/10.1111/j.1364-3703.2012.00806.x

Pruitt, R. N., Locci, F., Wanke, F., Zhang, L., Saile, S. C., Joe, A., Karelina, D., Hua, C., Fröhlich, K., Wan, W.-L., Hu, M., Rao, S., Stolze, S. C., Harzen, A., Gust, A. A., Harter, K., Joosten, M. H. A. J., Thomma, B. P. H. J., Zhou, J.-M., . . . Nürnberger, T. (2021). The EDS1–PAD4–ADR1 node mediates Arabidopsis pattern-triggered immunity. *Nature*, *598*(7881), 495-499. https://doi.org/10.1038/s41586-021-03829-0

Radutoiu, S., Madsen, L. H., Madsen, E. B., Felle, H. H., Umehara, Y., Grønlund, M., Sato, S., Nakamura, Y., Tabata, S., Sandal, N., & Stougaard, J. (2003). Plant recognition of symbiotic bacteria requires two LysM receptor-like kinases. *Nature*, *425*(6958), 585-592. https://doi.org/10.1038/nature02039

Radutoiu, S., Madsen, L. H., Madsen, E. B., Jurkiewicz, A., Fukai, E., Quistgaard, E. M., Albrektsen, A. S., James, E. K., Thirup, S., & Stougaard, J. (2007). LysM domains mediate lipochitin-oligosaccharide recognition and Nfr genes extend the symbiotic host range. *Embo j*, *26*(17), 3923-3935. https://doi.org/10.1038/sj.emboj.7601826

Redkar, A., Gimenez Ibanez, S., Sabale, M., Zechmann, B., Solano, R., & Di Pietro, A. (2022). Marchantia polymorpha model reveals conserved infection mechanisms in the vascular wilt fungal pathogen Fusarium oxysporum. *New Phytologist*, *234*(1), 227-241. https://doi.org/https://doi.org/10.1111/nph.17909

Reymond, P. (2021). Receptor kinases in plant responses to herbivory. *Current Opinion in Biotechnology*, *70*, 143-150. https://doi.org/https://doi.org/10.1016/j.copbio.2021.04.004

Robert, X., & Gouet, P. (2014). Deciphering key features in protein structures with the new ENDscript server. *Nucleic Acids Res*, *42*(Web Server issue), W320-324. https://doi.org/10.1093/nar/gku316

Salamaga, B., Turner, R. D., Elsarmane, F., Galley, N. F., Kulakauskas, S., & Mesnage, S. (2023). A moonlighting role for LysM peptidoglycan binding domains underpins Enterococcus faecalis daughter cell separation. *Communications Biology*, *6*(1), 428. https://doi.org/10.1038/s42003-023-04808-z

Sánchez-Vallet, A., Saleem-Batcha, R., Kombrink, A., Hansen, G., Valkenburg, D.-J., Thomma, B. P. H. J., & Mesters, J. R. (2013). Fungal effector Ecp6 outcompetes host immune receptor for chitin binding through intrachain LysM dimerization. *Elife*, *2*, e00790. https://doi.org/10.7554/eLife.00790

Scheuermann, T. H., Padrick, S. B., Gardner, K. H., & Brautigam, C. A. (2016). On the acquisition and analysis of microscale thermophoresis data. *Anal Biochem*, *496*, 79-93. https://doi.org/10.1016/j.ab.2015.12.013

Shimizu, T., Nakano, T., Takamizawa, D., Desaki, Y., Ishii-Minami, N., Nishizawa, Y., Minami, E., Okada, K., Yamane, H., Kaku, H., & Shibuya, N. (2010). Two LysM receptor molecules, CEBiP and OsCERK1, cooperatively regulate chitin elicitor signaling in rice. *Plant J*, *64*(2), 204-214. https://doi.org/10.1111/j.1365-313X.2010.04324.x

Shinya, T., Yamaguchi, K., Desaki, Y., Yamada, K., Narisawa, T., Kobayashi, Y., Maeda, K., Suzuki, M., Tanimoto, T., Takeda, J., Nakashima, M., Funama, R., Narusaka, M., Narusaka, Y., Kaku, H., Kawasaki, T., & Shibuya, N. (2014). Selective regulation of the chitin-induced defense response by the Arabidopsis receptor-like cytoplasmic kinase PBL27. *The Plant Journal*, *79*(1), 56-66. https://doi.org/https://doi.org/10.1111/tpj.12535

Somssich, M., & Simon, R. (2017). Studying Protein-Protein Interactions In Planta Using Advanced Fluorescence Microscopy. *Methods Mol Biol*, *1610*, 267-285. https://doi.org/10.1007/978-1-4939-7003-2_17

Strother, P. K., Battison, L., Brasier, M. D., & Wellman, C. H. (2011). Earth's earliest non-marine eukaryotes. *Nature*, *473*(7348), 505-509. https://doi.org/10.1038/nature09943

Suzuki, M., Shibuya, M., Shimada, H., Motoyama, N., Nakashima, M., Takahashi, S., Suto, K., Yoshida, I., Matsui, S., Tsujimoto, N., Ohnishi, M., Ishibashi, Y., Fujimoto, Z., Desaki, Y., Kaku, H., Kito, K., & Shibuya, N. (2016). Autophosphorylation of Specific Threonine and Tyrosine Residues in Arabidopsis CERK1 is Essential for the Activation of Chitin-

Induced Immune Signaling. *Plant Cell Physiol*, *57*(11), 2312-2322. https://doi.org/10.1093/pcp/pcw150

Suzuki, M., Watanabe, T., Yoshida, I., Kaku, H., & Shibuya, N. (2018). Autophosphorylation site Y428 is essential for the in vivo activation of CERK1. *Plant Signal Behav*, *13*(2), e1435228. https://doi.org/10.1080/15592324.2018.1435228

Tan, X., Wang, D., Zhang, X., Zheng, S., Jia, X., Liu, H., Liu, Z., Yang, H., Dai, H., Chen, X., Qian, Z., Wang, R., Ma, M., Zhang, P., Yu, N., & Wang, E. (2025). A pair of LysM receptors mediates symbiosis and immunity discrimination in Marchantia. *Cell*, *188*(5), 1330-1348.e1327. https://doi.org/https://doi.org/10.1016/j.cell.2024.12.024

Taylor, T. N., Remy, W., & Hass, H. (1992). Parasitism in a 400-million-year-old green alga. *Nature*, *357*(6378), 493-494. https://doi.org/10.1038/357493a0

Terwilliger, T. C., Liebschner, D., Croll, T. I., Williams, C. J., McCoy, A. J., Poon, B. K., Afonine, P. V., Oeffner, R. D., Richardson, J. S., Read, R. J., & Adams, P. D. (2024). AlphaFold predictions are valuable hypotheses and accelerate but do not replace experimental structure determination. *Nature Methods*, *21*(1), 110-116. https://doi.org/10.1038/s41592-023-02087-4

Teufel, F., Almagro Armenteros, J. J., Johansen, A. R., Gíslason, M. H., Pihl, S. I., Tsirigos, K. D., Winther, O., Brunak, S., von Heijne, G., & Nielsen, H. (2022). SignalP 6.0 predicts all five types of signal peptides using protein language models. *Nature Biotechnology*, *40*(7), 1023-1025. https://doi.org/10.1038/s41587-021-01156-3

Teyssier, E., Grat, S., Landry, D., Ouradou, M., Rich, M. K., Fort, S., Keller, J., Lefebvre, B., Delaux, P.-M., & Mbengue, M. (2025). A plant Lysin Motif Receptor-Like Kinase plays an ancestral function in mycorrhiza. *Proceedings of the National Academy of Sciences*, *122*(24), e2426063122. https://doi.org/10.1073/pnas.2426063122

Tian, H., Wu, Z., Chen, S., Ao, K., Huang, W., Yaghmaiean, H., Sun, T., Xu, F., Zhang, Y., Wang, S., Li, X., & Zhang, Y. (2021). Activation of TIR signalling boosts pattern-triggered immunity. *Nature*, *598*(7881), 500-503. https://doi.org/10.1038/s41586-021-03987-1

Trifinopoulos, J., Nguyen, L.-T., von Haeseler, A., & Minh, B. Q. (2016). W-IQ-TREE: a fast online phylogenetic tool for maximum likelihood analysis. *Nucleic Acids Research*, *44*(W1), W232-W235. https://doi.org/10.1093/nar/gkw256

Van Etten, J. L., Lane, L. C., & Meints, R. H. (1991). Viruses and viruslike particles of eukaryotic algae. *Microbiological Reviews*, *55*(4), 586-620. https://doi.org/10.1128/mr.55.4.586-620.1991

Visweswaran, G. R., Leenhouts, K., van Roosmalen, M., Kok, J., & Buist, G. (2014). Exploiting the peptidoglycan-binding motif, LysM, for medical and industrial applications. *Appl Microbiol Biotechnol*, *98*(10), 4331-4345. https://doi.org/10.1007/s00253-014-5633-7

Vollmer, W., Blanot, D., & De Pedro, M. A. (2008). Peptidoglycan structure and architecture. *FEMS Microbiology Reviews*, *32*(2), 149-167. https://doi.org/10.1111/j.1574-6976.2007.00094.x

Wang, D., Wei, L., Liu, T., Ma, J., Huang, K., Guo, H., Huang, Y., Zhang, L., Zhao, J., Tsuda, K., & Wang, Y. (2023). Suppression of ETI by PTI priming to balance plant growth and defense through an MPK3/MPK6-WRKYs-PP2Cs module. *Molecular Plant*, *16*(5), 903-918. https://doi.org/https://doi.org/10.1016/j.molp.2023.04.004

Willmann, R., Lajunen, H. M., Erbs, G., Newman, M.-A., Kolb, D., Tsuda, K., Katagiri, F., Fliegmann, J., Bono, J.-J., Cullimore, J. V., Jehle, A. K., Götz, F., Kulik, A., Molinaro, A., Lipka, V., Gust, A. A., & Nürnberger, T. (2011). Arabidopsis lysin-motif proteins LYM1 LYM3 CERK1 mediate bacterial peptidoglycan sensing and immunity to bacterial infection. *Proceedings of the National Academy of Sciences*, *108*(49), 19824-19829. https://doi.org/10.1073/pnas.1112862108

Xu, L., Wang, J., Xiao, Y., Han, Z., & Chai, J. (2023). Structural insight into chitin perception by chitin elicitor receptor kinase 1 of Oryza sativa. *J Integr Plant Biol*, *65*(1), 235-248. https://doi.org/10.1111/jipb.13279

Xue, D.-X., Li, C.-L., Xie, Z.-P., & Staehelin, C. (2019). LYK4 is a component of a tripartite chitin receptor complex in Arabidopsis thaliana. *Journal of Experimental Botany*, *70*(19), 5507-5516. https://doi.org/10.1093/jxb/erz313

Yamada, K., Yamaguchi, K., Shirakawa, T., Nakagami, H., Mine, A., Ishikawa, K., Fujiwara, M., Narusaka, M., Narusaka, Y., Ichimura, K., Kobayashi, Y., Matsui, H., Nomura, Y., Nomoto, M., Tada, Y., Fukao, Y., Fukamizo, T., Tsuda, K., Shirasu, K., . . . Kawasaki, T. (2016). The Arabidopsis CERK1-associated kinase PBL27 connects chitin perception to MAPK activation. *The EMBO Journal*, *35*(22), 2468-2483-2483. https://doi.org/https://doi.org/10.15252/embj.201694248

Yang, C., Liu, R., Pang, J., Ren, B., Zhou, H., Wang, G., Wang, E., & Liu, J. (2021). Poaceae-specific cell wall-derived oligosaccharides activate plant immunity via OsCERK1 during Magnaporthe oryzae infection in rice. *Nature Communications*, *12*(1), 2178. https://doi.org/10.1038/s41467-021-22456-x

Yang, C., Wang, E., & Liu, J. (2022). CERK1, more than a co-receptor in plant–microbe interactions. *New Phytologist*, *234*(5), 1606-1613. https://doi.org/https://doi.org/10.1111/nph.18074

Yotsui, I., Matsui, H., Miyauchi, S., Iwakawa, H., Melkonian, K., Schlüter, T., Michavila, S., Kanazawa, T., Nomura, Y., Stolze, S. C., Jeon, H. W., Yan, Y., Harzen, A., Sugano, S. S., Shirakawa, M., Nishihama, R., Ichihashi, Y., Ibanez, S. G., Shirasu, K., . . . Nakagami, H. (2023). LysM-mediated signaling in Marchantia polymorpha highlights the conservation of pattern-triggered immunity in land plants. *Curr Biol*, *33*(17), 3732-3746.e3738. https://doi.org/10.1016/j.cub.2023.07.068

Yu, X.-Q., Niu, H.-Q., Liu, C., Wang, H.-L., Yin, W., & Xia, X. (2024). PTI-ETI synergistic signal mechanisms in plant immunity. *Plant Biotechnology Journal*, *22*(8), 2113-2128. https://doi.org/https://doi.org/10.1111/pbi.14332

Yuan, M., Jiang, Z., Bi, G., Nomura, K., Liu, M., Wang, Y., Cai, B., Zhou, J.-M., He, S. Y., & Xin, X.-F. (2021). Pattern-recognition receptors are required for NLR-mediated plant immunity. *Nature*, *592*(7852), 105-109. https://doi.org/10.1038/s41586-021-03316-6

Zhang, X. C., Wu, X., Findley, S., Wan, J., Libault, M., Nguyen, H. T., Cannon, S. B., & Stacey, G. (2007). Molecular evolution of lysin motif-type receptor-like kinases in plants. *Plant Physiol*, *144*(2), 623-636. https://doi.org/10.1104/pp.107.097097

Zipfel, C. (2008). Pattern-recognition receptors in plant innate immunity. *Current Opinion in Immunology*, *20*(1), 10-16. https://doi.org/https://doi.org/10.1016/j.coi.2007.11.003

6. Supplemental figures and tables

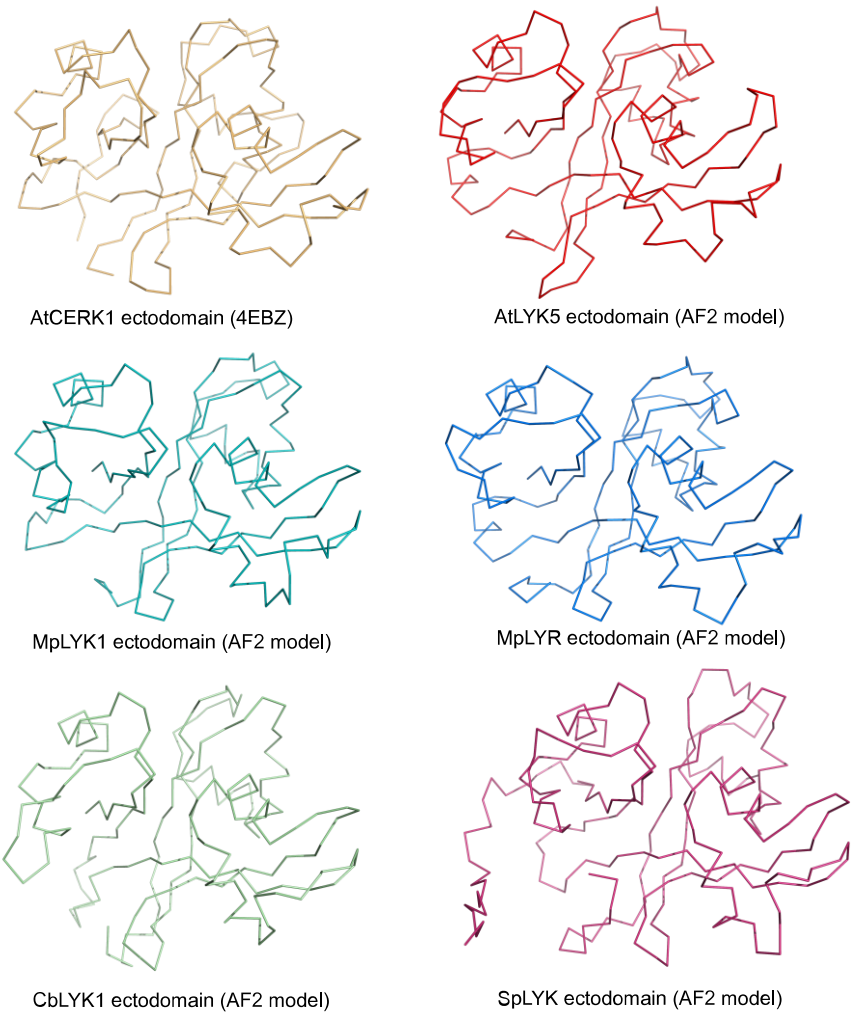

Supplemental Figure 1 LysM ECDs of AtCERK1 (PDB: 4EBZ), AtLYK5, MpLYK1, MpLYR, CbLYK1, and SplYK as predicted by AlphaFold2.

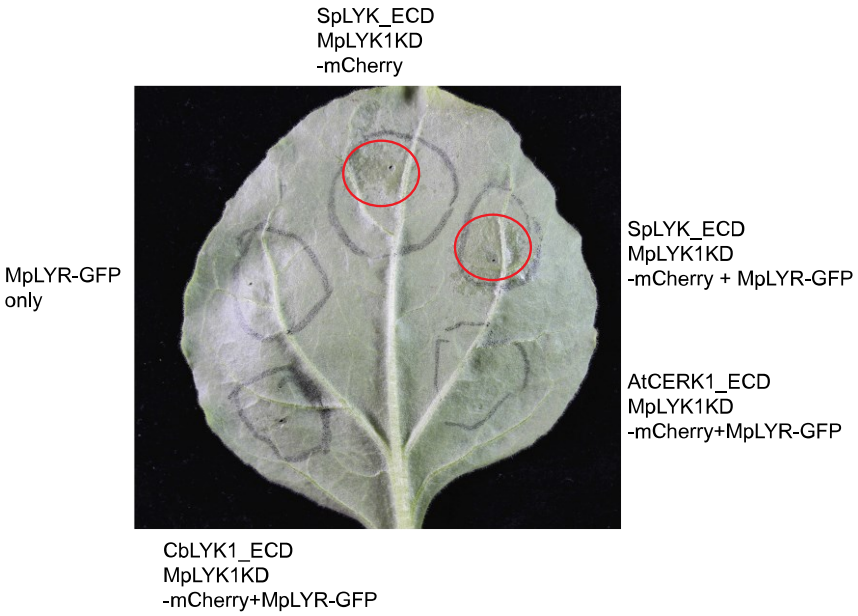

Supplemental Figure 2 Lesions on leaves (red circle) caused by infiltration of SpLYK_ECD-MpLYK1_KD chimera construct into *N. benthamiana.*

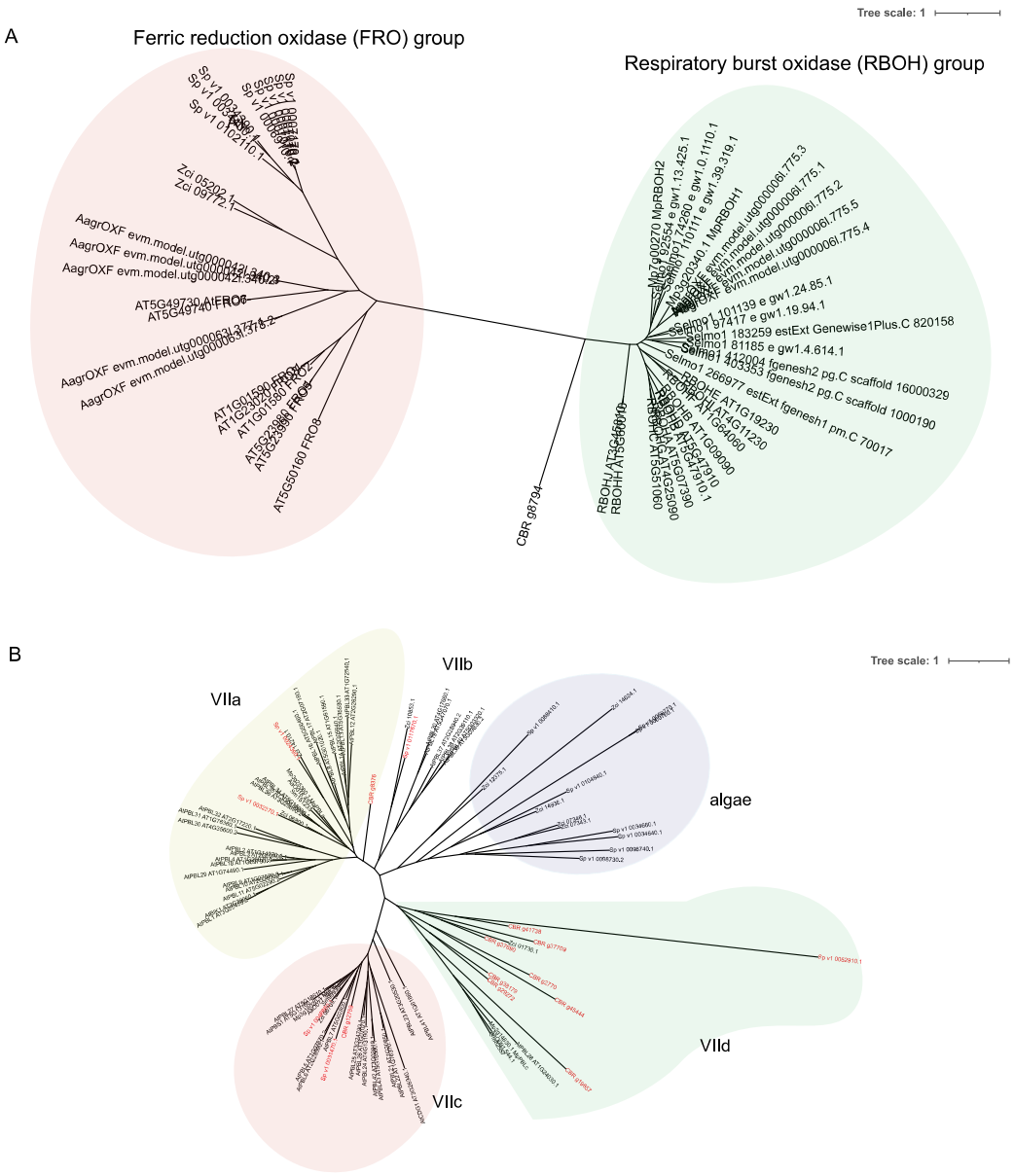

Supplemental Figure 3 (A) Unroot maximum likelihood phylogenetic tree of land plants and streptophyte algae NADPH oxidases. Streptophyte algae NADPH oxidases do not cluster with RBOH NADPH oxidase. Tree scale:1 **(B)** Unroot maximum likelihood phylogenetic tree of land plants and streptophyte algae (labeled in red) RLCK subfamily VII. Tree scale:1.

	Cytosolic P.G Quantity	Organelle P.G Quantity	Plasma membrane P.G Quantity
MpLYK1	16.4	17.9	19.4
MpLYP	21.5	20.7	22.1
MpLYK2	Not detected	Not detected	12.4
MpLYR	16.1	18.2	19.4

Supplemental table 1. LysM receptors identified by MS from the fractionation samples in *M. polymorpha*.